Aus der

Klinik für Allgemein-, Viszeral-, und Transplantationschirurgie

Klinikum der Ludwig-Maximilians-Universität München

Personalised Targeting of the Substance P/NK1R Axis in Pancreatic Ductal Adenocarcinoma: A Molecular and Sex-Specific Stratification Approach

Dissertation

zum Erwerb des Doctor of Philosophy (Ph.D.)

an der Medizinischen Fakultät

der Ludwig-Maximilians-Universität München

vorgelegt von

Iris Ittermann

aus

Potsdam / Deutschland

Jahr

2025

Mit Genehmigung der Medizinischen Fakultät der
Ludwig-Maximilians-Universität München

Erstes Gutachten:	Prof. Dr. Alexandr Bazhin
Zweites Gutachten:	Priv. Doz. Dr. Matthias Ilmer
Drittes Gutachten:	Priv. Doz. Dr. Julian Holch
Viertes Gutachten:	Prof. Dr. Julia Mayerle

Dekan: Prof. Dr. med. Thomas Gudermann

Tag der mündlichen Prüfung: 23.09.2025

Table of content

Abstract:

Background: The Neurokinin-1 receptor (NK1R) represents a promising target for pancreatic ductal adenocarcinoma (PDAC) therapy. Yet its complex expression patterns and functional implications remain incompletely understood.

Methods: A comprehensive multi-method approach was employed to investigate NK1R biology in PDAC, including transcriptomic analysis of multiple datasets, RT-qPCR analysis for isoform-specific expression profiling, Western blot analysis, functional assays with NK1R antagonist aprepitant (AP), as well as its ligand Substance P (SP), and bioinformatic analysis of sex-specific expression patterns.

Results: Differential expression of NK1R isoforms, encoded by *TACR1*, was demonstrated across PDAC cell lines with predominant expression of the truncated variant (NK1R-tr). Lower NK1R gene expression correlated with advanced tumour stage and poorer prognosis, while inversely correlating with EMT marker *ZEB1*. Treatment with the NK1R antagonist aprepitant demonstrated significant antiproliferative effects in PDAC cells, particularly in cancer stem cell-like populations, with the highest sensitivity in cell lines expressing elevated NK1R-tr. Mechanistically, aprepitant induced cell cycle arrest rather than apoptosis, modulating ERK*1/2* signalling. Bioinformatic analyses revealed distinct transcriptomic signatures associated with high versus low *TACR1* expression, with *TACR1*-high samples exhibiting enrichment of immune-related pathways. Unexpectedly, *TACR1* expression demonstrated strong sex-specific patterns, with substantially higher expression in female PDAC samples compared to male samples, accompanied by differential *XIST* expression, suggesting potential X-chromosome-linked regulatory mechanisms.

Conclusion: The SP/NK1R system exhibits complex expression patterns in PDAC with significant therapeutic and prognostic implications. NK1R inhibition represents a promising approach for targeted therapy, particularly in *TACR1*-high tumours. The pronounced sex-specific differences in *TACR1* expression highlight potential for personalised therapeutic strategies and suggest important biological differences in PDAC between males and females.

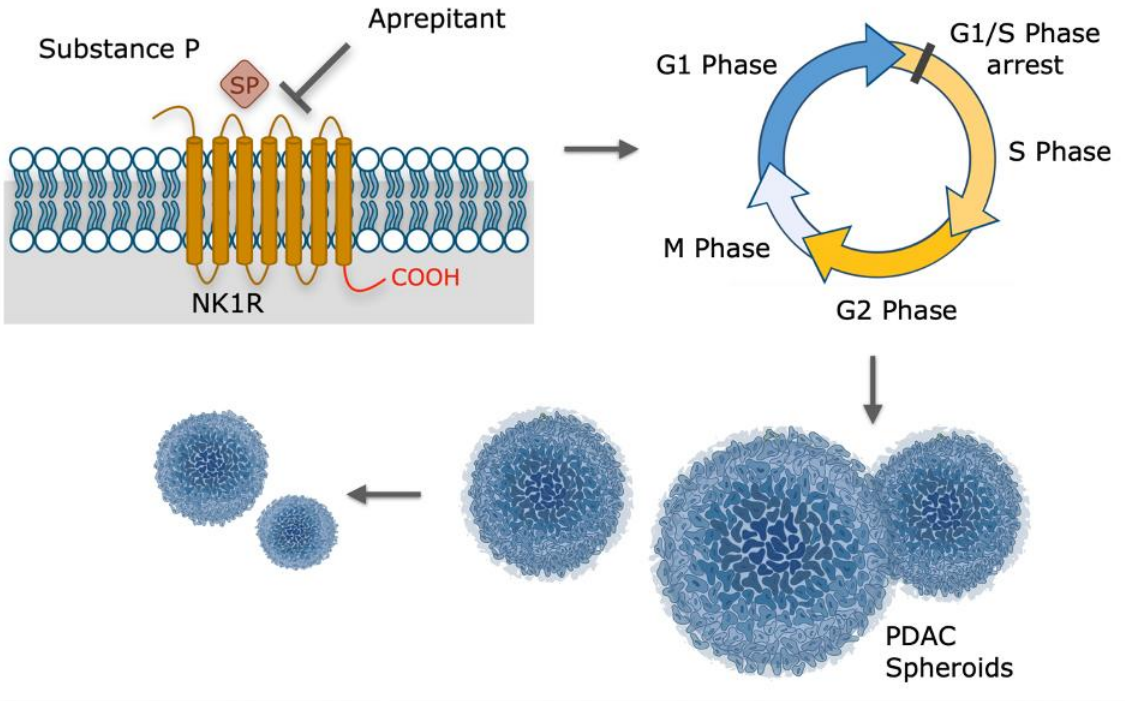

Figure 1: Graphical Abstract. Permission for print obtained from the publisher (1).*

* This has been previously published by the author (1).

List of figures

List of tables

List of abbreviations

ADEX	Aberrantly Differentiated Endocrine Exocrine
AP	Aprepitant
BDNF	Brain-Derived Neurotrophic Factor
BSA	Bovine Serum Albumin
CCLE	Cancer Cell Line Encyclopedia
CDH1	Cadherin-1 (E-cadherin)
CGRP	Calcitonin Gene-Related Peptide
CM	Conditioned Media
CSC	Cancer Stem Cell
DAPI	4′,6-Diamidin-2-phenylindol, Dihydrochloride
DEG	Differentially Expressed Gene
DMEM	Dulbecco's Modified Eagle's Medium
DMSO	Dimethyl Sulfoxide
ECL2	Second Extracellular Loop
ELISA	Enzyme-Linked Immunosorbent Assay
EMP	Epithelial-Mesenchymal Plasticity
EMT	Epithelial-Mesenchymal Transition
ERCP	Endoscopic Retrograde Cholangiopancreatography
ERK	Extracellular Signal-Regulated Kinase
FBS	Fetal Bovine Serum
FFPE	Formalin-Fixed Paraffin-Embedded
FGFR	Fibroblast Growth Factor Receptor
GAPDH	Glyceraldehyde 3-Phosphate Dehydrogenase
GEO	Gene Expression Omnibus
GO	Gene Ontology
GPCR	G-Protein Coupled Receptor
HTCR	Human Tissue and Cell Research
IC50	Half-Maximal Inhibitory Concentration
IPMN	Intraductal Papillary Mucinous Neoplasm
KEGG	Kyoto Encyclopedia of Genes and Genomes
LMU	Ludwig-Maximilian-University
MAPK	Mitogen-Activated Protein Kinase
MDSC	Myeloid-Derived Suppressor Cell
MTT	3-(4,5-Dimethylthiazol-2-yl)-2,5-Diphenyltertazolium Bromide
NGF	Nerve Growth Factor
NK1R	Neurokinin-1 Receptor
NK1R-fl	Neurokinin-1 Receptor Full-Length
NK1R-tr	Neurokinin-1 Receptor Truncated
PanIN	Pancreatic Intraepithelial Neoplasia

PBS	Phosphate-Buffered Saline
PCA	Principal Component Analysis
PCR	Polymerase Chain Reaction
PDAC	Pancreatic Ductal Adenocarcinoma
PDO	Patient-Derived Organoid
PI	Propidium Iodide
PNI	Perineural Invasion
PPT-A	Preprotachykinin-A
PSC	Pancreatic Stellate Cell
RT-qPCR	Reverse Transcription Quantitative Polymerase Chain Reaction
SDS-PAGE	Sodium Dodecyl Sulphate Polyacrylamide Gel Electrophoresis
SEM	Standard Error of the Mean
SFA	Sphere Formation Assay
SFM	Sphere Formation Medium
SP	Substance P
SSI	Surgical Site Infection
TAC1	Tachykinin 1 (Gene encoding for Substance P)
TACR1	Tachykinin Receptor 1 (Gene encoding for NK1R)
TACR1-fl	Tachykinin Receptor 1 Full-Length
TACR1-tr	Tachykinin Receptor 1 Truncated
TBST	Tris-Buffered Saline with Tween
TCGA	The Cancer Genome Atlas
TME	Tumour Microenvironment
XIST	X-Inactive Specific Transcript
ZEB1	Zinc Finger E-Box Binding Homeobox 1

1. Introduction

1.1 Pancreatic Ductal Adenocarcinoma

1.1.1 Epidemiology and Disease Burden

Pancreatic ductal adenocarcinoma (PDAC) stands as one of the most lethal malignancies in modern oncology, with a devastating 5-year survival rate that has remained stubbornly below 10% (2). Despite substantial progress in cancer treatment approaches, PDAC mortality continues to increase at an alarming rate (3). Current projections suggest it will become the second highest contributor to cancer mortality in the United States by 2030 (3). In 2022 more than 500,000 new pancreatic cancer cases were identified worldwide (4), while industrialized countries showed especially troubling upward trends in incidence rates (4,5). Pancreatic cancer's devastating impact stems largely from its stealthy progression (6). When finally detected, roughly 80-85% present with either locally advanced or metastatic cancer, which dramatically restricts available treatment options (6).

The disease burden extends far beyond mortality statistics years (Bryant et al., 2023; Yuan et al., 2022). PDAC disproportionately affects aging populations, with a median age of diagnosis of 70 years, though an alarming trend of increasing incidence among younger individuals has emerged in recent years (8,9).

The economic burden of PDAC is substantial, with significant variations between healthcare systems (7). In Europe, average total treatment costs per patient are €40,357 (median €15,991), with monthly costs averaging €3,656 (median €1,536) (7). These costs reflect the entire treatment course rather than annual expenses (7). In the United States, mean direct Medicare costs reach approximately $65,500 per patient (10). Total healthcare costs for PDAC in the US reached $2.55 billion in 2016, thus making it the second most expensive gastrointestinal cancer to treat (11). This significant economic impact is driven by several factors, such as complex treatment regimens, and frequent hospitalizations (12). Together with extensive supportive care requirements, this reflects the intensive resource utilization required for PDAC care (12).

1.1.2 Molecular Pathogenesis

The molecular development of PDAC occurs through multiple stages, marked by the gradual buildup of genetic mutations and epigenetic modifications (13). This progression occurs through well-defined precursor lesions, primarily pancreatic

intraepithelial neoplasias (PanINs) and intraductal papillary mucinous neoplasms (IPMNs) (14). The molecular landscape is characterized by four signature driver mutations that define PDAC's molecular signature (15). *KRAS* mutations, present in over 90% of cases, represent the earliest and most frequent genetic alteration, followed by inactivating mutations in tumour suppressor genes: *TP53* (75%), *CDKN2A* (90%), and *SMAD4* (55%) (15).

Beyond these canonical alterations, PDAC exhibits remarkable molecular heterogeneity (16). Complex patterns of chromosomal instability and structural variations affect key regulatory regions, while telomere dysfunction contributes to genomic instability (16,17). Constitutive activation of MAPK signalling through mutant *KRAS* (18), aberrant cell cycle regulation through *p16/CDKN2A* loss (19), and disrupted TGF-β signalling via *SMAD4* inactivation (20) collectively drive disease progression.

The molecular landscape is further complicated by extensive transcriptional reprogramming (21). This includes altered metabolic programming favouring aerobic glycolysis (22), activation of developmental pathways including Notch, Hedgehog, and WNT signalling, and EMT-related changes promoting invasive behaviour (23). Abnormal function of epigenetic regulators introduces additional complexity to how pancreatic ductal adenocarcinoma develops and progresses (24).

This intricate molecular profile creates significant therapeutic challenges, requiring novel targeted approaches that address PDAC's heterogeneity and treatment resistance.

1.1.3 Challenges in PDAC Treatment

PDAC remains one of the most difficult cancers to treat, largely due to late diagnosis, aggressive growth, and resistance against standard therapies (25). Even with progress in cancer research, these challenges continue to drive the poor survival rates associated with the disease (25).

The asymptomatic nature of early-stage PDAC remains a critical barrier to effective treatment (26). In most cases, the disease is already locally advanced or has metastasised by the time of diagnosis, leaving curative surgical options viable for only 15-20% of cases (27,28). Even among those who undergo resection, the likelihood of recurrence remains alarmingly high with approximately 80% (29). Efforts to develop reliable tools for early detection, such as biomarkers and advanced imaging techniques, have yet to yield sufficient sensitivity and specificity for routine clinical use (30).

Current systemic therapies, including FOLFIRINOX and gemcitabine-based regimens, offer only modest improvements in survival, often measured in months rather than years (31). These regimens are associated with significant toxicity, limiting their use to patients with strong performance status (32,33). The tumour microenvironment (TME) in PDAC, characterized by dense fibrosis and hypervascularity, further complicates treatment by impeding drug delivery and contributing to chemoresistance (34).

PDAC is notoriously resistant to immunotherapy, largely due to its immunosuppressive TME, which fosters immune evasion (35). Regulatory T cells, tumour-associated macrophages, and myeloid-derived suppressor cells (MDSCs) dominate the PDAC microenvironment, effectively neutralizing anti-tumour immune responses (36). Although immune checkpoint inhibitors have proven effective in various malignancies, their therapeutic benefit in PDAC has been limited (37). This highlights the need for alternative strategies to overcome the tumour's inherent resistance to immune-mediated therapies (37).

The extensive inter- and intra-tumoral heterogeneity of PDAC complicates treatment strategies by fostering therapeutic resistance and driving disease progression (38). Subpopulations of cancer cells within the same tumour can exhibit diverse genetic and epigenetic profiles, making single-agent therapies largely ineffective (39). Addressing this heterogeneity will require precision medicine approaches tailored to individual tumour characteristics (40).

The absence of reliable biomarkers to predict therapeutic response or reveal actionable targets limits the effectiveness of personalized treatment strategies in PDAC (41). While genomic and transcriptomic profiling efforts are advancing, the translation into widely applicable clinical interventions has not been achieved, yet (42). This leaves most patients without tailored treatment options (43).

In conclusion, the management of PDAC remains highly challenging, due to late-stage diagnosis, therapeutic resistance, and a highly complex tumour microenvironment. Addressing these challenges will require an integrative approach that combines innovations in early detection, molecular profiling, and novel therapeutic strategies.

1.1.4 Patient Stratification Approaches

Patient stratification in PDAC has emerged as a critical strategy to optimize treatment outcomes in this heterogeneous disease (44,45). Traditional approaches, such as anatomical staging, have been insufficient, which lead to the develop-

ment of molecular and biomarker-based stratification methods (28). The complexity of PDAC's molecular landscape, as previously discussed, offers both challenges and opportunities for patient classification (46).

Recent advances in molecular profiling have identified distinct PDAC subtypes with different therapeutic vulnerabilities (47–49). The commonly recognized subtypes include Squamous, Pancreatic Progenitor, Immunogenic, and Aberrantly Differentiated Endocrine Exocrine (ADEX) (44). Progenitor, also referred to as Classical, subtypes typically show better response to conventional chemotherapy, while the Squamous subtype demonstrates more aggressive behaviour and poorer outcomes (49).

Beyond molecular subtypes, emerging stratification approaches focus on specific biomarkers and signalling pathways (26). Of particular importance are receptor-based stratification strategies (50), as cell surface receptors represent both prognostic indicators and therapeutic targets (51).

Various receptor families have shown potential for patient stratification. These include growth factor receptors (52), G-protein coupled receptors (53), and cytokine receptors (54). Their expression patterns and activation states could serve as predictive indicators of therapeutic efficacy.

However, the development of effective patient stratification is hindered by several fundamental challenges (55). The limited availability of tissue for molecular analysis often restricts comprehensive profiling (55), while tumour heterogeneity and dynamic molecular changes during disease progression complicate consistent classification (56). Furthermore, the integration of multiple data types - from genomic and transcriptomic profiles to clinical parameters - remains complex (57). Despite these challenges, validated predictive biomarkers are essential for implementing personalized medicine strategies in PDAC treatment (46). As new therapeutic targets emerge, the ability to identify patient subgroups most likely to benefit from specific interventions becomes increasingly important for improving treatment outcomes (44).

1.1.5 Neural Aspects of PDAC

The neural network within the pancreas plays a crucial role in both normal organ function, in addition to driving pancreatic cancer onset and progression (58). The organ's complex innervation influence cellular behaviour, inflammatory responses, and cancer progression through multiple mechanisms (59).

The sympathetic nervous system regulates pancreatic blood flow and inhibits the secretion of both hormones and digestive enzymes, working in balance with parasympathetic stimulation to maintain proper pancreatic function (60). Parasympathetic innervation, mediated through the vagus nerve, regulates secretory activities and maintains metabolic homeostasis (61). Additionally, sensory nerve fibres, particularly peptidergic neurons containing substance P and calcitonin gene-related peptide (CGRP), are crucial for pain signalling and neurogenic inflammation (62).

In PDAC, this neural network undergoes significant remodelling characterized by multiple alterations (63). A key feature is perineural invasion (PNI), where cancer cells invade the perineural space of local nerves, using these structures as conduits for tumour spread (63). This process involves complex molecular interactions between tumour cells and neural elements, through which intrapancreatic nerves undergo neural hypertrophy and increased neural density (64). PNI correlates strongly with poor prognosis of PDAC patients and represents a major route for tumour dissemination beyond the primary site (65).

The development of neuroplastic changes in PDAC occurs through several mechanisms (66). Neurotrophic factors like nerve growth factor (NGF) and brain-derived neurotrophic factor (BDNF), secreted by cancer cells, facilitate axon formation and neural remodelling (64). This neuroplasticity creates a feedback loop where increased neural density provides additional routes for cancer cell invasion while simultaneously contributing to pain and inflammation through neuropeptide release (64).

Pain, a dominant symptom in PDAC, results from multiple neural mechanisms (67). Direct tumour invasion of nerves, inflammatory mediators, and increased intertumoral pressure all contribute to nociceptive signalling (67). The release of substance P and other neuropeptides from sensory nerve endings amplifies local inflammation and promotes tumour progression through specific receptor-mediated pathways (67).

Recent studies have revealed that neural remodelling in PDAC precedes visible tumour formation, suggesting its potential role as an early disease marker (65,67). Changes in neural density and morphology have been observed in precursor lesions, indicating that neural alterations may contribute to early stages of pancreatic carcinogenesis (65). These findings have important implications for both early detection strategies and therapeutic approaches (65,67). Furthermore, the recognition of neural-tumour interactions has led to the development of novel

therapeutic strategies targeting both neural signalling pathways and tumour-nerve interactions (67).

1.2 The Neurokinin-1 Receptor System

Cell surface receptors play a crucial role throughout tumour formation and disease progression, with G-protein coupled receptors (GPCRs) representing one of the largest and most diverse families of signalling molecules (68). Among these, the Substance P/Neurokinin-1 receptor (SP/NK1R) has emerged as a significant pathway in cancer biology, extending far beyond its initially characterized roles in neurogenic inflammation and pain transmission (69). This evolutionary conserved pathway gained attention in oncology research following the discovery of its significant overexpression in various malignancies (70,71).

The recognition of NK1R's role in cancer progression was initially driven by observations of its involvement in tumour cell proliferation, migration, and survival across multiple cancer types (72). In PDAC, interest in the SP/NK1R system intensified following discoveries of its contribution to the neural invasion that characterizes this aggressive malignancy (53,73). Given the complex neuroanatomy of the pancreas and the significant neural remodelling in PDAC described earlier, the SP/NK1R pathway represents a particularly compelling target for investigation (65). The extensive perineural invasion, neural hypertrophy, and increased neural density observed in PDAC create an environment where neuromodulatory systems like SP/NK1R can significantly influence disease progression and therapeutic response (65). The significant interplay between neural elements and neoplastic biology emphasizes the importance of elucidating neurogenic signalling pathways, as both potential prognostic biomarkers and therapeutic targets in PDAC management.

The presence of different NK1R isoforms (truncated and full-length) suggests potential therapeutic implications, as tumours with varying receptor expression profiles seem to respond differently to targeted treatments (74–78).

1.2.1 Substance P/Neurokinin-1 Receptor Signalling Pathway

SP is an 11-amino acid neuropeptide belonging to the tachykinin family, characterized by its conserved carboxyl-terminal sequence (79). Its primary structure, Arg-Pro-Lys-Pro-Gln-Gln-Phe-Phe-Gly-Leu-Met-NH2, facilitates high-affinity interaction with the neurokinin-1 receptor (NK1R) (71). SP is synthesized as part

of the preprotachykinin-A (PPT-A) precursor, undergoing post-translational modifications to yield its biologically active form (80). Stored in dense-core vesicles of neurons and immune cells, SP is released in response to noxious stimuli, tissue injury, and stress (81).

As both a neurotransmitter and neuromodulator, SP plays critical roles in pain perception, where it amplifies nociceptive signals in the dorsal horn of the spinal cord by acting on NK1R expressed on second-order neurons (82,83). SP also drives neurogenic inflammation, inducing vasodilation, plasma extravasation, and the release of pro-inflammatory mediators such as histamine and cytokines (84). Moreover, SP functions in immune modulation, recruiting and activating mast cells, macrophages, and lymphocytes, thereby linking the nervous and immune systems (85). It also regulates gastrointestinal motility and secretion via smooth muscle cells and enteric neurons (86).

Dysregulation of SP is implicated in numerous pathologies, including chronic pain syndromes (87), asthma (88), inflammatory bowel disease (89), and cancer, where SP promotes tumour proliferation, angiogenesis, and resistance to apoptosis (72). These multifaceted roles make SP a crucial mediator in health and disease (90).

Building on the structural basis of NK1R signalling, the SP/NK1R cascade extends into a complex network of second messenger systems and downstream effectors (91). Upon binding of SP to NK1R, the receptor undergoes a conformational change that facilitates the activation of Gq/11 proteins (92). These proteins, while occupying approximately 1-2% of the human genome, serve as signalling intermediaries downstream of G protein-coupled receptors (GPCRs) activation, thus initiating downstream signalling cascades (93).

To ensure precise regulation, the SP/NK1R cascade incorporates multiple layers of feedback and desensitization (94,95). PKC-mediated phosphorylation of NK1R recruits β-arrestin, a multifunctional adaptor protein that uncouples NK1R from G proteins, attenuating classical signalling (94). β-arrestins also promote receptor internalization by interacting with clathrin and adaptor protein complexes, sequestering NK1R into endosomes for recycling or degradation (95). This internalization not only limits ligand binding but also serves as a platform for non-canonical signalling pathways, such as β-arrestin-mediated ERK activation, which exhibits distinct dynamics critical for cellular differentiation, migration, and survival (96) (Figure 4).

1.2.2 Structure and Isoforms

The pathophysiological significance of the NK1R, encoded by *TACR1*, is fundamentally determined by its structural organization and downstream signalling mechanisms (97). As a class A G-protein coupled receptor characterized by seven hydrophobic transmembrane domains, it is connected by three extracellular and three intracellular loops (98,99). Extracellular loops, particularly the second extracellular loop (ECL2), play a critical role for NK1R by contributing to ligand specificity, facilitating ligand entry into the transmembrane binding pocket, and regulating receptor activation (100). Both, SP and Aprepitant, an NK1R antagonist, bind to that pocket in a competitive manner (Figure 2). As additional illustration, the structure of NK1R in its crystal form in complex with Aprepitant is shown in Figure 3.

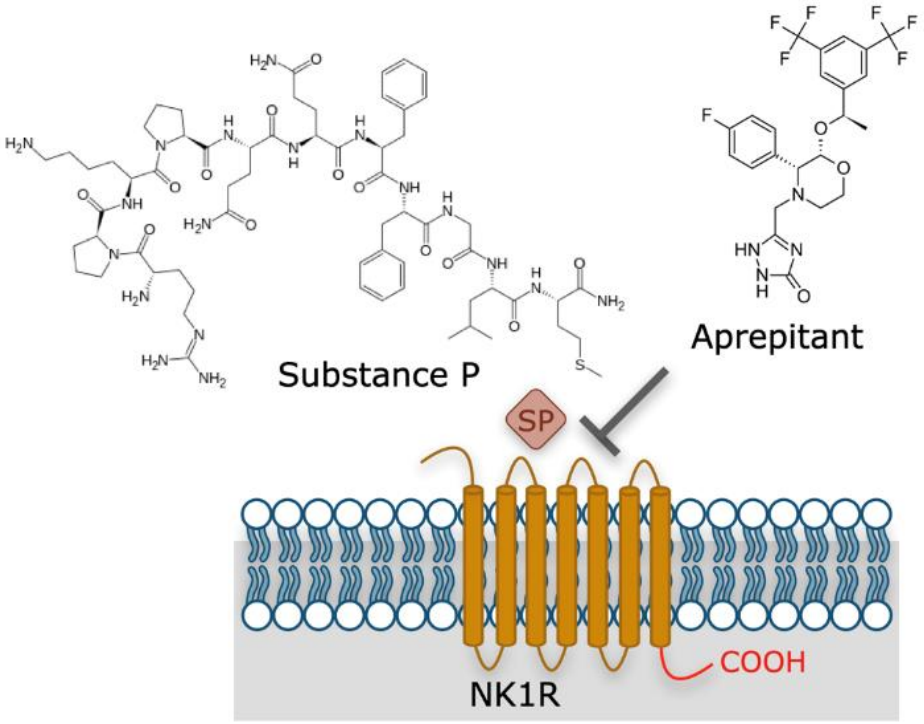

Figure 2: Molecular interactions at the NK1R receptor. Schematic representation of the NK1R (Neurokinin-1 receptor) embedded in the cell membrane, with its seven transmembrane domains shown in gold and the C-terminal tail (marked as COOH in red) extending into the cytoplasm (96). The diagram illustrates the competitive binding relationship between the endogenous ligand Substance P (SP, shown in pink) and the antagonist Aprepitant (101). The chemical structure of Substance P (left) shows the undecapeptide with its characteristic amino acid sequence, while Aprepitant (right) is depicted with its complex molecular structure containing multiple fluorine atoms and heterocyclic rings (102). The inhibitory action of Aprepitant is represented by the grey blocking bar, indicating how it prevents Substance P from activating the receptor, thereby inhibiting downstream signalling pathways. This competitive antagonism forms the basis for therapeutic targeting of the SP/NK1R system in pancreatic cancer. This figure was created by the author. Permission for print obtained from the publisher (1).

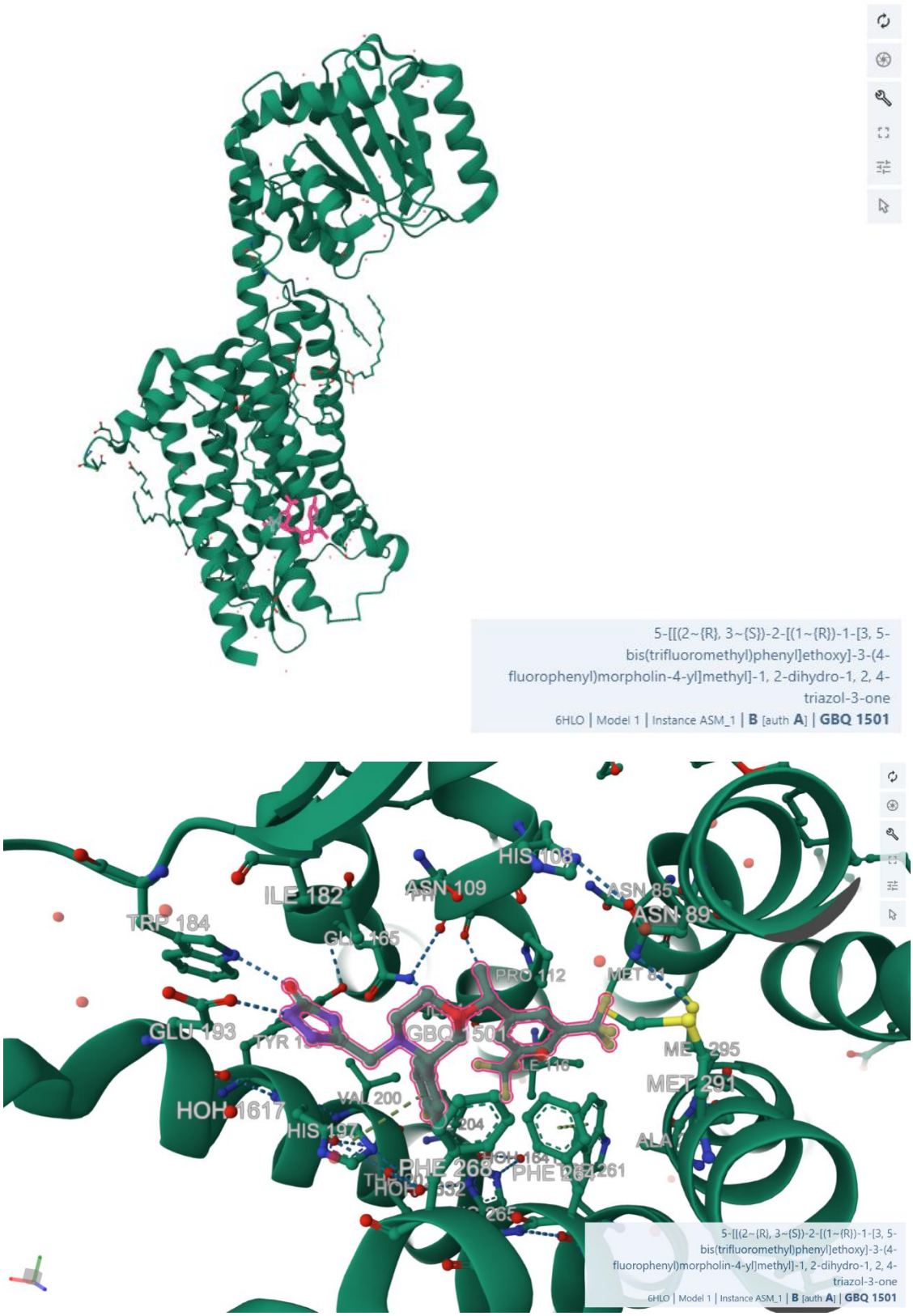

Figure 3: Crystal structure of NK1R in a complex with the small molecule antagonist Aprepitant. Top figure: Overall structure of the full-length NK1R with Aprepitant shown in pink binding to the appropriate pocket. Bottom figure: Zoom into the binding pocket on Aprepitant displaying the NK1R residues binding to Aprepitant. AP is shown in pink. This figure was generated by the author using the Protein Data Bank. The PDB identifier for this structure is 6HLO (103,104).

Alternative splicing of the *TACR1* gene produces two isoforms in humans: a full-length receptor (NK1R-fl) of 407 amino acids and a truncated variant (NK1R-tr) of 311 amino acids that lacks 96 amino acids at the carboxyl terminus (96).

Both the full-length NK1R (NK1R-fl) and the truncated NK1R (NK1R-tr) contain several key structural elements essential for signal transduction (96). The primary difference between the two forms lies in the intracellular C-terminus: NK1R-fl harbours phosphorylation sites necessary for β-arrestin recruitment and receptor internalization, while the truncated NK1R, resulting from alternative splicing of exon 5, lacks most of the C-terminal tail responsible for β-arrestin binding and receptor desensitisation (Figure 4) (105). This structural difference leads to profound functional consequences: NK1R-tr exhibits at least 10-fold lower binding affinity for SP compared to NK1R-fl and fails to undergo β-arrestin-mediated endocytosis (105). Both isoforms couple to Gq/11 proteins, triggering phospholipase C activation and subsequent calcium mobilization, but their downstream signalling cascades differ significantly due to the truncated variant's inability to form stable complexes with β-arrestin (96,106).

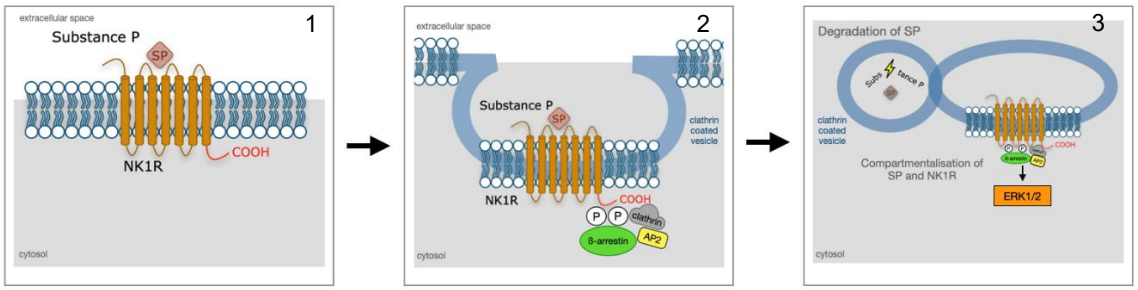

Figure 4: Internalization mechanism of the full-length NK1R. This diagram illustrates the sequential process of NK1R-FL internalization following activation by Substance P. 1) Substance P binds to and activates NK1R at the cell surface; 2) β-arrestin recruitment serves as an adapter for β-adaptin (AP2 and clathrin), coupling the activated receptor to clathrin-coated pits; 3) β-arrestin uncouples from Substance P, leading to compartmentalization, degradation of SP, and activation of ERK1/2 signalling; 4) NK1R undergoes recycling and returns to the cell surface (95,107). This figure was created by the author.

Receptor truncation delays the activation of extracellular signal-regulated kinase (ERK), with a peak occurring at 20-30 minutes, compared to the rapid activation observed in full-length NK1R (NK1R-fl), which peaks within 1 minute (96). ERK plays a critical role in cellular processes such as proliferation, differentiation, and survival (108). The delayed activation in truncated NK1R suggests impaired or altered signalling dynamics, which can significantly affect downstream cellular

responses to external stimuli like SP (96). This distinction highlights the importance of the carboxyl terminus in maintaining efficient signal transduction and physiological responses.

The molecular architecture of these isoforms determines their distinct tissue distribution patterns, with NK1R-fl predominantly expressed in the central nervous system and NK1R-tr more prevalent in peripheral tissues and malignant cells (109). This differential expression and structural variation has significant implications for therapeutic targeting, particularly in the context of cancer treatment (110,111).

1.2.3 NK1R in Cancer Biology

Initial investigations into oncogenic signalling pathways revealed aberrant expression and activation of GPCRs as critical factors in tumour development (112). Cancer cells commonly employ a strategy of abnormal GPCR upregulation coupled with receptor activation through autocrine and paracrine mechanisms (112). This process, where tumour or stromal cells release GPCR agonists that act upon the same or neighbouring cells, represents the predominant mechanism by which malignant cells activate GPCR signalling pathways (112). Among these, comprehensive molecular profiling has identified the SP/NK1R system as a key player across multiple cancer types, with distinct expression patterns and functional implications in different malignancies (69).

In breast cancer, a study has demonstrated high NK1R-tr expression in breast cancer tissues compared to normal breast epithelium, with expression levels positively correlating with tumour grade (77). The researchers found that while total NK1R is present across normal, benign and cancerous breast tissues, NK1R-fl expression significantly decreases in tumours, especially in metastatic cases. Notably, non-cancerous HBL-100 breast cells predominantly express NK1R-fl, while breast cancer cell lines (MDA-MB-231, MCF-7, T47D) express only NK1R-tr. (77).

In colorectal cancer, NK1R blocking exhibits significant anti-tumoral effects through multiple mechanisms (113). Molecular analyses have demonstrated that treatment with NK1R antagonists leads to robust growth inhibition of colorectal cancer cells, independent of their baseline Wnt activity status (113). Notably, NK1R blockade induces a striking inhibition of canonical Wnt signalling, characterized by increased membrane stabilization of β-catenin and decreased TCF/LEF-mediated transcription (113). This effect occurs regardless of mutations in the Wnt pathway, as observed in cell lines harbouring both APC and β-catenin

mutations. Furthermore, NK1R inhibition affects cancer stem cell-like populations, reducing the number and size of colorectal cancer spheroids in vitro, which suggests a potential impact on tumour-initiating cells (113).

In glioblastoma, NK1R signalling is critical for tumour cell viability and represents a potential therapeutic target (114). Inhibition of NK1R via *TACR1* gene silencing significantly reduces glioma cell proliferation in both GAMG and U-87 MG cell lines, with the latter showing greater sensitivity (114). Interestingly, Muñoz et al. (114) revealed full-length NK1R isoforms to predominantly reside in the nucleus, while truncated variants are enriched in the cytoplasm, suggesting isoform-specific roles in glioma biology. In contrast, silencing of TAC1 (encoding SP) has no effect on cell viability, indicating that glioma cell survival depends specifically on NK1R expression rather than its ligand (114). These findings position NK1R as a selective and functionally essential driver of glioma cell survival (114).

In liver cancers, NK1R exhibits distinct roles depending on tumour type (74). In hepatoblastoma, NK1R antagonism through aprepitant demonstrates significant anti-tumour effects as shown in Berger et al. (74). It was shown that hepatoblastoma cells predominantly express the truncated splice variant of NK1R, and targeting this receptor with antagonists like aprepitant, L-733,060, and L-732,138 led to dose-dependent growth inhibition and apoptosis (74). SP increased growth rates when added to hepatoblastoma cells and counteracted the anti-proliferative effects of NK1R antagonists (74). Importantly, oral administration of aprepitant (80 mg/kg/day) in HuH6 xenograft mouse models significantly reduced tumour growth, as evidenced by decreased tumour volume, weight, and alpha-fetoprotein serum levels (74). The treatment also inhibited in vivo angiogenesis, as shown by reduced vascularized area (74). Analysis of 17 human hepatoblastoma samples validated NK1R's relevance in a clinical context (74).

In non-small cell lung cancer (NSCLC), NK1R is significantly upregulated and associated with advanced clinical stages and poor prognosis (115). NK1R co-expresses and physically interacts with EGFR in tumour tissues, enabling it to transactivate EGFR phosphorylation and regulate ERK1/2 and Akt signalling (115). Activation of NK1R promotes cancer cell proliferation, colony formation, EMT, and migration, while its inhibition through aprepitant or genetic knockdown suppresses these malignant phenotypes both in vitro and in vivo (115). Notably, combining NK1R antagonists with EGFR tyrosine kinase inhibitors (gefitinib/osimertinib) produces synergistic anti-tumour effects, suggesting that targeting the NK1R-EGFR axis could overcome resistance to current EGFR-targeted therapies in NSCLC patients (115).

In summary, NK1R plays a context-specific yet consistently pro-tumorigenic role across a variety of malignancies. The receptor contributes to tumour growth across multiple cancers via distinct mechanisms. It drives proliferation and survival in glioblastoma, modulates Wnt and stemness pathways in colorectal cancer, promotes aggressive signalling in breast and lung cancers, and enhances tumour growth and angiogenesis in hepatoblastoma. These findings highlight NK1R as a versatile and promising therapeutic target.

1.2.4 NK1R Antagonists as Therapeutic Agents

The Neurokinin-1 Receptor (NK1R) antagonists, first approved for managing chemotherapy-induced nausea and vomiting, have shown potential as anti-cancer agents (116). Their ability to interfere with the SP/NK1R signalling pathway, which influences tumour growth and progression, has been demonstrated across several cancer types (116), as discussed above. The established safety profile of these drugs makes their investigation as cancer therapeutics particularly relevant (116) and therefore promote their use in the context of drug repurposing and patient stratification.

1.3 Goals and Objectives of this Study

Based on the evidence reviewed, this dissertation aims to investigate the role of the SP/NK1R complex in PDAC, with a particular emphasis on receptor isoform expression patterns and their potential utility for therapeutic stratification.

The primary goal of this research is to characterize the expression patterns of full-length and truncated NK1R isoforms in pancreatic cancer cell lines, and to correlate these patterns with clinical features and molecular subtypes of PDAC. Through detailed expression analysis at both mRNA and protein levels, I seek to establish the predominant isoform distribution across various models of pancreatic cancer and determine whether these patterns associate with specific tumour characteristics.

Building upon this characterization, I aim to examine the functional consequences of NK1R inhibition in PDAC models with varying levels of receptor isoform expression. This investigation will focus on determining how pharmacological inhibition of NK1R affects cell viability, cancer stem cell-like properties, and downstream signalling pathways, with particular attention to whether response patterns correlate with specific receptor isoform profiles. This functional analysis will

provide mechanistic insights into how the SP/NK1R complex contributes to PDAC progression and therapy resistance.

A critical component of this study involves analysing transcriptomic data from PDAC patient cohorts to identify potential molecular signatures associated with differential *TACR1* expression. Through computational approaches, my research will assess whether differential *TACR1* expression correlates with transcriptional signatures in PDAC, with the aim to identify molecular patterns that might allow for the classification of patients for personalised treatment approaches.

The combined investigation in this study could enhance to our understanding of the SP/NK1R pathway in pancreatic cancer. By examining NK1R variants, their responses to antagonists, and their expression patterns across different patient groups, I aim to uncover potential approaches for targeted treatment strategies. Ultimately, this research has the potential to identify patient subgroups that could respond to NK1R-targeted therapies, potentially opening new avenues for investigation in this challenging cancer type.

2. Material and Methods

2.1 List of Materials and Instruments

Table 1: Instruments

Instrument	Manufaturer
Autoclave	MMM Group, Planegg, Germany
Centrifuge for Cell Culture Rotina 420R	Hettich, Ebersberg, Germany
Centrifuge for Analysisl 5417R	Eppendorf, Hamburg, Germany
CO_2 Incubator	Binder GmbH, Tuttlingen, Gernany
ChemiDoc Imaging System	Bio-Rad Laboratories, California, USA
DNA/RNA work station	Uni Equip, Martinsried, Germany
FilterMax F3 Multi-Mode Microplate Reader	Molecular Devices, San Jose, CA, USA
Flow Cytometer LSRFortessa	BD Biosciences, Heidelberg, Germany
Fridges	Liebherr, Biberbach an der Riss, Germany
Laminar Flow	Heraeus, Thermo Scientific, Darmstadt, Germany
Liquid Nitrogen Tank	MVE Goch, Germany
Microscope AXI0	Carl Zeiss Microscopy GmbH, Oberkochen, Germany
NanoDrop ONE	Thermo Fisher Scientific, Darmstadt, Germany
Pipette Boy	Eppendorf, Hamburg, Germany
Pipette Boy Accu-jet pro	BRAND, Mannheim, Germany
Shaker, Incubating Mini	VWR, Avantor, Pennsylvania, USA
StepOnePlus Real-Time PCR System	Applied Biosystems, Thermo Fisher, Darmstadt, Germany
Thermomixer comfort	Eppendorf, Hamburg, Germany
Trans-Blot Turbo Transfer System	Bio-Rad Laboratories, California, USA
VersaMax Microplate Reader	Molecular Diagnostics, CA, USA
Vortex-Genie 2	Scientific Industries, New York, USA
Water bath	Memmert, Schwabach, Germany

Table 2: Disposables

Product	**Manufacturer**
6-well plate	Thermo Fisher Scientific, Darmstadt, Germany
96-well PCR plate	NUNC, Langenselbold, Germany
Adhesive Clear PCR Seal	Biozym Scientific GmbH, Oldendorf, Germany
Blotting Paper, Immun-Blot PVDF	Bio-Rad, California, USA
Cell culture flasks	Thermo Fisher Scientific, Darmstadt, Germany
Cell Scrapers	Greiner Bio-One, Kremsmünster, Austria
Gloves, Category III	SHIELD Scientific, Wageningen. The Netherlands
Plastic sterile pipettes	Greiner Bio-One, Frickenhausen, germany
Polystyrene test tubes	Falcon, Corning, Wiesbaden, Germany
Polyvinylidene difluoride membranes	Merck Group, Darmstadt, Germany
Safe-Lock Tubes 1,5 ml	Eppendorf, Hamburg, Germany
Sterile pipette tips	Eppendorf, Hamburg, Germany

Table 3: Chemicals and Reagents

Product	**Manufacturer**	**Cat. No.**
2-Mercaptoethanol	Aldrich Chemistry, Wisconsin, USA	M-7154
4x Laemmli Sample Buffer	Bio-Rad Laboratories, Hercules, California, USA	1610747
ab183713 Rb mAb to NK-1R	abcam, Cambride, UK	EPR6836(2)
Albumin Bovine Serum Solution	Sigma Life Sciences, USA	9048-46-8
Amphotericin B	PAN-Biotech, Aidenbach, Germany	P06-01050
Anti-rabbit Antibody	Cell Signalling Technology, Leiden, The Netherlands	7074
Apostat caspase detection kit	R&D Systems, Minneapolis, MN, USA	FMK012
Aprepitant	Tocris Bioscience, Bristol, UK	6486

Albumin Standard	Thermo Fisher, Rockford, USA	23209
B27	Gibco, Thermo Fisher, Darmstadt, Germany	17504044
Clarity Western ECL Substrate, Luminol	Bio-Rad Laboratories, Hercules, California, USA	1705060
Clarity Western ECL Substrate, Peroxide solution	Bio-Rad Laboratories, Hercules, California, USA	1705060
cOmplete ULTRA Tablets Mini EASY-pack	Roche, Mannheim, Germany	05 892 970 001
DAPI	Invitrogen, Carlsbad, CA, USA	D1306
DPBS	PAN Biotech, Aidenbach, Germany	P04-36500
DMEM	Gibco, Thermo Fisher, Darmstadt, Germany	41966-029
DMEM/F12	Gibco, Thermo Fisher, Darmstadt, Germany	11330-032
DMSO	Sigma-Aldrich, Karlsruhe, Germany	D2650
Ethanol 99%	AppliChem GmbH, Darmstadt, Germany	A8075, 2500PE
Ethidium bromide solution	Sigma, St Louis, MO, USA	E1510
FBS	Corning, Wiesbaden, Germany	35-079-CV
FITC Annexin V Apoptosis Detection Kit I	BD Biosciences, Heidelberg, Germany	556547
GAPDH Rabbit mAb	Cell Signalling Technology, Leiden, The Netherlands	2118
Glycerol 99%	Sigma, St Louis, MO, USA	G-5516
Human recombinant bFGF	Invitrogen, Carlsbad, CA, USA	13256-029
Human recombinant EGF	Invitrogen, Carlsbad, CA, USA	PHG0311L
Isopropanol	AV Liquid Production, GmbH, Flintsbach am Inn, Germany	0110005001
Methanol	Carl Roth, Karlsruhe, Germany	4627.4
Methylcellulose	Sigma-Aldrich, Taufkirchen, Germany	M0512
MTT	Invitrogen, Carlsbad, CA, USA	M6494
p44/42 MAPK Rabbit (ERK1/2) mAb	Cell Signalling Technology, Leiden, The Netherlands	4695

P-p44/42 MAPK Rabbit mAb	Cell Signalling Technology, Leiden, The Netherlands	4370
Penicillin/Streptomycin	PAN Biotech, Aidenbach, Germany	7980619
Piece BCA Protein Assay Reagent A	Thermo Fisher, Rockford, USA	23228
Pierce BCA Protein Assay Reagent B	Thermo Fisher, Rockford, USA	1859078
PhosSTOP EASYpack	Roche	04 906 837 001
Precision Plus Protein Dual Standards	Bio-Rad Laboratories, Hercules, California, USA	161-0363
QuantiTect Reverse Transcription Kit	QIAGEN, Hilden, Germany	205311
RIPA Lysis Buffer, 10X	EMD Millipore, Billerica, MA, USA	20-188
RNeasy Mini Kit	QIAGEN, Hilden, Germany	74104
RPMI 1640	Gibco, PAN-Biotech, Aidenbach, Germany	21875-034
SDS	VWR, Leuven, Belgium	83886.290
Substance P	Tocris Bioscience, Bristol, UK	1156
Substance P ELISA Kit	My BioSource, San Diego, CA, USA	MBS705162
Triton X-100	Merck, Darmstadt, Germany	106843
TRIzol Reagent	Ambion, Life Technologies, Carlsbad, CA, USA	15596018
Trypsin / EDTA	PAN Biotech, Aidenbach, Germany	P10-023100
Tween 20	Sigma, St Louis, MO, USA	P1379-100ML

Table 4: Software

Software and Version	**Manufacturer**
FACS Diva V.8.03	BD Biosciences
FlowJo 10.0	BD Biosciences
GraphPad Prism	GraphPad
StepOne 2.3	Applied Biosystems
SoftMax Pro 5	Molecular Devices, USA

2.2 Cell Culture for Cell Lines

For my research, I maintained eight established PDAC cell lines in two primary media types: RPMI 1640 medium supported BxPC-3, Capan-1, DanG, PSN-1, and AsPC-1 cell lines, while DMEM was used for HuP-T3, Panc-1, and MIA PaCa-2. Culture maintenance followed ATCC guidelines in their respective media obtained from Gibco®, Corning (Wiesbaden, Germany). Each medium was enriched with standardized additives, including fetal bovine serum at 10% concentration (Corning, Wiesbaden, Germany) alongside 1% streptomycin/penicillin antibiotic solution (PAN-Biotech, Aidenbach, Germany). Standard incubation parameters were maintained at 37°C under humidified conditions with 5% CO_2 atmosphere. To preserve cellular integrity, passage numbers were restricted to a maximum of 20 throughout all experimental procedures. For pancreatic stellate cell (PSC) cultivation, a distinct medium composition was employed. Gibco® DMEM/F-12 served as the foundation, enhanced with 10% FBS, 1% amphotericin B (PAN-Biotech, Aidenbach, Germany), and 1% streptomycin/penicillin. Standard PCR techniques were employed regularly to test for mycoplasma, with all cells confirmed negative for contamination. Cell authentication was performed externally by IDEX BioResearch located in Ludwigsburg, Germany.*

2.3 Production of Conditioned Media from Cultured PSCs

Conditioned media (CM) from pancreatic stellate cells was harvested after culturing primary PSCs at roughly 70% confluency for 24 hours. Prior to use, the collected CM was passed through a 0.4 µM membrane. The pancreatic cancer cell lines were subsequently grown in a mixture containing equal parts of their respective media and the filtered CM for the specified duration.*

2.4 Drugs

Aprepitant (NK1R antagonist) and substance P (NK1R agonist), both from Tocris Bioscience (Bristol, UK), were prepared as stock solutions in DMSO (50 mM) and distilled water (1 mM), respectively, with maintenance at −20°C.*

* This has been previously published by the author (1).

2.5 Viability Assay

Cellular viability assessment employed the 3-(4,5-Dimethylthiazol-2-yl)-2,5-Diphenyl-tetrazolium Bromide (MTT) colorimetric assay (Invitrogen, Carlsbad, CA, USA). Cells were seeded at 15,000 per well in 96-well plates (NUNC, Langenselbold, Germany) and allowed to adhere for 24 hours prior to treatment with varying aprepitant concentrations (5-50 µM) for an additional 24-hour period. For viability determination, MTT reagent (50 µL of 0.5 mg/mL solution prepared in 1X PBS; AppliChem, Darmstadt, Germany) was introduced to each well, followed by 30-minute incubation at 37°C. Following MTT solution removal, DMSO (50 µL; Sigma-Aldrich, Taufkirchen, Germany) was added to each well. Spectrophotometric measurements were performed at 570 nm with 670 nm background correction using a VersaMax Microplate Reader (Molecular Diagnostics, CA, USA).*

2.6 Sphere and Colony Formation Culture

Sphere cultivation methods followed previously published protocols (117). In brief, I prepared sphere formation medium (SFM) using Advanced DMEM/F-12 with 1% penicillin/streptomycin, further supplemented with 1% methylcellulose (Sigma-Aldrich, Taufkirchen, Germany). Essential growth factors were incorporated, comprising human recombinant βFGF (10 ng/mL), human recombinant EGF (20 ng/mL), and B27 serum-free supplement at 1X concentration (all sourced from Invitrogen, Carlsbad, CA, USA). After trypsinising and washing PDAC cells twice with DPBS, I seeded 500 cells per well in 96-well non-adherent plates (Corning, Wiesbaden, Germany) containing 100 µL SFM. Spheroid development occurred over a period of 10 to 14 days with bi-weekly medium replacement in designated treatments (20 µM aprepitant, 100 ng/mL substance P, or DMSO vehicle control) prior to counting.*

Colony formation analysis involved seeding 500 cells/well in standard 6-well plates. Following 24 hours of attachment, I began treatments with various concentrations of aprepitant (AP; 1 µM, 10 µM, 20 µM, and 40 µM) and substance P (SP) (20 nM SP), either individually or in combination. After 12 days, colony visualisation employed crystal violet staining (0.1% CV in 20% methanol) for 20 minutes, followed by overnight drying. Quantification was achieved through absorbance measurement at 570/670 nm using a spectrophotometric reader (Versa Max, Molecular Diagnostics, CA, USA).*

* This has been previously published by the author (1).

2.7 RNA Extraction and RT-qPCR

I performed RNA extraction utilizing the RNeasy Mini Kit (Qiagen, Hilden, Germany). Subsequently, cDNA synthesis was conducted with the QuantiTect Reverse Transcription Kit (Qiagen, Hilden, Germany) employing 1 µg of extracted RNA. cDNA generation was executed on an Eppendorf Mastercycler gradient.*

PCR amplification was implemented using the QuantiNova SYBR Green PCR Kit (Qiagen, Hilden, Germany). Quantitative PCR thermal cycling was performed on a StepOne Real-Time PCR System (Applied Biosystems, Carlsbad, CA, USA), comprising initial denaturation (95°C, 5 seconds), followed by 40 cycles of primer annealing and elongation (60°C, 10 seconds and 60°C, 60 seconds, respectively). Triplicate analyses were conducted for all experimental samples.*

I designed the primers using the NCBI Primer Blast Tool (118). The oligonucleotide primer sequences used are listed below.*

Table 5: List of Primers

TACR1-tr forward	5′-CAGGGGCCACAAGACCATCTA-3′
TACR1-tr reverse	5′-ATAAGTTAGCTGCAGTCCCCAC-3′;
TACR1-fl forward	5′-AACCCCATCATCTACTGCTGC-3′
TACR1-fl reverse	5′-ATTTCCAGCCCCTCATAGTCG-3′
TAC1 forward	5′-TCGTGGCCTTGGCAGTCTTT-3′
TAC1 reverse	5′-CTGGTCGCTGTCGTACCAGT-3′
GAPDH forward	5′-GTCTCCTCTGACTTCAACAGC-3′
GAPDH reverse	5'-ACCACCCTGTTGCTGTAGCCAA-3′
ZEB1 forward	5′-TTCACAGTGGAGAGAAGCCA-3′
ZEB1 reverse	5′-GCCTGGTGATGCTGAAAGAG-3′
CDH1 forward	5′-GAACGCATTGCCACATACAC-3′;
CDH1 reverse	5′-ATTCGGGCTTGTTGTCATTC-3′

All protocols followed manufacturer-provided guidelines. Primer functionality for truncated (tr) and full-length (fl) *TACR1*, as well as *TAC1* was validated in the hepatoblastoma cell line Hep G2. Hep G2 cDNA was sourced from Kolorz et al. (119).*

* This has been previously published by the author (1).

2.8 Western Blot Analysis

I conducted protein analysis on PDAC cell lines after double washing the cells with ice-cold PBS and extraction with lysis buffer containing protease and phosphatase inhibitors (Roche, Basel, Switzerland). Protein quantification employed the BCA Protein Assay kit from Thermo Fisher Scientific. Equal protein loading (25 µg per lane) was subjected to electrophoretic separation on 10% and 13% sodium dodecyl sulfate polyacrylamide gels (Bio-Rad Laboratories, Hercules, California, USA), followed by electrotransfer onto polyvinylidene difluoride membranes (Merck Group, Darmstadt, Germany). I performed membrane blocking using 5% BSA solution for 1 hour at ambient temperature and continued by overnight primary antibody incubation at 4°C. Triple TBST washing preceded 1-hour exposure to horseradish peroxidase-linked secondary antibodies at room temperature. Protein detection utilized enhanced chemiluminescent substrate (Bio-Rad Laboratories) with signal capture via ChemiDoc Imaging System (Bio-Rad Laboratories, Hercules, California, USA).

I used several antibodies in this study, including Rabbit p44/42 MAPK (Erk1/2) (1:1000 dilution), Rabbit Phospho-p44/42 MAPK (Erk1/2) (1:1000 dilution) from Cell Signaling Technology, Rabbit NK1R (1:1000) from Abcam, and Rabbit GAPDH (1:5000 dilution) from Santa Cruz Biotechnology. GAPDH served as the internal control for all membrane analyses.

2.9 Apoptosis Detection Assay

My apoptotic assessment employed flow cytometric analysis following cell seeding at 500,000/well in 6-well plates and attachment for 24 hours (37°C with 5% CO_2). AP and SP (both from Tocris Bioscience, Bristol, UK) were administered at the previously specified concentrations, followed by 24-hour incubation under standard conditions. Post-treatment, cells were examined microscopically for morphological alterations.*

I collected supernatants from each well into 5 mL designated round-bottom FACS tubes (Falcon, Corning, Wiesbaden, Germany). Cell harvesting involved DPBS washing with (1 mL; PAN-Biotech, Aidenbach, Germany), followed by gentle detachtment through addition of 300 µL accutase (Sigma-Aldrich, Taufkirchen, Germany) with 3-minute incubation at 37°C with 5% CO_2. Enzymatic activity was neutralized through administration of 1.5 mL medium containing 10% FBS (Falcon, Corning, Wiesbaden, Germany).*

* This has been previously published by the author (1).

I transferred the cell suspensions into the designated FACS tubes and pelleted via centrifugation (500 rpm, 5 minutes, Hettich Rotina 380R). Following resuspension in 1 mL DPBS and repeated centrifugation, I performed apoptotic staining at 37°C with 5% CO2 using 100 µL staining reagent (96 µL DPBS, 3 µL Annexin V, 1 µL propidium iodide) from the FITC Annexin V Apoptosis Detection Kit I (BD Biosciences, Heidelberg, Germany) for 15 minutes. I terminated staining by washing with 900 µL 1X ABB. I performed flow cytometric data acquisition using an LSRFortessa instrument (BD Biosciences, Heidelberg, Germany), with subsequent data processing via FlowJo software (BD Biosciences, version 10).*

2.10 Caspase Detection Assay

For caspase activity assessment employed 500,000 cells/well in 6-well culture plates, followed by 24 hours of attachment at 37°C under 5% CO_2 atmosphere. AP and SP treatments (both from Tocris Bioscience, Bristol, UK) were administered as specified. Prior to harvesting, I performed microscopic evaluation to assess cellular morphology.*

I collected supernatants from individual wells into polystyrene FACS tubes (5 mL, Falcon, Corning, Wiesbaden, Germany). Cell washing involved gentle DPBS application (1 mL/well, PAN-Biotech, Aidenbach, Germany) followed by enzymatic detachment through trypsin (500 µL, PAN-Biotech, Aidenbach, Germany) during a 3-minute incubation at 37°C with 5% CO_2. I halted trypsinisation by adding 1.5 mL complete medium supplemented with 10% FBS.*

I carefully transferred the cell suspensions to 5 mL polystyrene FACS tubes (Falcon, Corning, Wiesbaden, Germany) and subjected them to centrifugation (500 rpm for 5 minutes). Pellet resuspension in 1 mL DPBS preceded repeated centrifugation. For caspase staining, I employed a 30-minute incubation at 37°C with 5% CO_2 using 100 µL detection reagent (99 µL DPBS supplemented with 5% FBS and 1 µL FITC-VAD-FMK from Apostat intracellular caspase detection kit; R&D Systems, Minneapolis, MN, USA). Staining was terminated by DPBS washing (1 mL) and centrifugation. Final cell pellet resuspension in 1 mL DPBS enabled flow cytometric analysis, with data interpretation using FlowJo software (version 10, BD).*

* This has been previously published by the author (1).

2.11 Cell Cycle Analysis

For cell cycle analysis, I seeded 500,000 cells/well in a 6-well culture plates with 24-hour incubation (37°C, 5% CO_2). Afterwards, I applied AP and SP treatments at their previously described concentrations, followed by additional 24-hour incubation. Similarly to the protocols above, I harvested the individual supernatants into FACS tubes (Falcon, Corning, Wiesbaden, Germany) for further washing in 1 mL of DPBS. Cell detachment was achieved through trypsinisation (500 µL) and additional 3 min incubation at 37°C, 5% CO_2. Enzymatic activity was neutralised by addition of 1.5 mL complete medium containing 10% FBS. Following pellet resuspension in 1 mL DPBS and repeated centrifugation (500 rpm, 5 minutes), cellular fixation employed gradual 70% ice-cold ethanol addition. I enhanced the fixation efficacy through overnight incubation at 4°C. Ethanol removal involved centrifugation with subsequent repeated DPBS washing (1 mL).*

For nuclear staining I utilised 1 mL 4′,6-Diamidin-2-phenylindol, Dihydrochlorid (DAPI) solution (1 µg/mL DAPI (Invitrogen, Carlsbad, CA, USA) and 1% Triton X (Merck, Darmstadt, Germany) in DPBS) for 15 min in dark incubation. Afterwards, I performed flow cytometric analysis with data processing conducted using the software FlowJo v.10 by BD Biosciences (San Jose, CA, USA).*

2.12 ELISA

Substance P quantification employed conditioned medium collection from MIA Paca-2, Panc-1, DanG, and HuP-T3 cell lines following 24-hour cultivation periods. Analysis scope encompassed both cancer patient sera and control group samples. This study received approval from the ethics committee of the Ludwig-Maximilian-University (LMU) Munich, Germany (approval number 19-233).*

Sample preparation involved supernatant centrifugation at 4°C using 16,000 x g for 10 minutes. ELISA procedures utilized 100 µL test sample volumes applied to manufacturer-provided pre-coated plates, with subsequent protocol adherence following Substance P ELISA Kit guidelines (My BioSource, San Diego, CA, USA). Spectrophotometric detection occurred at 450 nm wavelength using a VersaMax instrument (Molecular Diagnostics, CA, USA). Assay sensitivity achieved a minimum detectable substance P threshold of 0.175 ng/mL.*

* This has been previously published by the author (1).

2.13 Analysis of RNA-Sequencing data

2.13.1 Data Selection Methodology

I applied a systematic selection process to identify suitable transcriptomic datasets for PDAC analysis. My search was conducted between May 2022 and April 2025. Due to inconsistent metadata standards across public repositories, strict quality criteria were established to ensure data reliability and comparability. Dataset identification was performed using specific search terms: "PDAC," "pancreas," "pancreatic cancer," and "pancreatic tumour". Datasets were required to: (1) contain explicitly labelled PDAC or pancreatic tissue samples; (2) originate from Homo sapiens; (3) utilize Illumina sequencing technology; (4) derive from non-genetically modified specimens without laboratory manipulations such as transfection or experimental treatments; and (5) include RNA sequencing data. Importantly, only datasets containing tissue samples were considered for analysis, while those derived from cell lines were excluded to ensure physiological relevance.

2.13.2 Selected Datasets

The following chapters allows insight into the metadata given for each included open source dataset.

2.13.2.1 PRJNA719796 Dataset

The first dataset (accession: PRJNA719796; GEO: GSE171485) comprises RNA-sequencing data from 6 PDAC specimens and 6 non-tumour adjacent tissues. These sequencing libraries were constructed from polyadenylated-RNA extracted from clinical specimens for the identification of novel oncogenes in PDAC. Sequencing was performed on the Illumina HiSeq 2000 platform. Following resection, tumour tissues underwent pathological examination before being placed in cryotubes with RNAlater reagent, frozen in liquid nitrogen, transported on dry ice, and stored at -80°C. Total RNA was isolated using RNeasy mini kit (Qiagen) following manufacturer's protocol. Sample quality and quantity were assessed using NanoDrop 2000 spectrophotometer and Agilent 2100 Bioanalyzer. The library construction utilized cDNA selection with a single-end read layout.

2.13.2.2 PRJNA1133919 Dataset

The second dataset (accession: PRJNA1133919; SRP523219) contains RNA-sequencing data from human PDAC samples aimed at detecting differentially expressed genes between low-perineural and high-perineural PDAC samples. This resource contains 10 SRA experiments. Sequencing was performed on the Illumina HiSeq 2000 platform using a library preparation method designated as "common method" in the metadata. The selection method employed PCR-based techniques, and the sequencing utilized a paired-end read layout.

2.13.3 Overview of selected Datasets

Table 6: Selected Datasets for Open Source Transcriptomic Analysis

Dataset ID	# of Samples	Sample Types	Sequencing Platform	Publication Year
PRJNA719796	12	6 PDAC, 6 adjacent non-tumour	Illumina HiSeq 2000	2021
PRJNA1133919	10	PDAC samples	Illumina HiSeq 2000	2024
Total	**22**			

2.13.4 RNA-seq Data Processing

The analysis of RNA sequencing (RNA-seq) data was conducted using the web-based platform, www.usegalaxy.eu (120,121). Raw sequencing reads were downloaded from the NCBI SRA server (122) using the "Faster Download and Extract Reads in FASTQ" tool (Galaxy Version 2.11.0+galaxy1).

To investigate molecular signatures associated with differential *TACR1* expression, I used the reference-based RNA-seq data analysis pipeline developed by Batut et al. (2018) for the Galaxy platform. This well-established workflow includes quality control, mapping, read counting, differential expression analysis, and functional annotation steps. This approach allowed for efficient utilization of existing data while avoiding redundant experimentation.

I assessed raw sequence data quality using “FastQC Read Quality reports” (Galaxy Version 0.74+galaxy1). The analysis was performed on both single-end and paired-end reads according to their respective sequencing layouts. FastQC anal-

ysis was performed using default parameters with minimal configuration. The appropriate read format (single-end or paired-end) was selected according to each dataset's specifications. All optional parameters were left unspecified. All standard FastQC modules were executed, including: Basic Statistics, Per Base Sequence Quality, Per Sequence Quality Scores, Per Base Sequence Content, Per Base GC Content, Per Sequence GC Content, Per Base N Content, Sequence Length Distribution, Sequence Duplication Levels, Overrepresented Sequences, and K-mer Content.

Following individual “FastQC” analysis, “MultiQC” (Galaxy Version 1.11+galaxy0) was employed to aggregate quality control reports across all samples, facilitating comparative assessment of sequence quality metrics across datasets.

For adapter and quality trimming, fastp (Galaxy version 0.23.2+galaxy0) was used rather than the trimming tools specified in the original protocol. This alternative was selected for its efficiency, as fastp combines adapter trimming, quality filtering, and base correction in a single tool (124). For human RNA-seq samples with limited metadata and varying library qualities, this approach seemed more appropriate, as it balances speed, robustness, and comprehensiveness. “fastp” was run in either single-end or paired-end mode, matching the layout of each dataset, with adapter trimming, quality filtering, length filtering, and overrepresented sequence analysis enabled using default settings. Adapter trimming was enabled with auto-detection of adapter sequences. Default quality filtering thresholds were maintained.

RNA-seq specific optimizations were implemented, including forced polyG tail trimming with the default minimum length of 10 bases to handle potential sequencing artifacts from Illumina platforms. Additionally, polyX tail trimming was enabled to remove homopolymer sequences, particularly polyA tails commonly found in mRNA-seq data. In this configuration, polyG trimming was performed first, followed by polyX trimming as per the tool's processing logic. Overrepresented sequence analysis was also enabled to identify potential contamination or biases.

Following read preprocessing with “fastp”, “MultiQC” was employed to aggregate quality control reports across all samples, facilitating comparative assessment of sequence quality metrics before proceeding to alignment.

Pre-processed reads were then aligned to the human reference genome using “RNA STAR” (Galaxy Version 2.7.8a+galaxy1). The human reference genome

GRCh38.p13 was used to create a temporary index, supplemented with gene model annotation from GENCODE v42 (in GTF format) to improve the accuracy of splice junction mapping.

Following the alignment data quality was manually evaluated using the Integrative Genomics Viewer (IGV). Specifically, read coverage for housekeeping genes and *TACR1* was visually inspected to confirm sufficient read depth and transcript representation before proceeding with downstream differential expression analysis.

Following alignment of RNA-seq reads to the reference genome, the strandedness configuration of the libraries was determined using the “Infer Experiment tool” (RSeQC Version 5.0.3+galaxy0). I performed this analysis to determine the strand orientation of the sequencing libraries used in all datasets. Gene quantification was generated using “featureCounts**”** (Galaxy Version 2.0.1+galaxy2).

2.13.5 Stratification and Differential Expression Analysis

Samples were stratified based on *TACR1* (ENSG00000115353.11) expression. Gene-specific counts were extracted with the “Search in textfiles tool” (Galaxy Version 9.5+galaxy0) and sorted in descending order using the “Sort” tool (Galaxy Version 9.5+galaxy0).

To divide samples into *TACR1*-low and *TACR1*-high groups, I employed an expression-gap stratification method. After calculating the dataset mean, multiple threshold distances were tested by adding and subtracting various percentages (±10%, ±20%, and ±25%) from the average expression value. The optimal threshold was selected based on the following key criteria: (1) maximizing sample size retention in both groups due to the very limited number of samples available for each dataset, (2) a minimum of three samples for each comparison group to ensure statistical power, and (3) generating a sufficient number of differentially expressed genes (DEGs) that yielded significant pathways in downstream GO and KEGG analyses. The ±25% threshold best satisfied these criteria throughout the datasets, with samples below the mean-25% classified as *TACR1*-low and samples above the mean+25% classified as *TACR1*-high.

Differential expression analysis was conducted using “DESeq2” (Galaxy Version 2.11.40.7+galaxy2) to compare count tables between the defined groups. Significant changes in gene expression were identified using an adjusted p-value threshold of $p<0.05$ and filtered with the "Filter" (Galaxy Version 1.1.1) method.

“DESeq2” includes integrated count normalization to account for differences in sequencing depth and library composition. Results were then annotated using the "Annotate DESeq2/DEXSeq output tables" (Galaxy Version 1.1.0) function.

To identify enriched biological functions, Gene Ontology (GO) analysis was performed using the "goseq" package (Galaxy Version 1.50.0+galaxy0), with Benjamini-Hochberg [FDR] (1995) applied for multiple hypothesis correction.

2.13.5.1 RNA-seq Differential Exon Usage Analysis

Differential exon usage analysis was performed using DEXSeq (Galaxy Version 1.48.0+galaxy0) within the Galaxy platform. The analysis consisted of three main steps: annotation preparation, exon abundance quantification, and statistical testing for differential exon usage.

The analysis began with preparing a DEXSeq-compatible annotation file using the “DEXSeq-Count” tool (Galaxy Version 1.48.0+galaxy0) in "Prepare annotation" mode. The GENCODE v42 annotation (gencode.v42.annotation.gtf) was used as the reference GTF file. During annotation preparation, the "Aggregate genes with exons" option was enabled, which merged genes sharing exons into aggregate genes. This flattening process transformed the standard GTF annotation into a DEXSeq-compatible format where overlapping exonic regions were split into non-overlapping counting bins, each uniquely assigned to a gene or aggregate gene.

For exon abundance quantification, RNA-seq reads aligned to the reference genome (BAM files generated by RNA STAR) were processed using the DEXSeq-Count tool in "Count reads" mode with the previously prepared flattened GTF annotation. The analysis was performed with paired-end sequencing data using a non-strand-specific library protocol. The alignments were position-sorted, and the default minimum alignment quality threshold was applied.

The count tables generated in the previous step were used as input for the DEXSeq statistical analysis tool. The analysis was configured with a primary experimental factor, with count files from the first condition assigned to factor level 1 and count files from the second condition assigned to factor level 2. DEXSeq utilizes a negative binomial generalized linear model to test for differential exon usage while accounting for biological variability. The statistical framework incorporates variance estimation across biological replicates, normalization for sequencing depth differences, and correction for multiple testing using the Benjamini-Hochberg procedure. Results were visualized through an HTML report, and an RDS file was generated to allow for detailed visualization of individual genes.

Exons with an adjusted p-value (FDR) below the specified threshold were considered as showing significant differential usage between conditions.

2.13.5.2 RNA-seq Differential Isoform Usage Analysis

Differential isoform usage analysis was performed using the Galaxy platform, following an adapted version of the Galaxy training protocol for differential isoform expression (125). The analysis consisted of transcript assembly, quantification, and isoform switch detection between two experimental conditions.

RNA-seq reads aligned to the reference genome using RNA STAR were processed through StringTie (version 2.2.3+galaxy0) for transcript assembly. The initial assembly was performed using GENCODE v42 annotation as a guide. Resulting transcripts from all samples were merged using StringTie merge (version 2.2.3+galaxy0) to create a unified reference transcriptome. GffCompare (version 0.12.6+galaxy0) was then used to assess the quality of the assembled transcriptome by comparing it to the reference annotation.

Transcript sequences were extracted using gffread (version 2.2.1.4+galaxy0) with the GRCh38.p13 reference genome. A second pass of StringTie was performed using the merged transcriptome as a reference to ensure consistent quantification across all samples, with output configured for Ballgown format.

Isoform switching analysis was conducted using IsoformSwitchAnalyzeR (Galaxy Version 1.20.0+galaxy5). The analysis was configured to include novel isoforms, with average read length specified as 50 base pairs. The "Fix StringTie annotation problem" option was enabled to correct annotation issues arising during transcript assembly. Significant isoform switches were identified using a threshold of $q < 0.05$ and a minimum difference in isoform fraction (dIF) of 0.1.

The functional consequences of identified isoform switches were predicted by analysing changes in protein domains, signal peptides, intrinsically disordered regions, and sensitivity to nonsense-mediated decay.

2.14 Statistical Methods

Data are shown as mean ± standard error of the mean (SEM). Statistical analyses were conducted using one-way ANOVA for multiple group comparisons and unpaired parametric *t*-tests for dual-group comparisons via GraphPad Prism biostatistics software (version 9.0.0, 86, San Diego, CA, USA). Significance levels are indicated as follows: *, $p \leq 0.05$; **, $p \leq 0.01$; ***, $p \leq 0.001$; ****, $p \leq 0.0001$.

3. Results

3.1 Divergent Expression Patterns of *TACR1* and *TAC1* in PDAC versus Normal Pancreatic Tissue

To assess SP/NK1R-complex significance in PDAC, I performed RT-qPCR-based expression profiling of associated genes. I conducted gene expression analysis across eight PDAC cell lines (Figure 5a), specifically targeting both NK1R variants (*TACR1*-tr and -fl) alongside *TAC1*. Additionally, I applied identical expression assessment protocols to primary stellate cells.*

I found that *TACR1*-fl expression remained undetectable across all RT-qPCR analyses, while *TACR1*-tr demonstrated variable expression patterns among pancreatic cancer cell lines. I noted expression absence in Capan-1 and HuP-T3, whereas I detected *TACR1*-tr in the remaining six PDAC lines and at minimal levels within PSCs. Relative to the hepatoblastoma positive control (Hep G2), I found that all examined PDAC cells exhibited significantly reduced *TACR1*-tr expression (p-value < 0.0001). *TAC1* expression variations did not achieve statistical significance; nevertheless, I confirmed SP-encoding gene presence in Panc-1, MIA PaCa-2, Hep G2, and PSCs, while remaining PDAC cell lines yielded negative detection results in my analysis (Figure 5a).*

In contrast to the RT-qPCR findings, SP quantification using ELISA demonstrated SP presence across all cell lines examined, with MIA PaCa-2 exhibiting the highest concentration (Figure 5b). This analysis was extended to human serum samples to compare SP levels between control subjects and PDAC patients. The investigation revealed reduced SP blood serum concentrations in PDAC patients relative to the control group, though this difference did not reach statistical significance (Figure 5c).*

* This has been previously published by the author (1).

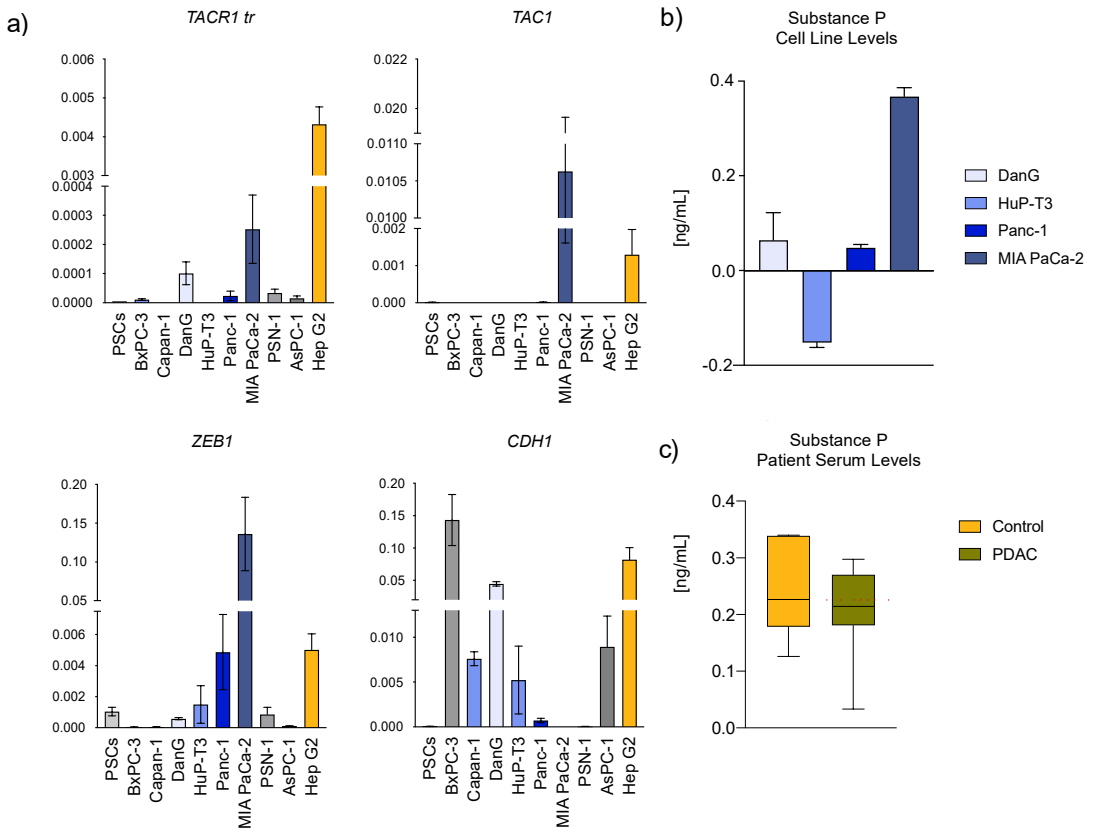

Figure 5: Characterization of SP/NK1R expression in pancreatic cancer models and clinical samples. (A) Quantitative assessment of transcript levels using RT-qPCR across multiple pancreatic cancer cell lines. Data are presented as ΔCt values with standard deviation (SD), demonstrating variable expression patterns of SP/NK1R pathway components among the examined cell lines. (B) Protein-level quantification of Substance P in conditioned media from cultured PDAC cell lines measured by enzyme-linked immunosorbent assay (ELISA), revealing distinct secretion profiles. (C) Comparative analysis of circulating Substance P concentrations in serum samples from healthy controls (n = 7) versus PDAC patients (n = 7), highlighting disease-associated alterations in this signalling peptide. Permission for print obtained from the publisher.*

To further validate the expression patterns of SP/NK1R complex-related genes, I analysed publicly accessible bioinformatic datasets. Comparative examination of PDAC datasets from Gene Expression Omnibus (GEO), the Cancer Genome Atlas (TCGA), and Cancer Cell Line Encyclopedia (CCLE) revealed that *TACR1* is significantly downregulated in tumour tissue compared to normal pancreatic cells (Figure 6a). However, it should be noted that these public databases lacked information distinguishing between the two receptor splice variants.*

* This has been previously published by the author (1).

GEO data analysis revealed interesting patterns of differential gene expression associated with tumour progression. Specifically, GSE microarray data indicated a trend toward decreasing total *TACR1* expression with advancing tumour stages, while *TAC1* expression showed an opposite trend, increasing with higher stages (Figure 6b). Survival analysis demonstrated that elevated *TACR1* expression significantly correlated with improved overall survival for PDAC patients (Figure 6c, accessed via OncoLnc.org).*

* This has been previously published by the author (1).

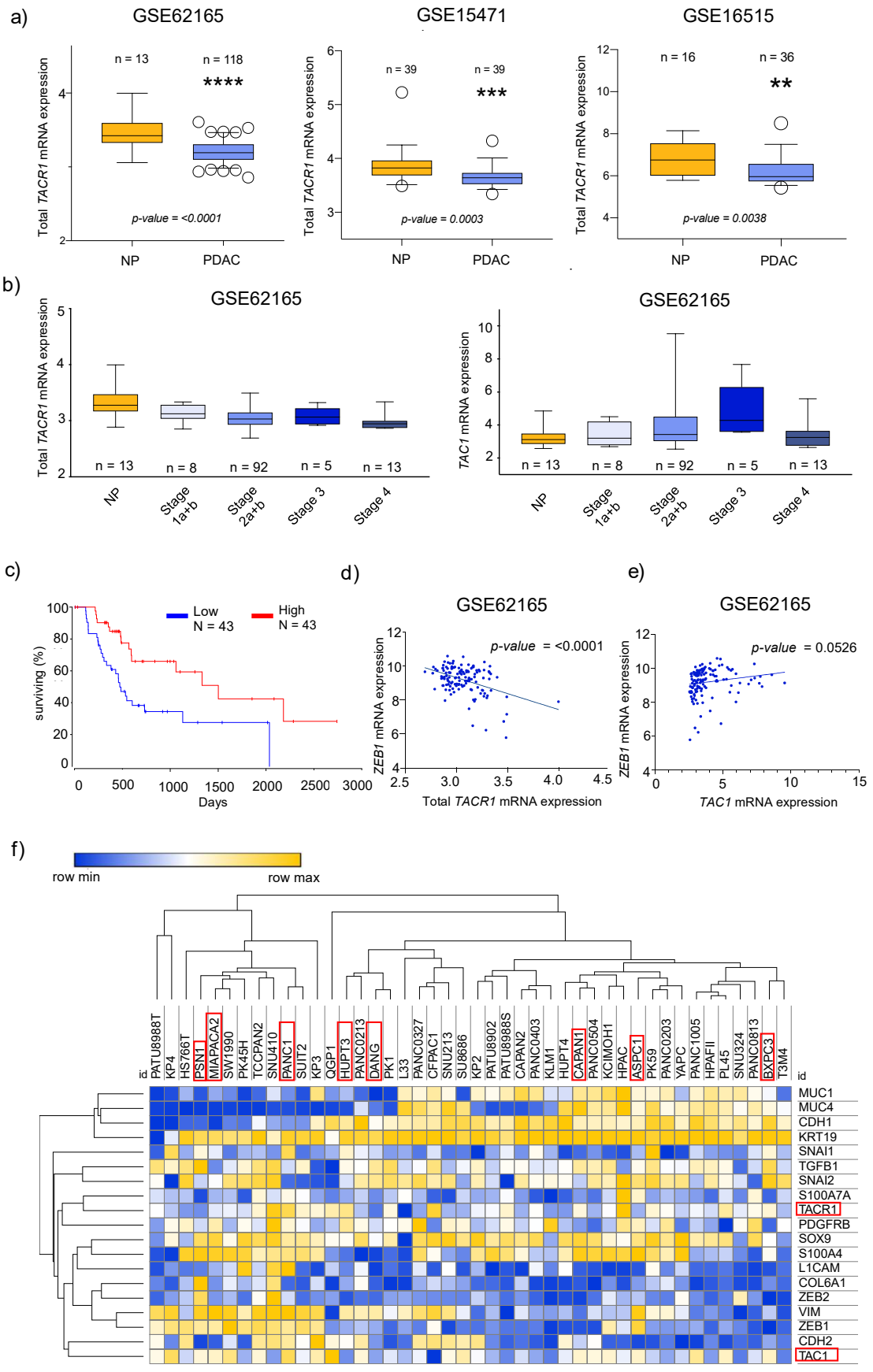
a)
GSE62165
GSE15471
GSE16515
Total TACR1 mRNA expression
n = 13
n = 118
****
p-value = <0.0001
NP
PDAC
n = 39
n = 39
***
p-value = 0.0003
n = 16
n = 36
**
p-value = 0.0038
b)
GSE62165
Total TACR1 mRNA expression
n = 13
n = 8
n = 92
n = 5
n = 13
NP
Stage 1a+b
Stage 2a+b
Stage 3
Stage 4
GSE62165
TAC1 mRNA expression
c)
Low
N = 43
High
N = 43
surviving (%)
Days
d)
GSE62165
p-value = <0.0001
ZEB1 mRNA expression
Total TACR1 mRNA expression
e)
GSE62165
p-value = 0.0526
ZEB1 mRNA expression
TAC1 mRNA expression
f)
row min
row max
PATU8988T
KP4
HS766T
PSN1
MIAPACA2
SW1990
PK45H
TCCPAN2
SNU410
PANC1
SUIT2
KP3
QGP1
HUPT3
PANC0213
DANG
PK1
L33
PANC0327
CFPAC1
SNU213
SU8686
KP2
PATU8902
PATU8988S
CAPAN2
PANC0403
KLM1
HUPT4
CAPAN1
PANC0504
KCIMOH1
HPAC
ASPC1
PK59
PANC0203
YAPC
PANC1005
HPAFII
PL45
SNU324
PANC0813
BXPC3
T3M4
id
MUC1
MUC4
CDH1
KRT19
SNAI1
TGFB1
SNAI2
S100A7A
TACR1
PDGFRB
SOX9
S100A4
L1CAM
COL6A1
ZEB2
VIM
ZEB1
CDH2
TAC1

Figure 6: Transcriptome-based characterization of the SP/NK1R pathway in PDAC. (A) Comparative analysis of multiple transcriptomic datasets demonstrated significantly reduced expression of *TACR1* mRNA in PDAC tissue compared to normal pancreatic (NP) tissue. Statistical significance was determined using unpaired Student's t-tests. (B) Analysis of stage-specific expression patterns from the indicated GEO dataset revealed differential expression of both *TACR1*-total and *TAC1* genes across progressive stages of pancreatic cancer. (C) Survival analysis using OncoLnc demonstrated prognostic relevance of *TACR1*-tr expression in PDAC patients. Patients were stratified by high (top 25%) versus low (bottom 25%) expression levels. (D) Correlation analysis identified a significant negative relationship between the epithelial-to-mesenchymal transition marker *ZEB1* and *TACR1* expression in the examined transcriptomic dataset (p-value determined by Pearson's Correlation). (E) Assessment of the relationship between *ZEB1* and *TAC1* expression within the indicated dataset revealed distinct correlation patterns. (F) Hierarchical clustering analysis of PDAC cell lines from the Cancer Cell Line Encyclopedia (CCLE) based on gene expression profiles (clustering method: one minus Pearson's Correlation). SP/NK1R pathway genes are highlighted in red, along with specifically marked cell lines selected for subsequent functional experiments. Permission for print obtained from the publisher.*

3.2 NK1R Isoform Distribution and ERK Pathway Activity in PDAC Cell Lines

To assess NK1R protein expression in PDAC, I performed Western blot analysis in six human pancreatic cancer cell lines (MIA PaCa-2, Panc-1, DanG, Capan-1, BxPC3, and AsPC1). Two distinct immunoreactive bands were detected in MIA PaCa-2, Panc-1, DanG, and Capan-1. The upper band was consistently observed at approximately 48 kDa, while a second, lower band appeared at approximately 36-40 kDa. In BxPC3 and AsPC1, only the upper band was present.

According to the manufacturer's data, only a single band was observed in their Western blot assays. However, since *TACR1* is known to exhibit tissue- and context-specific expression patterns, including differential isoform expression, depending on the cell type used by the manufacturer, the appearance of one band is likely, which also matches the observed results for BxPC3 and AsPC1 (Figure 7).

To confirm the appearance of the double bands, I calculated the theoretical molecular weights as follows, based on the average molecular weight of 110 Da per amino acid (126):

NK1R-fl: $407 \text{ amino acids} \times 110 \text{ Da} = 44{,}770 \text{ Da} \approx 45 \text{ kDa}$

NK1R-tr: $311 \text{ amino acids} \times 110 \text{ Da} = 34{,}210 \text{ Da} \approx 34 \text{ kDa}$

* This has been previously published by the author (1).

Taking post-translational modifications and gel migration behaviour into account, these isoforms are expected to appear at approximately 48 kDa according to the manufacturers instructions and 36-40 kDa on SDS-PAGE, respectively, which aligns with the observed results. Therefore, the higher molecular weight band corresponds to the full-length NK1R isoform (NK1R-fl), which consists of 407 amino acids. The lower band corresponds in size to the truncated NK1R isoform (NK1R-tr), which consists of 311 amino acids and lacks the C-terminal 96 residues. The presence of both bands confirms the co-expression of both isoforms at the protein level.

Interestingly, no treatment effects can be observed throughout all cell lines, suggesting that AP and SP treatments may affect NK1R signalling activity rather than total protein levels.

GAPDH was used as a loading control and showed uniform expression across all samples, confirming equal loading (with slight variation in Panc-1) and efficient transfer. Band patterns were consistent across biological replicates and treatment conditions. No additional bands, non-specific signals, or degradation products were observed. These results are shown in Figure 7.

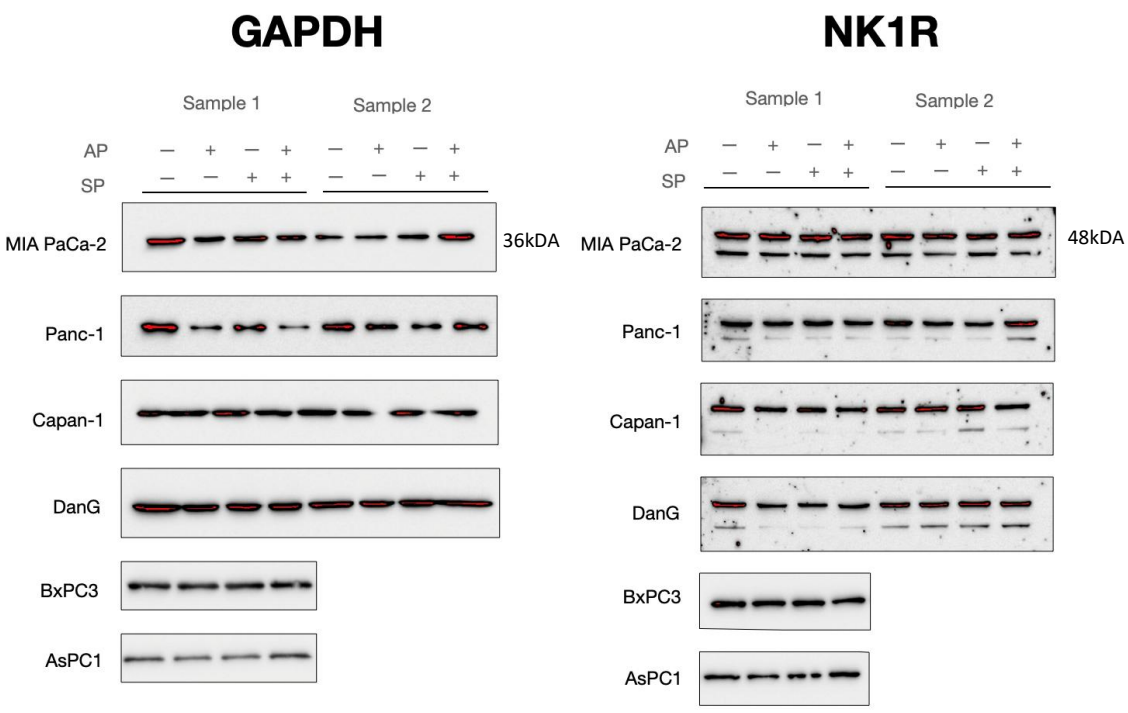

Figure 7: Expression of GAPDH and NK1R proteins in pancreatic cancer cell lines under AP and SP treatment conditions. Western blot analysis showing GAPDH (left panel) and NK1R (right panel) protein expression in six pancreatic cancer cell lines (MIA PaCa-2, Panc-1, Capan-1, DanG, BxPC3, and AsPC1) under various treatment conditions. Cells were treated with AP (+) or vehicle control (-) in combination with SP (+) or its control (-), with two independent experimental replicates (Sample 1 and Sample 2). GAPDH levels (left) demonstrate consistent protein loading across all samples and conditions, serving as a reference control for NK1R. NK1R protein expression (right) exhibits distinct double-band patterns in most cell lines, likely representing the full-length (upper band) and truncated (lower band) isoforms of the receptor. All six pancreatic cancer cell lines express detectable levels of NK1R, though with varying patterns and intensities across cell lines. MIA PaCa-2 cells show particularly strong NK1R expression, with both isoforms clearly visible. No consistent treatment-dependent changes in NK1R expression are observed across the cell lines.

To assess downstream signalling activity of NK1R in PDAC cell lines, I analysed total ERK1/2 and phosphorylated ERK1/2 (pERK1/2) protein levels by Western blot following treatment with aprepitant (AP), substance P (SP), or their combination. Total ERK1/2 expression remained stable across all cell lines and treatment conditions. In MIA PaCa-2, Panc-1, Capan-1, DanG, BxPC3, and AsPC1, no change in ERK1/2 band intensity was observed between control, AP-, SP-, or AP+SP-treated samples, indicating that ERK1/2 expression is not modulated by NK1R-targeted interventions.

In contrast, pERK1/2 levels varied in response to treatment in MIA PaCa-2 and Panc-1, where phosphorylation of ERK1/2 was detectable. In MIA PaCa-2,

pERK1/2 levels were strongly increased upon treatment with AP, especially for ERK2 (lower band). Co-treatment with SP did not display restorative effects.

I found a similar, though less pronounced, pattern in Panc-1 cells, where AP treatment led to a visible increase in pERK1/2 signal. These patterns were consistent across biological replicates, e.g. as displayed in both, Sample 1 and Sample 2. These results are shown in Figure 8. GAPDH was used as reference control, as these experiments were performed on the identical sample set (see Figure 7).

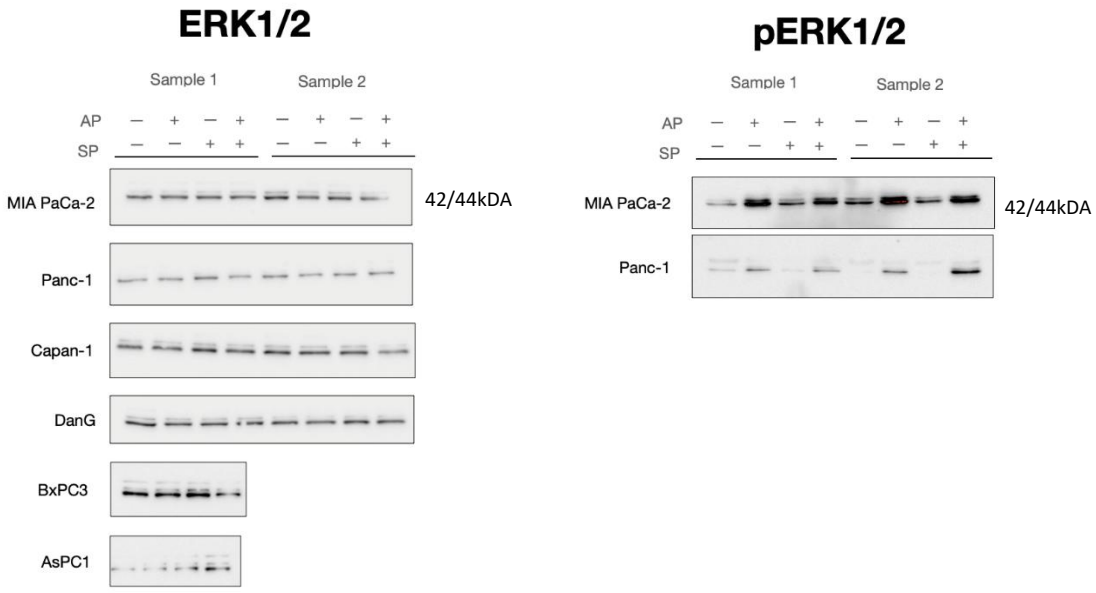

Figure 8: Comparative analysis of total ERK1/2 and phosphorylated ERK1/2 (pERK1/2) expression in pancreatic cancer cell lines. Western blot analyses depicting protein expression profiles under AP and SP treatment conditions. Left panel: Total ERK1/2 protein expression across six pancreatic cancer cell lines (MIA PaCa-2, Panc-1, Capan-1, DanG, BxPC3, and AsPC1) with BxPC3 and AsPC1 analysed in sample set 1. Right panel: Phosphorylation status of ERK1/2 (pERK1/2) in MIA PaCa-2 and Panc-1 cell lines under identical treatment conditions. Cells were exposed to AP (+/-) and SP (+/-) in all combinations across two independent experiments (Sample 1 and 2). While total ERK1/2 levels remain relatively consistent across conditions in all cell lines (left), the phosphorylation patterns (right) reveal distinct responses to treatment. Both, MIA PaCa-2 and Panc-1 cells exhibit pERK1/2 activation with AP treatment regardless of SP status, with MIA PaCa-2 demonstrating a stronger reaction. Notably, differential phosphorylation patterns are observed between ERK1 (44 kDa, upper band) and ERK2 (42 kDa, lower band), with the lower ERK2 band showing predominant phosphorylation in response to treatments, particularly in MIA PaCa-2 cells.

3.3 Correlations between EMT Status and SP/NK1R Pathway

Epithelial-mesenchymal plasticity (EMP) represents an alteration in tissue homeostasis that drives cellular transformation and promotes heterogeneity, a phenomenon especially pronounced in PDAC (127). As a driver for cancer progression and metastasis (128), I investigated whether there might be a correlation between *TACR1* expression and epithelial-to-mesenchymal transition (EMT) in PDAC. Recent experimental biological data and transcriptomic bioinformatical analyses have established a strong connection between elevated mesenchymal marker expression, particularly zinc finger E-box binding homeobox 1 (*ZEB1*), and poorer patient prognosis (129). Performing gene expression correlation analysis, I was able to identify a significant inverse relationship between *TACR1*-total and *ZEB1*, where high *ZEB1* expression corresponded with low *TACR1*-total levels (Figure 6d). Conversely, a positive correlation was observed between *ZEB1* and *TAC1* expression (Figure 6e).*

Gene clustering analyses demonstrated that *TACR1* and *TAC1* formed distinct groupings with different EMT markers. *TACR1* grouped with epithelial characteristic genes (including *S100A7A*, *SNAI2*, *KRT19*, *CDH1*), while *TAC1* associated with mesenchymal markers (such as *ZEB1*, *CDH2*, *VIM*, *ZEB2*), supporting the previously mentioned findings. For subsequent investigations representing PDAC's heterogeneous nature, PDAC cell lines (Capan-1, DanG, HuP-T3, Panc-1, and MIA PaCa-2) with varying EMT states and differing *TACR1* and *TAC1* gene expression profiles according to the CCLE database were selected (Figures 5a and 6f). Table 7 outlines relevant cell line characteristics, displaying the EMT classification of eight cell lines alongside a simplified gene expression categorisation system derived CCLE data (see also Figure 6f).*

* This has been previously published by the author (1).

Table 7: Transcriptional Profiling and Phenotypic Characterization of Pancreatic Cancer Models

PDAC Cell Line	EMT State	*TAC1*	*TACR1*
BxPC-3	epithelial	+	+
Capan-1	epithelial	+	+
DanG	epithelial	− −	− −
HuP-T3	epithelial/mesenchymal	− −	+ +
Panc-1	epithelial/mesenchymal	+ +	+ +
MIA PaCa-2	mesenchymal	+	−
PSN-1	mesenchymal	+	−
AsPC-1	mesenchymal	+	+

To validate EMT state and expression levels of EMT markers, I performed RT-qPCR using primers for *ZEB1* and epithelial cadherin-1 (*CDH1*), in addition to the previously mentioned primer sets. The expression patterns of EMT markers observed aligned with classifications reported in previous literature (130). Specifically, *CDH1* expression was significantly elevated in DanG compared to other PDAC cell lines, with no detectable expression in MIA PaCa-2 and PSN-1. *ZEB1* expression was detected in multiple cell lines (BxPC-3, AsPC-1, PSN-1, DanG, HuP-T3, Panc-1, Hep G2), with MIA PaCa-2 demonstrating significantly higher expression compared to all other cell lines (Figure 5a).*

3.4 Impact of Aprepitant on Growth of PDAC Cell Lines and Cancer Stem Cell-Like Subpopulations

The effects of NK1R-targeted therapy on PDAC cell growth were investigated by treatment with the NK1R antagonist AP, followed by determination of 50% inhibitory concentration using MTT cell viability assay. Hep G2 IC50 values from Kolorz et al. (119) served as positive control. AP exposure resulted in dose-dependent growth inhibition of PDAC cells over 24 hours. The observed sensitivity gradient to AP treatment (from lowest to highest) was: PSCs (32 µM), Panc-1 (30 µM), Capan-1 (30 µM), HuP-T3 (29 µM), DanG (26 µM), and MIA PaCa-2 (19 µM) (Figure 9a). A similar IC50 value for Capan-1 has been reported previously (27.4 µM) (131).*

* This has been previously published by the author (1).

Given that PSC-conditioned media is known to enhance pancreatic cancer cell metabolism and promote tumour cell proliferation and colony formation (132), IC50 values (MTT) were determined for both normal and PSC-conditioned media across all cell lines to exclude potential discrepancies from SP secretions in the immediate PDAC microenvironment represented by PSCs. Interestingly, cells cultured in PSC-conditioned media exhibited higher susceptibility to AP treatment (Figure 9b), though the difference between growth conditions was not statistically significant (unpaired *t*-test).*

Colony and spheroid formation assays, established *in vitro* surrogate techniques for identifying cells with stem-like characteristics (117,133,134), showed exceptional dose-dependent responses to AP treatment after 14 days of culture. SP presence partially attenuated these effects, particularly in co-treatments with higher AP concentrations, most notably in MIA PaCa-2. Consistently, MIA PaCa-2 demonstrated the highest sensitivity to AP treatment. I observed a profound and significant inhibition of colony and spheroid formation at 40 µM concentration across all cell lines ($p < 0.0001$). SP addition appeared beneficial exclusively for Panc-1 under CFA growth conditions ($p = 0.0005$), while AP effects were diminished by SP addition in SFAs with MIA PaCa-2. No significant difference was observed between control and SP-only treatment in SFA (Figure 9c).*

Beyond quantitative changes in colonies and spheroids, I also noticed morphological alterations following treatment. Figure 9d illustrates spheroids derived from DanG, MIA PaCa-2, and Panc-1, highlighting distinct phenotypic features including size, shape, and texture. Specifically, manipulation of the SP/NK1R system resulted in loss of tightly packed spheroid structure in all cases, with surface blebbing indicative of apoptosis initiation following antagonistic treatment (Figure 9d, right panels).*

In summary, dose-dependent decreases in PDAC cell viability were observed, manifested as reductions in sphere size and cell numbers, along with altered cell morphology following exposure to the NK1R antagonist AP.*

* This has been previously published by the author (1).

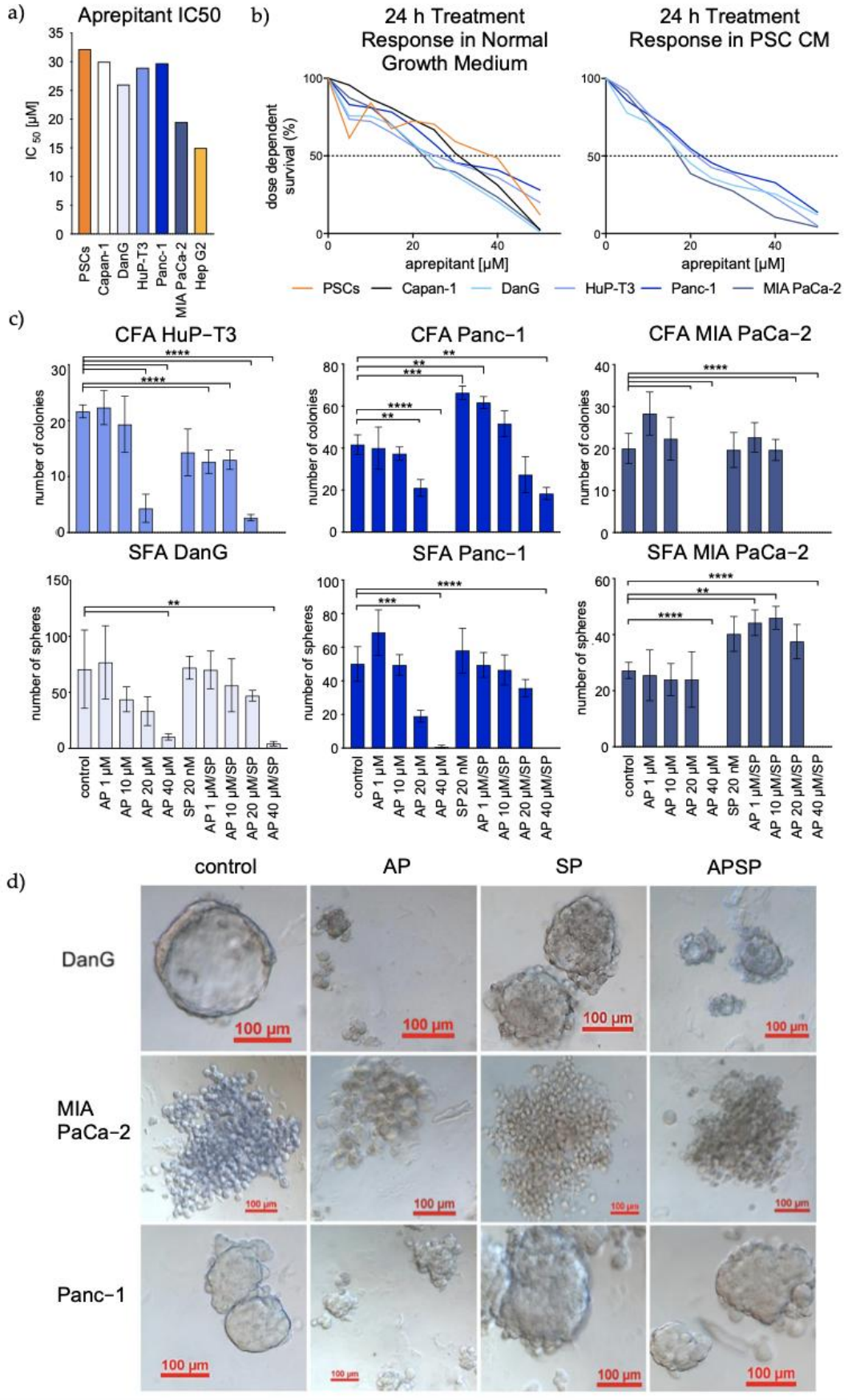
a)
Aprepitant IC50
IC 50 [µM]
PSCs
Capan-1
DanG
HuP-T3
Panc-1
MIA PaCa-2
Hep G2
b)
24 h Treatment Response in Normal Growth Medium
24 h Treatment Response in PSC CM
dose dependent survival (%)
aprepitant [µM]
PSCs
Capan-1
DanG
HuP-T3
Panc-1
MIA PaCa-2
c)
CFA HuP-T3
CFA Panc-1
CFA MIA PaCa-2
SFA DanG
SFA Panc-1
SFA MIA PaCa-2
number of colonies
number of spheres
control
AP 1 µM
AP 10 µM
AP 20 µM
AP 40 µM
SP 20 nM
AP 1 µM/SP
AP 10 µM/SP
AP 20 µM/SP
AP 40 µM/SP
d)
control
AP
SP
APSP
DanG
MIA PaCa-2
Panc-1
100 µm

Figure 9: Response to NK1R blockade in various pancreatic cancer model systems. (A) Half-maximal inhibitory concentration (IC50) values determined for selective NK1R antagonist treatment across a panel of PDAC cell lines, demonstrating differential sensitivity. (B) Dose-response curves illustrating PDAC cell viability following NK1R antagonist administration under standard culture conditions (left) compared to pancreatic stellate cell (PSC)-conditioned medium (right), highlighting microenvironment-dependent effects. (C) Quantitative assessment of clonogenic potential (upper) and three-dimensional growth capacity (lower) under various treatment regimens as indicated on the horizontal axis, showing dose-dependent inhibitory effects of NK1R blockade. (D) Representative images from sphere formation assays depicting morphological alterations in DanG (top row), MIA PaCa-2 (middle row), and Panc-1 (bottom row) spheroids following exposure to different treatment conditions, revealing cell line-specific responses to NK1R pathway modulation.*

3.5 Aprepitant-Mediated Modulation of Cell Cycle Progression in PDAC Cell Lines

To investigate the cellular mechanisms underlying the anti-proliferative effects of NK1R antagonism, I performed FITC Annexin V/PI staining to assess treatment-induced apoptosis rates (Figure 10a), while pan-caspase labelling was utilized to quantify caspase activity via flow cytometric analysis (Figure 10b). The analyses revealed no significant differences in apoptosis rates between treatment conditions across all PDAC cell lines examined. Furthermore, pan-caspase detection demonstrated only a minor leftward shift in MIA PaCa-2 cells, suggesting minimal caspase involvement in apoptosis induction under these conditions (Figure 10b).*

* This has been previously published by the author (1).

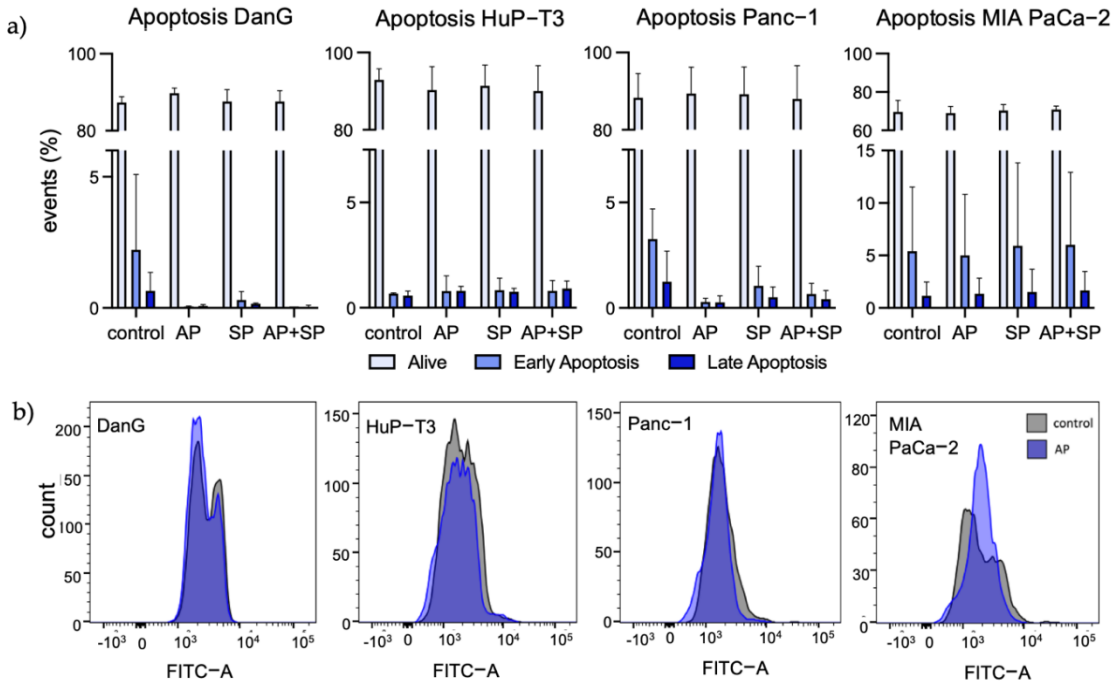

Figure 10: Assessment of apoptotic markers and caspase activity in PDAC cells under NK1R antagonist treatment. (A) Apoptosis analysis using dual-parameter flow cytometry with Annexin V-FITC and propidium iodide staining. Pancreatic cancer cells were subjected to vehicle control, NK1R antagonist (25 µM), or Substance P (20 nM) treatments. Quantitative analysis showed no statistically significant differences in Annexin V-positive populations across treatment conditions, suggesting limited classical apoptosis induction. (B) Intracellular caspase activity evaluation using the pan-caspase substrate FITC-VAD-FMK across multiple PDAC cell lines. Flow cytometric analysis revealed minimal leftward shifts in fluorescence intensity following NK1R antagonist exposure, indicating subtle, non-significant changes in caspase activation. Cell lines are arranged from epithelial (left) to mesenchymal (right) phenotypes, revealing potential EMT-associated differences in response patterns.*

Given these findings, I analysed cell cycle distribution using DAPI staining and flow cytometry to evaluate the effects of NK1R modulation on cell cycle progression. Flow cytometric analysis revealed pronounced aprepitant-induced alterations in G1 and S phase distributions in DanG, Panc-1, and MIA PaCa-2 cell lines compared to untreated controls. In contrast, Capan-1 and HuP-T3 cells, which lack expression of both truncated and full-length *TACR1* isoforms, exhibited no alterations in cell cycle distribution following aprepitant administration. Notably, substance P treatment did not induce cell cycle modulation in any of the examined cell lines. Representative histograms depicting aprepitant-induced changes in cell cycle progression are provided in the appendix (Appendix A).*

* This has been previously published by the author (1).

Collectively, these data demonstrate that pharmacological inhibition of NK1R in PDAC cells expressing the truncated TACR1 isoform results in substantial cell cycle arrest, primarily affecting G1 and S phases (Figure 11).*

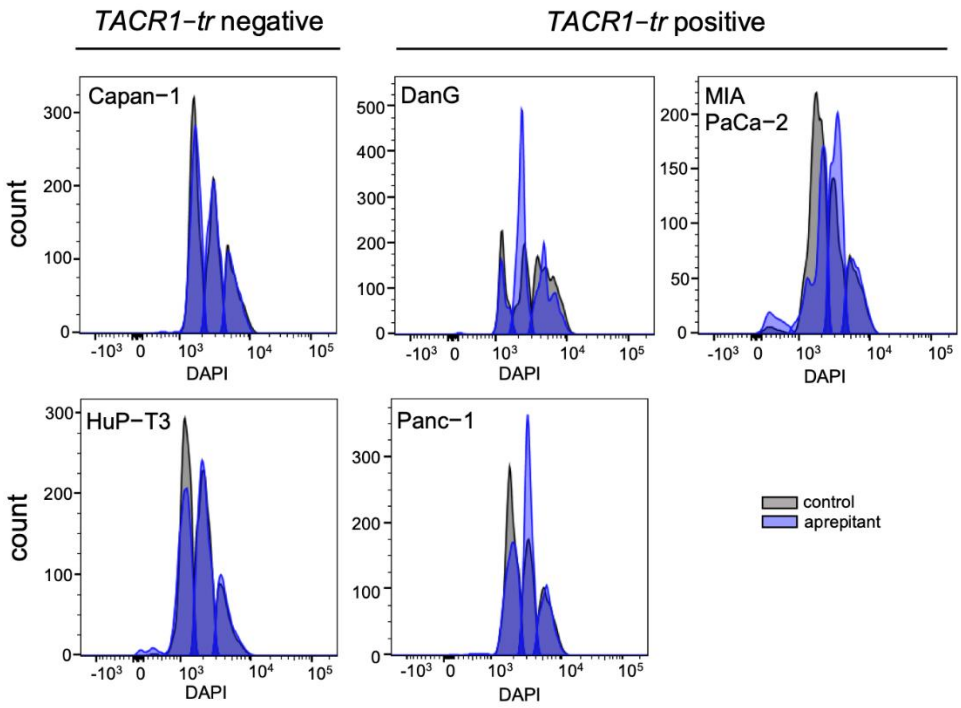

Figure 11: Differential cell cycle responses to NK1R pathway inhibition based on receptor expression status. (A) Representative DNA content analysis by flow cytometry using DAPI staining in control and NK1R antagonist-treated pancreatic cancer cells (10,000 events per condition). The left panels display *NK1R-tr* negative cell lines showing minimal alteration in cell cycle distribution following treatment with 25 µM NK1R antagonist. In contrast, right panels demonstrate *NK1R-tr* positive cell lines exhibiting pronounced shifts in cell cycle phase distribution upon identical treatment conditions. (B) Univariate histograms reveal receptor expression-dependent effects, where only *NK1R-tr* positive cells demonstrate significant redistribution across G0/G1, S, and G2/M phases following exposure to the NK1R antagonist (25 µM), while Substance P treatment (20 nM) shows distinct effects. Additional quantitative analyses of phase-specific changes are provided in Supplementary Data (Appendix A).*

* This has been previously published by the author (1).

3.6 Bioinformatic Exploration of *TACR1* Expression Patterns in PDAC

The observations described above suggested that *TACR1* expression might serve as a clinically relevant stratification factor in PDAC, as previously published (1). However, current public transcriptomic databases present a significant limitation by not distinguishing between the full-length and truncated isoforms of NK1R, despite substantial evidence indicating important functional and regulatory differences between these variants. This critical knowledge gap necessitated a more nuanced analytical approach. Therefore, I undertook a systematic bioinformatic investigation using raw RNA-seq data from publicly available datasets to directly assess *TACR1* isoform expression patterns. By accessing and reprocessing primary sequencing data from PRJNA719796 and PRJNA1133919, I aimed to distinguish between NK1R isoforms and characterize their expression profiles in pancreatic cancer. Furthermore, I employed DESeq2 differential expression analysis to compare transcriptional profiles between subjects with low versus high total *TACR1* expression within individual cohorts, stratifying samples based on a ±25% threshold from the mean expression value. This approach, described in more detail in the following, enabled me to identify molecular signatures and pathways specifically associated with *TACR1* expression levels, potentially revealing novel therapeutic vulnerabilities while addressing the isoform-specific roles that conventional databases fail to capture.

3.6.1 PRJNA719796 Dataset Analysis: Transcriptomic Profiling and *TACR1* Expression-Based Stratification in PDAC and Adjacent Tissue

3.6.1.1 Transcriptional Profiling of PDAC vs Adjacent Tissue

To establish a foundational understanding of PDAC-specific transcriptomic alterations within the PRJNA719796 dataset, I first compared tumour samples to their control group, adjacent non-malignant tissue, to identify core disease related patterns before introducing stratification by *TACR1.* This initial comparison also served to confirm the robustness of the separation between tumour and non-tumour tissue, as well as the within-group homogeneity, ensuring reliable foundation for subsequent stratification analysis.

Principal component analysis (PCA) of normalized gene expression profiles after differential gene expression analysis revealed a clear separation between PDAC and adjacent non-malignant tissue (control) samples. PCA identified multiple

principal components, of which the first two (PC1 and PC2) explained the largest proportion of variance, 53% and 13%, respectively, accounting for 66% of the total variance. PDAC samples formed a tight cluster on the left side of PC1 and were exclusively located within the positive PC2 range, indicating a relatively homogeneous transcriptomic signature among tumour samples. In contrast, control samples exhibited a broader spread along PC1, ranging from negative to positive values, but were consistently confined to negative PC2 values. This distinct separation along PC2 suggests that it captures disease-related transcriptional differences between tumour and non-tumour tissues.

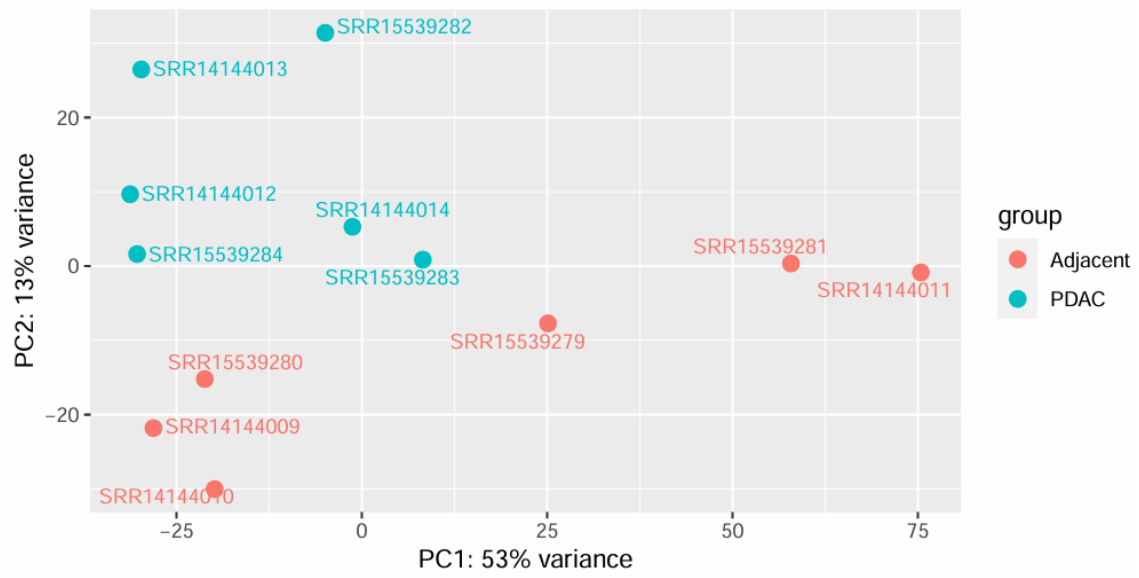

Figure 12: PCA of normalized gene expression data from PDAC and adjacent tissue samples. Each point represents one sample, coloured by group (PDAC: blue; Adjacent: red). PC1 and PC2 account for 53% and 13% of the total variance, respectively. PDAC samples cluster on the left side of PC1 and are exclusively located in the positive PC2 range. Adjacent samples span a wider range across PC1, from negative to positive values, but are all located in the negative PC2 space. The separation of samples along PC2 indicates a distinct transcriptomic signature between tumour and non-tumour tissues.

While PCA demonstrated clear separation of samples based on tissue type (PDAC vs. adjacent), the sample-to-sample distance matrix revealed a less distinct clustering pattern. Although some grouping by tissue origin was observed, overlap between PDAC and adjacent samples suggests inter-sample variability or shared transcriptional features that limit clear separation in hierarchical clustering (Figure 13).

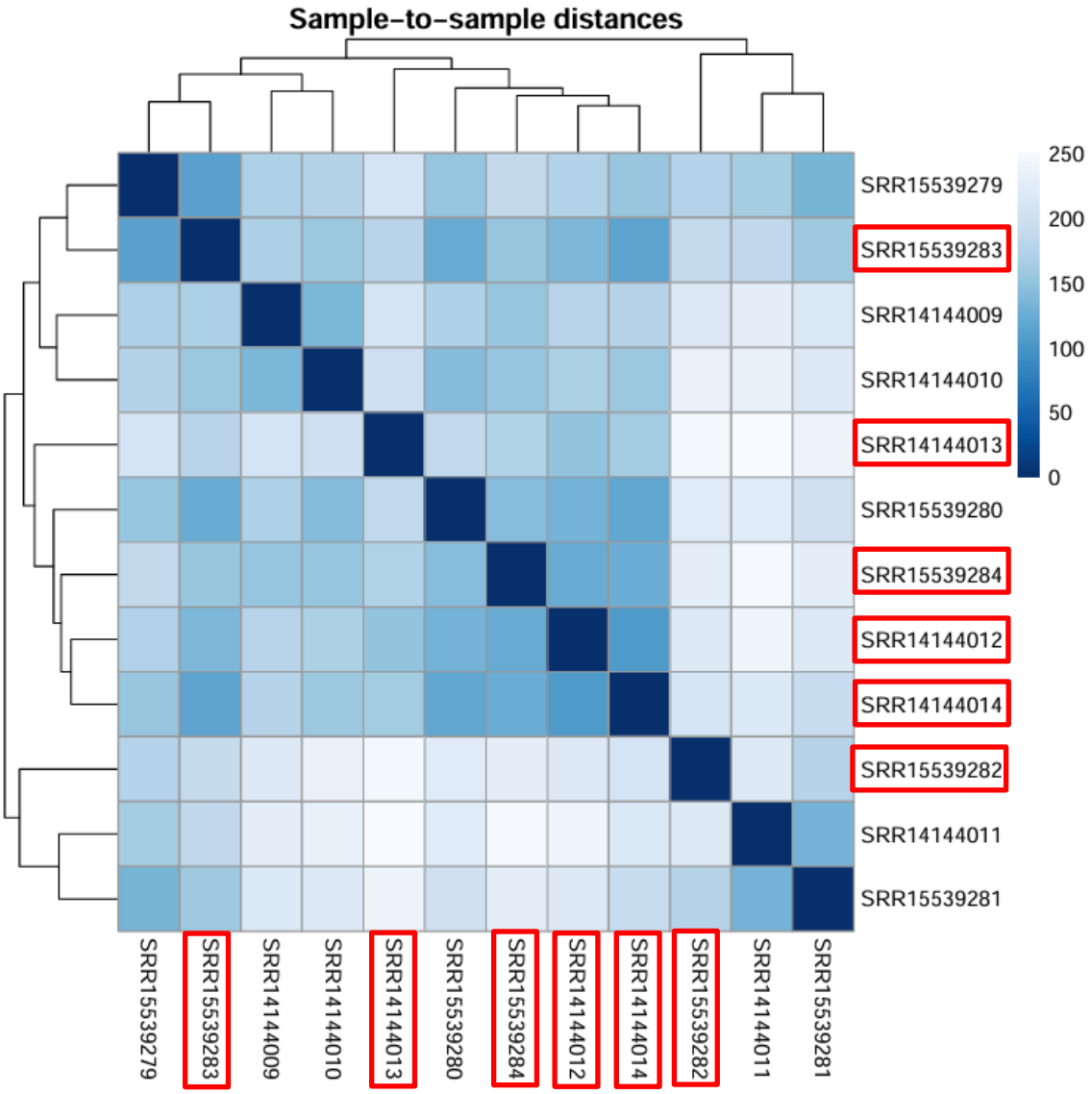

Figure 13: Sample-to-sample distance heatmap of transcriptomic profiles from the PRJNA719796 dataset. This hierarchical clustering visualization illustrates the pairwise distances between all samples in the dataset, with darker blue indicating greater similarity (smaller distance) and lighter blue representing greater dissimilarity (larger distance). The dendrogram at the top shows the hierarchical relationship between samples based on their transcriptional profiles. While some grouping patterns are evident, the clustering is less distinct than observed in the PCA plot, suggesting more complex relationships between samples beyond the primary tumour/normal distinction. The diagonal line of dark blue squares represents each sample's perfect correlation with itself. Three general clusters are observed: one including samples SRR15539279, SRR15539283, SRR14144009, and SRR14144010; another containing SRR14144013, SRR15539280, SRR15539284, SRR14144012, and SRR14144014; and a third cluster with SRR15539282, SRR14144011, and SRR15539281. Tumour samples are marked in red. While these clusters may reflect biological similarities, including potential tumour-adjacent sample pairings, no subject-level metadata were available to confirm such relationships.

Dispersion estimation analysis demonstrated the expected inverse relationship between gene expression level and biological variability. Initial gene-wise estimates (black) showed greater variability among lowly expressed genes, while final shrunken estimates (blue) closely followed the fitted trend (red), confirming appropriate variance modelling using DESeq2's empirical Bayes shrinkage approach (Figure 14).

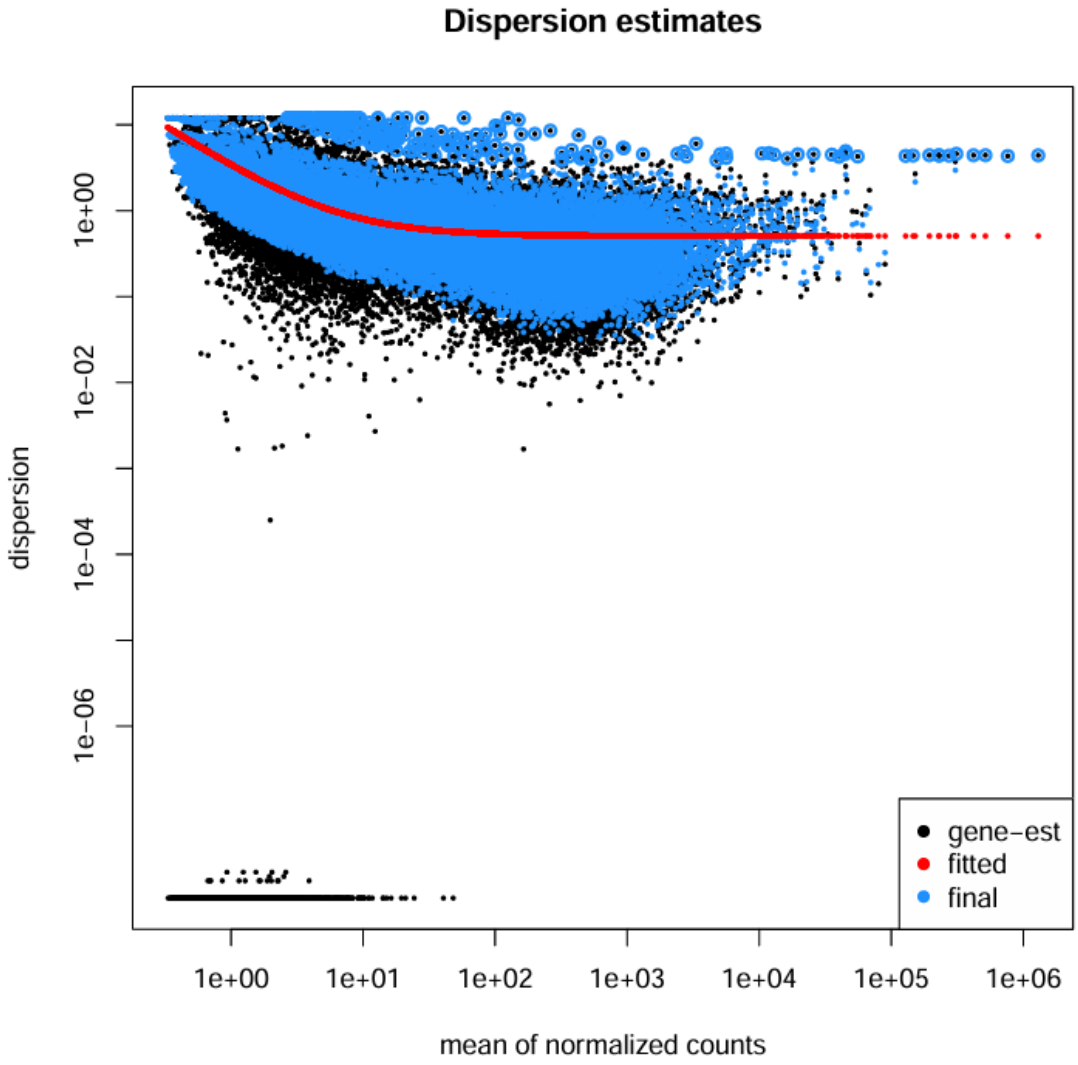

Figure 14: Dispersion estimates plot from DESeq2 analysis of the PRJNA719796 dataset. This plot illustrates the relationship between gene expression levels (x-axis, mean of normalized counts) and biological variability (y-axis, dispersion) on logarithmic scales. Black dots represent gene-wise dispersion estimates for individual genes, showing the typical pattern of higher variability among lowly expressed genes. The red curve shows the fitted trend line that captures the expected dispersion-mean relationship. Blue dots represent the final dispersion values after empirical Bayes shrinkage, which pulls the gene-wise estimates toward the fitted curve, particularly for genes with less information. This shrinkage approach improves the accuracy of differential

expression testing by borrowing information across genes. The plot demonstrates the expected inverse relationship between expression level and dispersion, confirming appropriate variance modelling in the DESeq2 analysis.

The MA plot visualizes $\log_2$ fold changes (PDAC vs. adjacent tissue) against the mean normalized expression for each gene. Significantly differentially expressed genes are highlighted in blue (padj < 0.05), while non-significant genes are shown in grey. The majority of significant genes exhibit positive fold changes, indicating increased expression in PDAC compared to adjacent tissue (Figure 15).

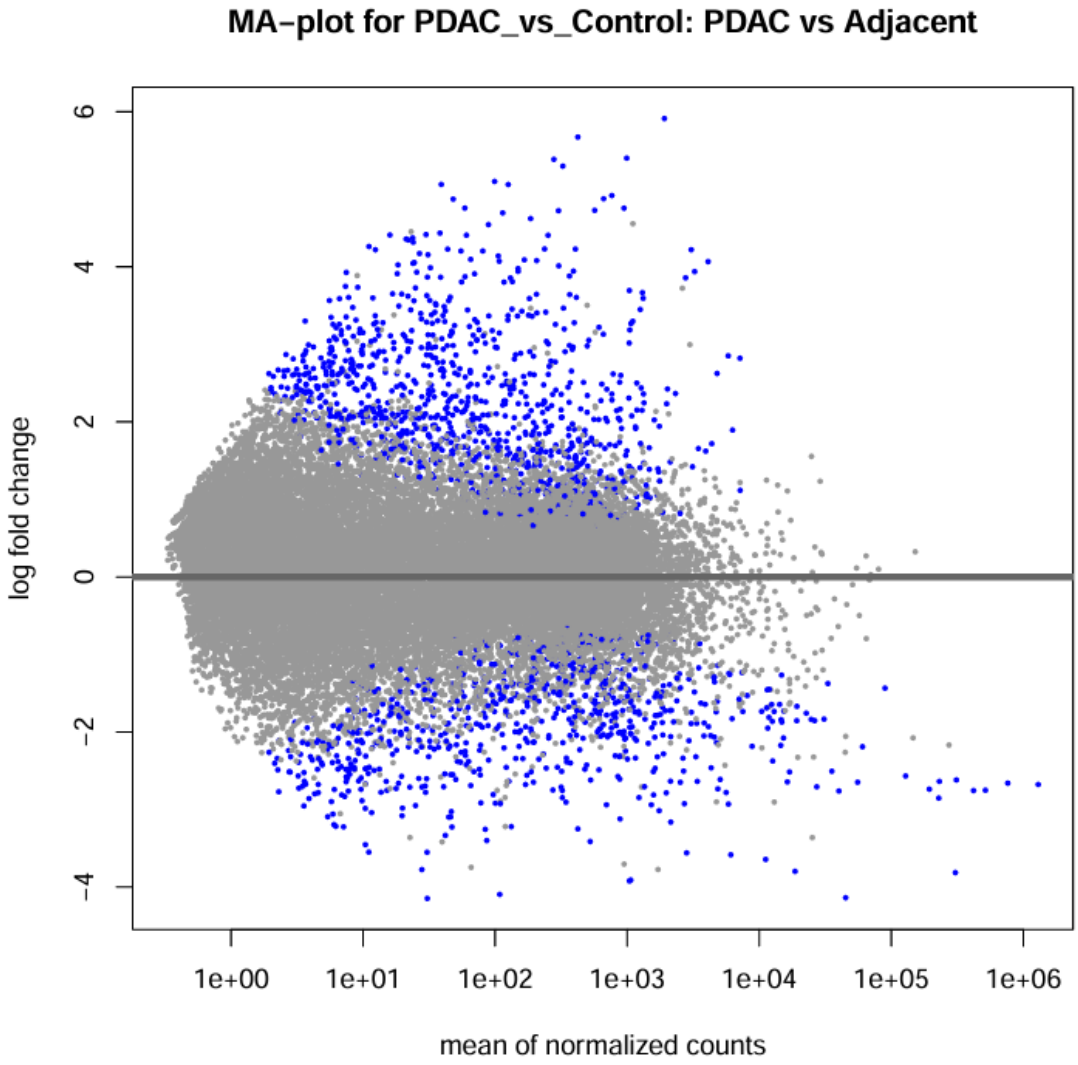

Figure 15: MA-plot showing differential gene expression between PDAC and adjacent normal tissue in the PRJNA719796 dataset. This plot visualizes the relationship between mean expression level (x-axis, mean of normalized counts on log scale) and fold change (y-axis, log2 fold change) for all genes analysed. Each point represents a gene, with significantly differentially expressed genes (adjusted p-value < 0.05) highlighted in blue, while non-significant genes are shown in grey. The horizontal line at y=0 represents no change in expression between conditions.

The plot shows a symmetric distribution of up- and down-regulated genes at lower expression levels, with more significantly upregulated genes (62.43%; positive log fold changes) at higher expression levels. This pattern indicates substantial transcriptional differences between PDAC and adjacent normal tissue, with many highly expressed genes showing increased expression in tumour samples relative to normal tissue.

A total of 978 genes were identified as significantly differentially expressed based on an adjusted p-value threshold of 0.05. *TACR1* is downregulated with a log2FC of -0.73, did however not show statistical significance (padj = 0.58). This negative trend matches the observation in other public data sets, as described in Figure 6a and 6b.

Among the top upregulated genes in PDAC compared to control tissue were *TNS4* (log2FC = 5.67; padj =2.12x10^{-7}), *SERPINB5* (log2FC = 4.70; padj = 3,43x10^{-5}), *COL17A1* (log2FC = 5.40; padj = 1,26x10^{-3}), and *MSLN* (log2FC = 5.91; padj = 1,83x10^{-3}). *TNS4* was previously identified to be overexpressed in pancreatic cancer and shown to act through promotion of colony formation in Panc-1 and PSN-1(135). *COL17A1* is known for its ability to regulate tumour growth in PDAC (136). Both genes, *COL171A* (136) and *MSLN*, a tumour-associated antigen (137), were shown as overexpressed in PDAC. Moreover, I found the six genes, *SERPINB5*, *TMPRSS4*, *CEACAM5*, *S100P*, *AHNAK2*, and *ECT2*, to also be significantly upregulated, which match the transcriptomic PDAC classifiers described by Bhasin et al. (138).

This diverse set of differentially expressed genes suggests substantial alterations in multiple cellular processes in the PDAC group with upregulation of known PDAC-associated markers and clear transcriptomic separation from the control group.

Gene Ontology enrichment analysis using GOseq revealed significant enrichment of biological processes related to cell cycle regulation and nuclear division in PDAC compared to adjacent tissue. The most significantly enriched GO terms included regulation of nuclear division (GO:0051783, p-adjust = 7.02E-08), regulation of mitotic nuclear division (GO:0007088, p-adjust = 7.02E-08), and nuclear division (GO:0000280, p-adjust = 8.73E-08). Additionally, the extracellular region (GO:0005576, p-adjust = 1.88E-07) was the most significantly enriched cellular component term. The data indicates that PDAC is characterized by dysregulation of cell cycle processes, particularly those related to mitosis and chromosome segregation, as well as alterations in extracellular components. These results are consistent with current high-throughput studies, that identified enrichment of

genes involved in mitosis, cell cycle control, and extracellular matrix remodelling in PDAC (139–141). Specifically, Long et al. (139) also identified cell cycle and mitosis pathways to be enriched in their GO and pathway enrichment analysis comparing PDAC to non-neoplastic pancreatic tissue samples. Similarly, Nwosu et al. (140) confirmed cell cycle pathways to be upregulated in 5 human PDAC datasets. Further confirmation is found in Lv et al. (141), which also show the upregulation of the extracellular region and its related pathways, such as extracellular space. The data suggest transcriptional reprogramming in pancreatic cancer tissue compared to adjacent non-tumour tissue, offering a basis for in-depth exploration of the molecular mechanisms involved in PDAC pathogenesis.

3.6.1.2 *TACR1* Expression-Based Stratification and Analysis

Next, I aimed to investigate whether the variation of *TACR1* expression could be associated with broader transcriptomic differences. Therefore, I stratified samples based on *TACR1* (ENSG00000115353.11) expression levels to explore potential downstream effects. Gene expression-based stratification is a very common method for subgroup generation in transcriptomic studies, including cancer (142–144). While many approaches rely on centroid-based classifications or clustering (144), these approaches were not suited to my study due to the limited sample size and the hypothesis-driven focus on a single gene of interest with its function in cancer.

Therefore, following the initial comparison described in 3.6.1.1, I calculated the dataset mean of the gene of interest, and divided samples into *TACR1*-low (below mean-25%) and *TACR1*-high (above mean+25%) groups. I selected this stratification approach after testing multiple threshold distances (±10%, ±20%, and ±25%), with the ±25% threshold best satisfying the criteria of maximizing sample retention while enabling downstream pathway analyses. Further details regarding this method are included in the methods section.

Interestingly, subsequent DESeq2 analysis comparing *TACR1*-high to *TACR1*-low PDAC samples showed that *TACR1* itself did not reach statistical significance in differential expression between these groups (log2 fold change = -0.906, adjusted p-value = 0.636), despite the initial stratification based on raw count values. The *TACR1* raw counts in the PDAC samples ranged from 2 to 61, showing substantial variability across the limited sample set (n=6). The non-significant differential expression result likely reflects a combination of factors including the small sample size, high biological variability in PDAC samples, normalization methods employed by DESeq2, and multiple testing correction. Therefore, the

TACR1-based stratification was maintained to explore whether transcriptomic or pathway-level differences might still emerge between these biological distinct expression groups.

The main focus of this research was to explore how different levels of *TACR1* expression affect PDAC transcriptional profiles. Hence, additional comparisons of *TACR1*-high vs. control tissue (in the following referred to as “control”), and *TACR1*-low vs. control were performed. This comparison strategy was chosen because DESeq2 clustering revealed stronger and more distinct sample grouping when comparing the stratified PDAC groups to the control group rather than directly to each other, as well as to the lack of statistical difference between *TACR1* low versus high expression values.

Comparing the DESeq2 results from *TACR1*-high vs. control and *TACR1*-low vs. control analyses revealed notable differences in the transcriptional profiles. The *TACR1*-high vs. control comparison yielded 1,787 significantly differentially expressed genes (adjusted p-value < 0.05, log2FC > 1), while the *TACR1*-low vs. control comparison identified only 290 differentially expressed genes using the same criteria. This substantial variation in the number of differentially expressed genes suggests that PDAC tumours with higher *TACR1* expression may exhibit more extensive transcriptional dysregulation compared to those with lower *TACR1* expression.

Analysis of shared and unique differentially expressed genes between these comparisons revealed a core set of genes that were consistently dysregulated in PDAC regardless of *TACR1* expression levels. However, within the set of shared genes, many genes showed stronger differential expression in the *TACR1*-high context. For instance, *TRIM29*, a biomarker for PDAC that mediates radioresistance (145,146), showed a log2FC of 5.13 (padj = 3.35×10^{-12}) in *TACR1*-high vs. control but 4.62 (padj = 2.04×10^{-15}) in *TACR1*-low vs. control. Similarly, *TNS4* (log2FC = 5.61 vs. 5.58), *COL17A1* (log2FC = 5.60 vs. 5.17), both mentioned above, demonstrated more pronounced upregulation in the *TACR1*-high condition. The stepwise increase in biomarker expression from *TACR1*-low to *TACR*-1 high samples suggests a potential link between *TACR1* expression and tumour progression, positioning *TACR1* not only as a stratification marker but also as possible indicator of disease severity. In summary, this pattern could suggest that higher *TACR1* expression may enhance or potentiate specific oncogenic pathways in PDAC. Additionally, this indicates that *TACR1*-high and *TACR1*-low PDAC samples may involve different regulatory mechanisms.

Further analysis identified a subset of 124 genes that were uniquely differentially expressed in *TACR1*-low vs. control comparison, but not in the *TACR1*-high vs. control dataset. Among the top unique genes in *TACR1*-low PDAC was the mesothelin precursor *MSLN* (log2FC = 6.43) (137) described above, as well as the *AQP5* (log2FC = 4.16), an aquaporin involved in cellular water transport and biomarker for PDAC associated with tumour stage (147). Other notable uniquely expressed genes in *TACR1*-low PDAC included *HTR1D* (log2FC = 4.36, padj = $1.05x10^{-5}$), which promotes pancreatic cancer via PI3K-AKT signalling pathway (148); and *CDC20* (log2FC = 3.90, padj = $1.05x10^{-5}$), a cell division cycle protein critical for mitotic progression and associated with PDAC differentiation (149). This distinct gene expression pattern in *TACR1*-low PDAC suggests that lower *TACR1* expression may be associated with activation of alternative oncogenic pathways compared to *TACR1*-high tumours.

Conversely, a much larger set of 1,621 genes were uniquely differentially expressed in *TACR1*-high vs. control but not in *TACR1*-low vs. control comparison. Among the most significantly upregulated genes unique to *TACR1*-high PDAC were *LINC02086* (log2FC = 5.59, padj = $6.54x10^{-11}$) a long non-coding RNA that inhibits ferroptosis in pancreatic cancer cells (150); *B3GNT6* (log2FC = 6.11), which is significantly associated with *KRAS* mutations in colorectal cancer (151), and stabilised by *IGF2BP2*, found to promote PDAC (152).

Moreover, *SLC6A14* (log2FC = 5.40, padj = $2.97x10^{-8}$), a basic amino acid transporter, which was previously identified as a drug target in PDAC (153), and *XIST* (log2FC = 4.77), a long non-coding RNA known to promote pancreatic cancer proliferation (154) and perineural invasion (155), were upregulated in this group. Furthermore, *CXCL5*, upregulated with a log2FC = 4.73 (padj 0 $5.63x10^{-6}$), has been described as a marker for poor prognosis and correlated with immune infiltration in PDAC (156).

Interestingly, the *TACR1*-high tumours also showed significant downregulation of several Y-chromosome genes including *UTY* (log2FC = -4.94, padj = $4.32x10^{-5}$) (157), *RPS4Y1* (log2FC = -5.01, padj = $5.50x10^{-5}$) (158), and *EIF1AY* (log2FC = -4.91, padj = $7.40x10^{-5}$) (159), among others, suggesting potential sex-specific differences in gene expression patterns. Unfortunately, the metadata from this study does not reveal gender specific information (160).

This extensive set of *TACR1*-high-specific genes highlights the more profound transcriptional reprogramming that occurs in PDAC with higher *TACR1* expression and points to distinct biological mechanisms differing from the *TACR1*-low group that may drive disease behaviour in these tumours.

3.6.1.3 *XIST* as a Marker of *TACR1*-High PDAC: Evidence for Aberrant X-Chromosome Inactivation Dynamics

Given that *XIST* (ENSG00000229807.13) was among the top differentially expressed genes, as described in chapter 3.6.1.2, I investigated its expression pattern in more detail, revealing striking differences.

XIST is a long non-coding RNA gene located in the X inactivation centre (XIC) that plays an essential role in X-chromosome inactivation in females, a process that transcriptionally silences one X chromosome to provide dosage equivalence between males and females (161). Raw count analysis demonstrated that *TACR1*-low PDAC samples exhibited minimal *XIST* expression (counts of 4, 23, and 1), while *TACR1*-high PDAC samples showed dramatically elevated expression levels (counts of 11881, 9898, and 5200). The control tissue samples displayed relatively low and variable *XIST* expression (counts of 81, 5, 15, 2, 128, and 49). The differential expression analysis identified *XIST* as significantly upregulated in *TACR1*-high vs. control comparison with a log2FC of 4.77. This extreme difference in *XIST* expression between *TACR1*-high and *TACR1*-low PDAC samples represents one of the most pronounced gene expression disparities observed between these stratified groups.

3.6.2 PRJNA1133919 Dataset Analysis: *TACR1* Expression-Based Stratification in PDAC Tumour Samples (male vs female)

3.6.2.1 Dataset Overview and Sex-Based Expression Patterns

To further investigate the role of *TACR1* expression PDAC, I analysed the PRJNA1133919 dataset, which contains exclusively PDAC tumour tissue samples. Unlike the PRJNA719796 dataset, this collection lacks adjacent non-malignant tissue, thus providing an opportunity to examine intra-tumoral gene expression patterns specifically. A notable advantage of this dataset is the availability of patient sex information in the metadata, which revealed a striking biological pattern, next to the higher number of PDAC samples available (n = 10).

Examination of *TACR1* expression levels by sex showed a remarkable distribution pattern (Table 8). Female samples exhibited substantially higher *TACR1* expression (range: 70-150 feature counts) compared to male samples (range: 0-138 feature counts, with most male samples showing very low expression). Specifically, after employing the identical subgrouping method described above, four out of five female samples clustered in the high expression group with *TACR1* feature counts of 70, 102, 120, and 150, while five out of six male samples showed minimal expression with feature counts of 0, 0, 0, 2, and 28, with only one male sample exhibiting high expression (138 feature counts).

Table 8: Sex distribution across all included samples in PRJNA1133919

Sex	Sample ID	Feature Counts
female	SRR30045792	150
male	SRR30045786	138
female	SRR30045794	120
female	SRR30045788	102
female	SRR30045790	70
male	SRR30045791	28 (Outlier)
male	SRR30045789	2
male	SRR30045787	0
male	SRR30045793	0
male	SRR30045795	0

During preprocessing, one sample (SRR30045791) with a *TACR1* feature count of 28 was identified as an outlier and excluded from further analysis. This sample exhibited moderate expression levels that would have clouded the clear differentiation between high and low expression cohorts. The decision to remove this outlier was made to maintain clear separation between the stratified groups, thereby enhancing the ability to detect distinct molecular signatures associated with different levels of *TACR1* expression.

3.6.2.2 Stratification Approach and Transcriptomic analysis of PDAC samples

After removing the outlier, the stratification resulted in the following sample groupings: *TACR1*-high group included SRR30045792 (female, 150 counts), SRR30045786 (male, 138 counts), SRR30045794 (female, 120 counts), and

SRR30045788 (female, 102 counts). The *TACR1*-low group consisted of SRR30045789 (male, 2 counts), SRR30045787 (male, 0 counts), SRR30045793 (male, 0 counts), and SRR30045795 (male, 0 counts) (see also Table 8).

The mean *TACR1* expression in the *TACR1*-low group was 0.5 (range: 0-2), compared to 127.5 (range: 102-150) in the *TACR1*-high group, representing a 255-fold difference. The stratification by *TACR1* expression level showed significant separation between those groups (log2FC = 6.36, padj = 9.32×10^{-8}), which was not achieved in the first dataset described above, as well as a strong correlation with patient sex. The *TACR1*-high group consisted of 3 female samples and 1 male sample, while the *TACR1*-low group was composed exclusively of 4 male samples.

As shown in Figure 16, PCA revealed distinct clustering of *TACR1*-high and *TACR1*-low samples. PC1 explained 56% of the variance and PC2 13%. Notably, samples segregated cleanly along PC2, with *TACR1*-low and *TACR1* high forming distinct clusters. Additionally, separation along PC1 can be observed, with two *TACR1*-low samples and one *TACR1*-sample clustering on the far right, while the remaining samples grouped predominantly on the left, including both other *TACR1*-low samples on the far left.

Figure 16: PCA of *TACR1*-high versus *TACR1*-low PDAC samples from the PRJNA1133919 dataset. This PCA plot illustrates the distribution of samples based on their global gene expression profiles. The first principal component (PC1) captures 56% of the overall variance, whereas the second principal component (PC2) explains 13% of the variance. *TACR1*-low samples (red points) are exclusively positioned in the upper portion of the plot with positive PC2 values, while *TACR1*-high samples (blue points) cluster exclusively in the lower portion with negative PC2 values. Each sample is labelled with its corresponding identifier (SRR number). This distribution pattern reveals that the sample stratification based on *TACR1* expression correlates more strongly with PC2 than PC1, suggesting that *TACR1* expression might be associated with specific transcriptional programs in PDAC that contribute to the second most important source of variation in the dataset.

Sample-to-sample distance analysis revealed similar patterns to the previously described dataset with less distinct clustering. MA-plot demonstrated the primarily upregulated genes as expected due to the comparison of High vs Low *TACR1* (Figure 17).

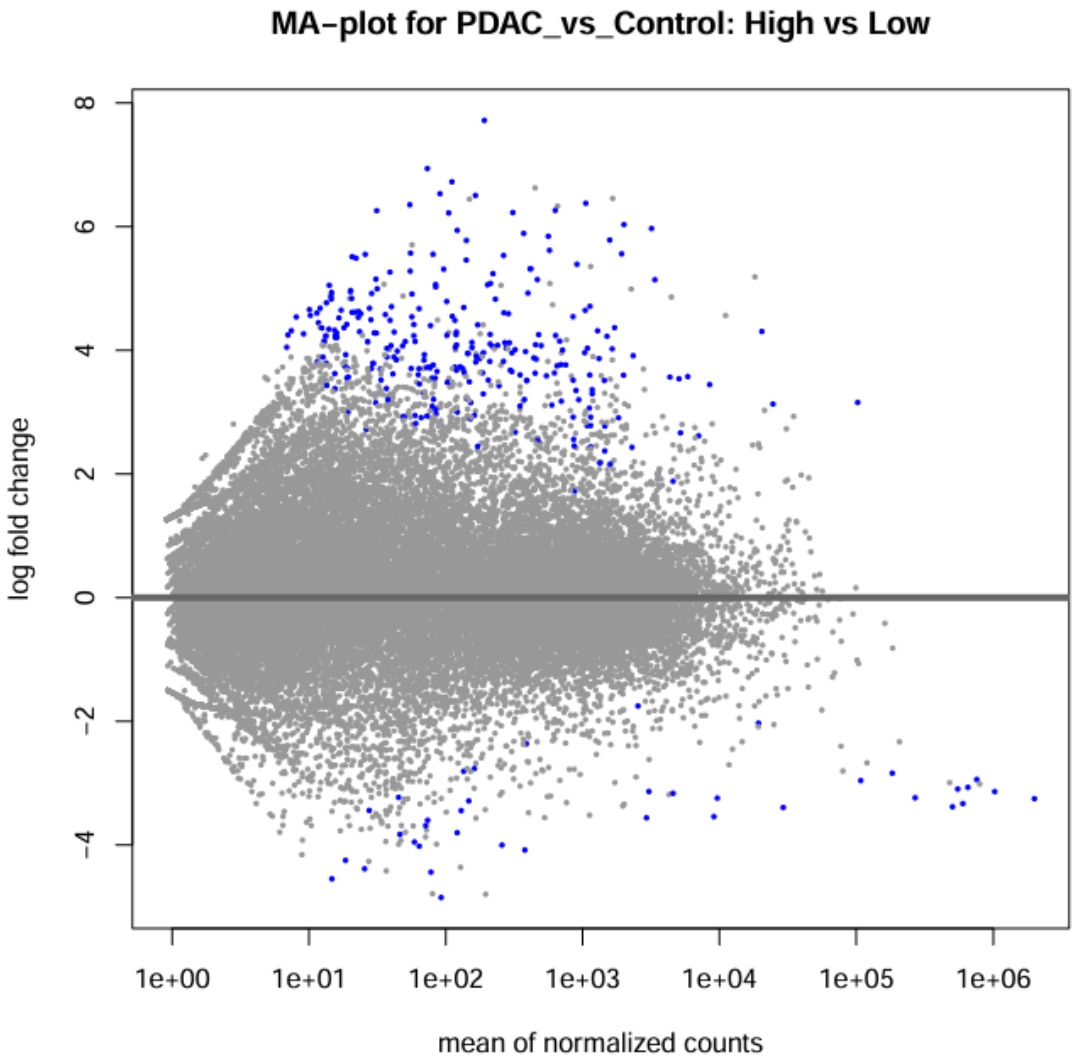

Figure 17: MA-plot comparing gene expression between *TACR1*-high and *TACR1*-low PDAC samples in the PRJNA1133919 dataset. This plot visualizes the relationship between mean expression level (x-axis, mean of normalized counts on log scale) and fold change (y-axis, log2 fold change) for all genes analysed. Each point represents a gene, with significantly differentially expressed genes (adjusted p-value < 0.05) highlighted in blue, while non-significant genes are shown in grey. The horizontal line at y=0 represents no change in expression between conditions. There is a notable asymmetry in the distribution of significant genes, with more upregulated genes (87.92% positive log fold changes) than downregulated genes, particularly at moderate expression levels. This pattern suggests that *TACR1*-high tumours are characterized by the activation of specific gene programs rather than general transcriptional amplification, revealing distinct molecular signatures associated with *TACR1* expression levels in PDAC.

3.6.2.4 Differential Gene Expression Analysis and Functional Enrichment Analysis

As mentioned previously, *TACR1* (ENSG00000115353.11) itself showed substantial differential expression with a log2 fold change of 6.36 (adjusted p-value = 9.32×10^{-8}), confirming the effective stratification of samples. The top 20 up- and downregulated genes are listed in Appendix B and C.

The top upregulated genes in the *TACR1*-high group are *IGKV1D-39, IGGL5*, and *CD79A*, all genes related to immunoglobulins, among others in the top differentiated genes (162–164), *SHISA8* (according to NCBI (2025)) *and CBLN1 (166)*, both predicted as players in regulation of neuronal synaptic plasticity, *GFRA1*, contributing to chemoresistance in osteosarcoma (167), and *ITIH5*, a metastasis suppressor gene in PDAC (168).

Gene Ontology (GO) enrichment analysis identified biological pathways and cellular components significantly associated with differentially expressed genes. In *TACR1*-high samples, significantly enriched GO terms included immunoglobulin complex (p-adj = 1.24e-11), adaptive immune response (p-adj = 4.66e-08), B cell activation (p-adj = 1.04e-05), antigen binding (p-adj = 1.54e-05), immunoglobulin production (p-adj = 3.08e-05), B cell proliferation (p-adj = 9.80e-04), external side of plasma membrane (p-adj = 2.02e-03), and signalling receptor activity (p-adj = 2.16e-03). These enriched terms confirm a strong B-cell-mediated immune signature in *TACR1*-high samples. The top ten enriched genes are shown in Figure 18.

In *TACR1*-low samples, significantly enriched GO terms included intracellular membrane-bounded organelle (padj = 1.10×10^{-2}), nucleus (padj = 1.00×10^{-3}), intracellular organelle (padj = 8.43×10^{-4}), and intracellular anatomical structure (padj = 1.43e-06).

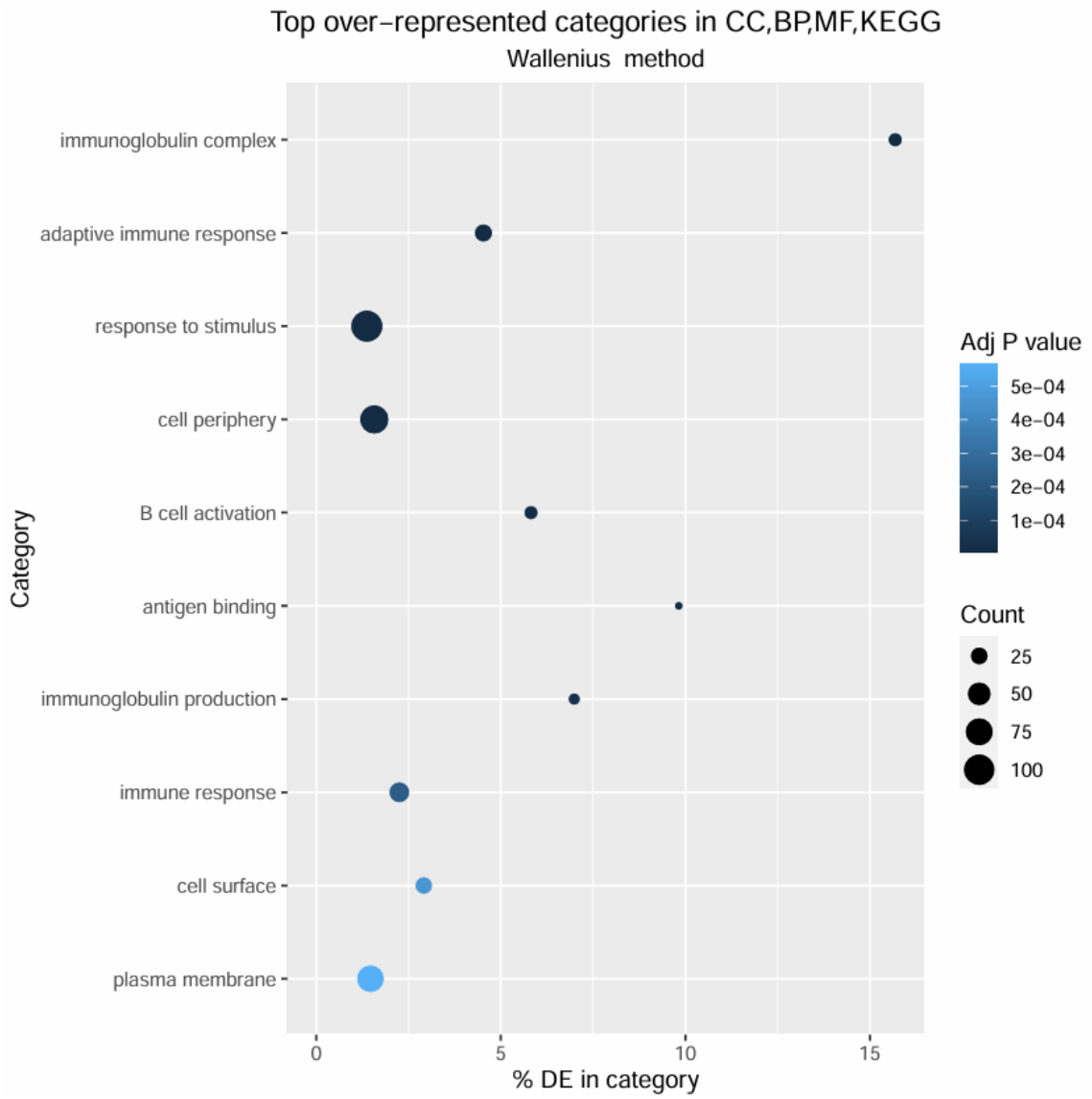

Figure 18:. Gene Ontology enrichment analysis of differentially expressed genes in *TACR1*-high versus *TACR1*-low PDAC samples from the PRJNA1133919 dataset. This dot plot shows the top over-represented functional categories identified through Gene Ontology (GO), Biological Process (BP), Molecular Function (MF), and KEGG pathway analysis using the Wallenius method. The x-axis represents the percentage of differentially expressed genes in each category, while the y-axis lists the functional categories. The size of each dot corresponds to the count of differentially expressed genes in that category, and the colour intensity (darker blue) indicates higher statistical significance (lower adjusted p-value). Notably, immune-related pathways are prominently enriched, including immunoglobulin complex, adaptive immune response, B cell activation, and immunoglobulin production. Other significant functional categories include response to stimulus, cell periphery, and plasma membrane, suggesting that *TACR1* expression levels are associated with distinct immune response profiles and cell surface signalling mechanisms in PDAC.

3.6.2.5 *XIST* Expression Analysis and Sex-Specific Transcriptomic Patterns

Given the strong correlation between *TACR1* expression and patient sex, additional analyses were performed to investigate sex-specific gene expression patterns. In the analysis of the PRJNA719796 dataset, *XIST* (a long non-coding RNA involved in X-chromosome inactivation in females) showed dramatically elevated expression in *TACR1*-high samples compared to *TACR1*-low samples.

To explore whether this finding was consistent in the current dataset and directly attributable to sex differences, a follow-up differential expression analysis was conducted using only female samples in the *TACR1*-high group compared against the *TACR1*-low group (which consisted entirely of male samples). The results showed that *XIST* (ENSG00000229807.13) exhibited a positive log2 fold change of 1.66, indicating higher expression in female *TACR1*-high samples than in male *TACR1*-low samples, a trend that is consistent with the results of the other dataset. However, this difference did not reach statistical significance (p-value = 0.184, adjusted p-value = 0.954).

3.6.3 NK1R Expression Patterns Across PDAC Transcriptomes

To investigate whether distinct *TACR1* isoforms contribute to expression differences, alternative splicing analysis was conducted on the *TACR1* gene utilizing two independent computational methodologies: DEXSeq and IsoformSwitchAnalyzeR. Both analytical approaches were attempted on two PDAC datasets with different experimental designs. For PRJNA719796 (n=12), analysis focused on comparing PDAC tissue samples (n=6) versus adjacent non-tumor tissue (n=6). With the limited number of PDAC samples available, I decided to refrain from direct *TACR1* low vs high comparison in this dataset. For PRJNA1133919 (n=10), all samples were PDAC tissues stratified into *TACR1*-high and *TACR1*-low expression groups based on the 25% deviation threshold from mean expression values.

DEXSeq analysis was successfully completed for both datasets and revealed no statistically significant differential exon usage patterns for *TACR1* (adjusted p-value threshold: 0.05) in any comparison group. Analysis of the PRJNA719796 transcriptomic dataset revealed the exon usage patterns of *TACR1* between PDAC and adjacent normal pancreatic tissue. Examination across exons E001-E009 showed a subtle reduction in expression of exon E001 in PDAC samples compared to adjacent normal tissue (Figure 19). E001 distinguishes between the full-length and truncated isoforms. This modest difference, though not reaching

statistical significance, potentially indicates a slight decrease in full-length *TACR1* (NK1R-fl) expression in tumour tissue. However, the overall exon usage patterns remained largely comparable between tumour and normal samples across the gene body. Visualization of aligned reads via IGV confirmed adequate coverage across *TACR1* exons, validating that the non-significant findings from DEXSeq analysis were not attributable to insufficient sequencing depth.

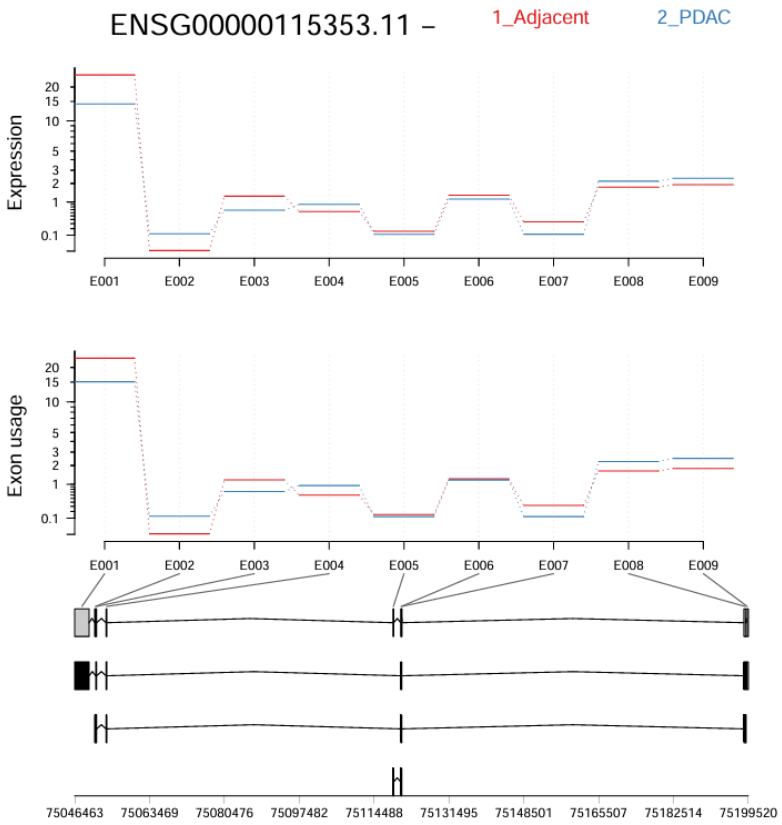

Figure 19: DEXSeq analysis of *TACR1* (ENSG00000115353.11) exon usage in PDAC versus adjacent normal tissue from the PRJNA719796 dataset. This visualization shows differential exon usage patterns across the nine exons (E001-E009) of the *TACR1* gene. The top panel displays expression levels (y-axis, log scale) for each exon in adjacent normal tissue (red line, 1_Adjacent) and PDAC samples (blue line, 2_PDAC). The middle panel shows the normalized exon usage values. The bottom panel illustrates the gene structure with various transcript isoforms. Exon E001 shows slightly higher expression in adjacent normal tissue compared to PDAC samples, though this difference does not reach statistical significance. This subtle reduction in E001 usage in tumor tissue might suggest a potential shift toward relatively greater expression of the truncated NK1R isoform in PDAC, as E001 is specific to the full-length receptor variant. However, the overall exon usage patterns remain largely similar between tumor and normal samples across the gene body, indicating no statistically significant differential splicing of *TACR1* between these tissue types.

IsoformSwitcher analysis failed to complete execution for both datasets, generating an error during the initiation of the splicing analysis step: "Error in txtProgressBar(min = 1, max = numberOfGenes, style = 3): must have 'max' > 'min'". This technical error suggests that the algorithm could not properly establish a progress tracking parameter, likely due to insufficient number of genes meeting the tool's internal filtering criteria.

4. Discussion

4.1 Downregulation and Isoform-Specific Expression of *TACR1* in PDAC

4.1.1 Transcriptomic Evidence for *TACR1* Downregulation in PDAC

My transcriptomic analyses consistently revealed downregulation of *TACR1* in PDAC tissue compared to normal pancreatic tissue across multiple datasets, including TCGA, GSE62165, GSE15471, and GSE16515. Additionally, in the PRJNA719796 dataset, *TACR1* showed a negative trend in differential expression, although it did not reach statistical significance. GEO microarray data further demonstrated a stage-dependent decline in *TACR1* expression, with lower expression levels observed in more advanced tumour stages. Conversely, expression of the neuropeptide-encoding gene *TAC1* increased with tumour stage. These findings were reinforced by survival analysis, which revealed that higher *TACR1* expression was significantly associated with improved overall survival in PDAC patients. Collectively, these observations suggest that *TACR1* expression is reduced in PDAC tissue and progressively decreases during tumour development, highlighting its potential as a biomarker for tumour progression and patient prognosis. The contradicting trend previously published by Friess at al. (53) is discussed in chapter 4.9.

4.1.2 Predominance of Truncated NK1R Isoform in PDAC Cell Lines

My thorough examination of *TACR1* isoform expression patterns in PDAC shows a complex picture with important consequences for understanding tumour development and designing targeted treatments. The analysis of multiple PDAC cell lines demonstrated predominant expression of the truncated NK1R isoform (NK1R-tr) over the full-length variant (NK1R-fl) at the transcriptional level, while protein-level analysis revealed a more nuanced picture with both isoforms detectable in several cell lines. This finding aligns with previous studies reporting tissue-specific isoform distribution, where NK1R-fl predominates in neuronal tissues while NK1R-tr is more prevalent in peripheral tissues and certain cancer types (74,77,109).

Taken together, these findings suggest that the expression of NK1R isoforms, particularly the balance between NK1R-fl and NK1R-tr, may not simply reflect

tumour burden but rather represent a dynamic regulatory mechanism during PDAC progression.

4.1.3 Technical Limitation in Computational Analysis of *TACR1* Alternative Splicing

The absence of statistically significant alternative splicing events in *TACR1* via DEXSeq analysis across both datasets, coupled with the inability of IsoformSwitchAnalyzeR to successfully execute, requires critical evaluation of multiple technical and biological factors, particularly in light of the subtle exon usage differences observed.

While DEXSeq analysis did not identify statistically significant differential exon usage, the subtle reduction in exon E001 expression in PDAC samples compared to adjacent normal tissue is particularly noteworthy. This region differentiates the full-length (NK1R-fl) from the truncated (NK1R-tr) *TACR1* isoforms, which indicates a possible trend toward higher relative expression of the shortened variant in PDAC. Though this difference did not reach statistical significance, it represents a biologically plausible pattern that warrants further investigation.

The execution failure of IsoformSwitchAnalyzeR provides additional context. The specific error message indicated a parameter configuration issue where the maximum progress value was not greater than the minimum, a condition typically arising when the software cannot identify eligible genes for splicing analysis after its initial filtering steps. This suggests that while subtle differences may exist, they may not meet the tool's threshold criteria for formal isoform switching events.

Technical limitations of the utilized datasets represent primary considerations. Despite implementation of rigorous quality control protocols, the inherent constraints of publicly sourced RNA-sequencing data include potential variability in specimen processing, RNA preservation methods, and library construction protocols. The sequencing depth provided by the platforms used in both datasets may be suboptimal for detection of low-abundance isoforms, particularly for genes with moderate expression profiles such as *TACR1*.

Statistical power constraints likely contributed significantly to my inability to achieve statistical significance for the observed exon E001 differences. The PRJNA719796 dataset's restricted sample size (6 PDAC, 6 non-tumour adjacent tissues) and PRJNA1133919's limited cohort (10 PDAC samples) were further diminished after expression-based stratification, potentially precluding detection of subtle splicing alterations. These limitations have special significance for alternative splicing analyses, as they generally require larger sample sizes compared

to differential expression studies to identify statistically meaningful changes. A larger sample size would likely provide the necessary statistical power to determine whether the observed exon E001 usage pattern represents a genuine biological phenomenon.

From a biological standpoint, the minor variation in exon E001 usage corresponds with existing knowledge of *TACR1* biology, specifically how the ratio of full-length to truncated isoforms may affect various downstream signalling pathways. The cellular heterogeneity characteristic of PDAC specimens may further dilute these differences, as isoform switching might occur predominantly within specific cell populations or microenvironmental niches.

Single-cell RNA sequencing methodology would address several of these limitations by enabling cell type-specific analysis of *TACR1* isoform distribution. This approach would permit deconvolution of the heterogeneous tumour microenvironment and identification of potential cell-specific splicing patterns. Additionally, targeted validation using isoform-specific RT-PCR would provide an orthogonal approach to verify and quantify the suggested differences in exon E001 usage in a larger cohort of PDAC samples.

4.1.4 Consequences of Impaired Receptor Internalisation on ERK Signalling

The structural features of NK1R-tr, result in impaired receptor internalization and desensitization (94). Due to its lack of a C-terminal β-arrestin binding domain, NK1R-tr fails to undergo β-arrestin-mediated internalization and desensitization (105). As a result, its G protein-mediated signalling may be prolonged, potentially altering downstream dynamics such as ERK activation. Indeed, previous studies have shown that, compared to NK1R-fl, NK1R-tr is associated with delayed ERK activation, likely due to its inability to engage β-arrestin scaffolds (96). This altered signalling profile may influence cellular processes such as survival, proliferation, or migration differently. Furthermore, prolonged pathway activity in the absence of desensitization could engage feedback mechanisms that suppress *TACR1* transcription, possibly explaining the detection of NK1R-tr protein despite low mRNA levels in some PDAC cell lines. These findings emphasize the importance of evaluating functional signalling activity rather than transcript abundance alone when assessing the SP/NK1R axis as a therapeutic target.

Finally, these findings invite future research into whether reactivation of NK1R expression or modulation of its downstream effectors could influence EMT status,

sensitize cells to chemotherapy or reduce metastatic potential. If NK1R contributes to the maintenance of epithelial features, its targeted modulation might help stabilize less aggressive phenotypes or interfere with progression toward a mesenchymal state - a process closely linked to PDAC aggressiveness (169).

4.2 Molecular Characterisation of *TACR1*-Stratified PDAC Subtypes

My stratification approach applied to both datasets divided samples within each dataset into two groups, *TACR1*-low and high, based on gene expression. I selected this approach after testing multiple threshold distances, with the average ±25% best satisfying the criteria of maximising sample retention while enabling downstream pathway analysis.

The differences in transcriptomic profiles between *TACR1*-high and *TACR1*-low tumours represent an intriguing finding of my study. For the PRJNA719796 dataset, the *TACR1*-high vs. control comparison yielded 1,787 significantly differentially expressed genes, while the *TACR1*-low vs. control comparison identified only 290 differentially expressed genes using the same criteria. This substantial difference in the number of differentially expressed genes suggests that PDAC tumours with higher *TACR1* expression may exhibit more extensive transcriptional dysregulation compared to those with lower *TACR1* expression. This quantitative difference in transcriptional perturbation indicates that *TACR1*-high tumours may possess different regulatory networks compared to their *TACR1*-low counterparts, though further validation would be required.

My observation that established PDAC biomarkers show enhanced expression in *TACR1*-high contexts suggests potential interactions between *TACR1* signalling and oncogenic pathways. For instance, *TRIM29*, a biomarker for PDAC that mediates radioresistance (145,146), showed a log2FC of 5.13 in *TACR1*-high vs. control but 4.62 in *TACR1*-low vs. control. Similarly, *TNS4*, previously characterized by its overexpression in pancreatic cancer and its role in facilitating colony formation (135), and *COL17A1,* associated with tumour growth control in PDAC (136), demonstrated more pronounced upregulation in the *TACR1*-high condition. This pattern of biomarker expression could reflect a distinct disease state or possibly indicate a specific cellular differentiation program associated with neurokinin receptor activity.

The analysis identified a subset of 124 genes that were uniquely differentially expressed in *TACR1*-low vs. control comparison, but not in the *TACR1*-high vs.

control dataset. Among the top unique genes in *TACR1*-low PDAC was the mesothelin precursor *MSLN* (137), as well as *HTR1D*, which promotes pancreatic cancer via PI3K-AKT signalling pathway (148), and *CDC20*, a cell division cycle protein critical for mitotic progression and associated with PDAC differentiation (149).

Notably, *AQP5*, a known biomarker associated with tumour progression and poor prognosis in PDAC (147), was exclusively expressed in the *TACR1*-low group and absent in *TACR1*-high vs. control comparisons. Considering the survival curve, which associate lower *TACR1* expression with poorer prognosis, and upregulated genes, such as *AQP5*, with its established role in promoting invasiveness, epithelial-mesenchymal transition, and metastasis (147), such selective expression in *TACR1*-low samples could further imply that this group represents a more aggressive PDAC subtype. This hypothesis will be further strengthened by the consistent identification of additional genes associated with aggressiveness in *TACR1*-low samples in future studies.

The molecular signature of *TACR1*-high tumours, with a much larger set of 1,621 genes, is characterized by upregulation of genes like *LINC02086*, a long non-coding RNA that inhibits ferroptosis in pancreatic cancer cells (150), and *SLC6A14*, a potential drug target (153). Besides these genes, *B3GNT6*, which is significantly associated with KRAS mutations in colorectal cancer (151), and *XIST*, a long non-coding RNA known to promote pancreatic cancer proliferation and perineural invasion (Cheng et al., 2024; Wei et al., 2017; Xiao et al., 2022), were upregulated in this group. Furthermore, upregulated *CXCL5* has been described as a marker for poor prognosis and correlated with immune infiltration in PDAC (156). Collectively, this suggests these tumours might possess distinct metabolic properties and therapeutic sensitivities. This molecular distinction seems to involve more than just gene expression variations, affecting basic biological functions, which indicates that *TACR1* levels may represent important characteristics of tumour cell behaviour in PDAC.

Interestingly, the *TACR1*-high tumours also showed significant downregulation of several Y-chromosome genes including *UTY*, *RPS4Y1*, and *EIF1AY*, suggesting potential sex-specific differences in gene expression patterns (157–159).

4.3 *TACR1* Expression Levels as a Potential Marker of Epithelial Phenotype Maintenance in PDAC

The observed inverse correlation between *TACR1* expression and EMT marker *ZEB1* implies a potential suppressive role of NK1R in maintaining epithelial characteristics. As tumours progress and undergo EMT, they may reduce dependence on NK1R signalling, potentially as a strategy to escape growth-limiting feedback or immune recognition (170). This observation is additionally validated by public database analyses, which demonstrated reduced *TACR1* expression in PDAC tissues relative to normal pancreatic tissue, showing a gradual decrease in expression as tumour stages progress (Figure 6b).

From a therapeutic perspective, my findings suggest that *TACR1*-tr expression is present in a range of PDAC phenotypes, including mesenchymal-like cell lines such as MIA PaCa-2, which showed the highest expression among those tested. This indicates that *TACR1*-tr is not restricted to epithelial-like or early-stage tumour models and may remain expressed in more aggressive or transcriptionally reprogrammed states. The observation that SP protein was detectable across all PDAC cell lines, despite variable *TAC1* mRNA levels, further supports the potential biological relevance of this pathway. Therefore, *TACR1*-tr expression may serve as a functional marker to guide patient stratification for NK1R-targeted therapies, such as aprepitant, independent of EMT status. Rather than relying solely on phenotypic classification, assessing receptor expression directly could provide a more precise basis for identifying tumours likely to benefit from pathway inhibition.

The distinct transcriptomic signatures of *TACR1*-high and *TACR1*-low PDAC tumours may reflect underlying differences in differentiation status or epithelial-mesenchymal plasticity. In the *TACR1*-high group, the upregulation of *COL17A1* may suggest the retention of certain epithelial traits or structural features (171). As a transmembrane collagen component of hemidesmosomes, *COL17A1* plays a role in maintaining epithelial polarity and cell-ECM adhesion (172,173). In epithelial cancers, its misexpression has been associated with altered tissue architecture and invasive behaviour, potentially reflecting a partial or transitional epithelial phenotype (174). Similarly, *TNS4*, also more strongly expressed in *TACR1*-high samples, is known to modulate cell adhesion and motility via focal adhesion signalling in pancreatic cancer (135).

In contrast, *TACR1*-low tumours showed exclusive upregulation of *AQP5*, a gene well-established to promote epithelial-mesenchymal transition (EMT) and metastasis in PDAC. *AQP5* has been associated with loss of E-cadherin, increased

cancer cell migration, and poor prognosis, marking it as a strong indicator of a more mesenchymal and invasive tumour phenotype (175,176). Additionally, *CDC20*, another gene elevated in *TACR1*-low samples, is a key regulator of mitotic progression (177) and has been linked to poor differentiation and increased tumour aggressiveness in PDAC (149), although it is not a classical EMT marker

Together, these patterns suggest that *TACR1*-high tumours may maintain more epithelial-like features, while *TACR1*-low tumours exhibit molecular traits associated with EMT, high proliferative capacity, and increased invasiveness. This supports the hypothesis that *TACR1* expression stratifies PDAC into biologically distinct subtypes with potential clinical relevance for prognosis and therapeutic targeting. However, *TNS4* this gene has also been shown to downregulate E-cadherin in colorectal cancer (178), thus contradicting this hypothesis. Studying its role in pancreatic cancer might reveal further insight.

4.4 Functional Consequences of NK1R Inhibition in PDAC Models

4.4.1 Antiproliferative Effects Correlate with *TACR1*-tr Expression Levels

My functional studies demonstrated significant antiproliferative effects of the NK1R antagonist aprepitant (AP) across multiple PDAC cell lines, with varying sensitivity correlating broadly with *TACR1*-tr expression levels. The antitumoral effect of NK1R antagonists is consistent with previous findings (74,113,131). Notably, as mentioned above, MIA PaCa-2 cells exhibited the highest expression of truncated *TACR1* alongside substantial *TAC1* presence. This mesenchymal cell line demonstrated the greatest sensitivity to AP treatment across all growth inhibition experiments, including colony formation assay (CFA) and spheroid formation assay (SFA). I also noted a modest increase in pan-caspase activity exclusively in this cell line, suggesting AP has particular efficacy against these highly undifferentiated cancer cells. Similar patterns were observed in DanG cells, which displayed the second-highest *TACR1*-tr levels. My findings suggest that PDAC subgroups with higher *TACR1*-tr expression may be more responsive to AP as an anti-cancer therapy. Therefore, I propose further clinical investigation to evaluate *TACR1*-tr measurement as a potential marker for therapeutic stratification in PDAC patients.

The western blot analysis of ERK1/2 activation provided mechanistic insight into the downstream signalling alterations induced by NK1R inhibition in PDAC cells. The marked modulation of ERK1/2 phosphorylation in response to AP treatment,

despite stable receptor protein levels, confirms that the observed effects are mediated through functional inhibition of NK1R signalling rather than alterations in receptor expression.

Interestingly, my results also suggest potential differential signalling dynamics between NK1R isoforms. Previous studies have shown that the truncated variant exhibits delayed ERK1/2 activation compared to the full-length receptor, with peak phosphorylation occurring at 20-30 minutes versus 1-2 minutes, respectively (96). The varied responses to AP treatment across cell lines with different isoform expression profiles may reflect these distinct signalling kinetics.

4.4.2 Enhanced Sensitivity of Cancer Stem Cell-like Populations to NK1R Inhibition

Spheroid generation from cells resistant to anoikis is widely used as an *in vitro* marker of cancer stemness (117), enabling identification of cells with cancer stem cell (CSC)-like properties while facilitating drug testing in three-dimensional culture models (117,133,134). Given that CSCs represent rare tumour initiators with significant chemoresistance (133,134), inhibiting their growth presents a promising approach to enhance therapeutic outcomes. Most cell lines in my study demonstrated capacity for both colony and spheroid formation, with notable dose-dependent responses to AP treatment over 14 days of culture. Importantly, cells in colony and spheroid formations showed greater sensitivity to AP than parental cells, suggesting lower concentrations may effectively inhibit growth.

These results indicate NK1R blockade may efficiently target CSC-like cells, offering potential for tumour initiator inhibition. Further studies are needed to determine potential alterations in SP/NK1R-related gene expression.

While direct identification of CSCs in patients remains challenging, putative markers such as CD44, CD133, or EpCAM are commonly used in PDAC tissue samples and could be assessed via immunohistochemistry or flow cytometry to explore clinical relevance (179). A logical next experimental step would be to evaluate NK1R expression and AP responsiveness in patient-derived organoids (PDOs), which would offer a more clinically representative model and help validate the CSC-targeting potential of NK1R inhibition in human PDAC (180,181).

4.4.3 Cell Cycle Arrest as the Primary Mechanism of NK1R Antagonist Activity

Following the substantial decrease in viability observed across all assays after AP treatment, I examined the cellular mechanisms involved. Notably, there was

little indication of apoptotic pathway activation. Since consistent findings from several apoptosis assays indicated that cell death processes were not driving the AP-induced growth suppression, I investigated other potential mechanisms. Cell cycle progression analysis revealed AP-induced cell cycle arrest, particularly affecting G1 and S phases. This pattern is consistent with the known role of NK1R in promoting cell proliferation in human cancers (182).

Interestingly, a previous study linked NK1R internalization and β-arrestin-mediated signalling to cell cycle progression (183). In glioblastoma cells, β-arrestin 1 (*ARRB1*) was shown to mediate NK1R-induced proliferation and regulate key cell cycle proteins such as CDC25C, CDK1, and cyclin B1 (183). *ARRB1* knockdown led to G2/M arrest and disrupted long-term ERK1/2 and Akt signalling (183). Although my study did not observe a G2/M phenotype but instead revealed a G1/S Phase arrest after pharmacological NK1R inhibition in PDAC, these findings suggest that β-arrestin-dependent signalling downstream of NK1R may have context-dependent effects on cell cycle regulation and may also contribute to the non-apoptotic effects observed after NK1R blockade in PDAC. Further investigation into cell-cycle-related proteins is needed to fully understand the mechanisms behind this arrest.

4.5 Transcriptomic Profiling of PDAC versus Adjacent Control Tissue

Initial analysis comparing PDAC to adjacent non-malignant pancreatic tissue revealed substantial transcriptional alterations (with 978 significantly differentially expressed genes), consistent with the established understanding of cancer. The PCA demonstrated clear separation between tumour and non-tumour samples, thus providing a solid foundation for subsequent stratification analysis, though the limited samples size necessitates cautious interpretation of my results.

The most significantly enriched GO terms included regulation of nuclear division, regulation of mitotic nuclear division, and nuclear division. The dysregulation of cell cycle and mitotic processes aligns with the fundamental understanding that uncontrolled proliferation represents a core cancer hallmark (184,185). Additionally, the extracellular region was the most significantly enriched cellular component term, suggesting active remodelling of the tumour microenvironment (186), a process that could contribute to metastatic progression and therapeutic resistance in pancreatic cancer (187). These transcriptional changes likely reflect complex interactions between tumour cells and stromal components (188). The consistency of these findings with earlier research (139–141) from various patient

groups indicates these are likely core features of PDAC pathobiology rather than findings specific to a particular cohort, although more extensive studies would be required for conclusive verification.

My examination of *TACR1* expression uncovered a complex relationship with PDAC pathobiology. The consistent downregulation of *TACR1* across multiple transcriptomic datasets points to sophisticated regulatory mechanisms that probably involve more than just transcriptional regulation. This pattern may reflect context-dependent functions in cancer, potentially influenced by post-transcriptional mechanisms, alternative splicing events generating functionally distinct isoforms, or signalling pathway interactions.

While published literature mostly reports on *TACR1* overexpression in various cancers (69), my findings align with emerging evidence that its expression can be heterogeneous and even suppressed in certain malignant contexts (74–78). This variability underscores the potential value of *TACR1* as a stratification marker rather than a universal diagnostic indicator. The lack of statistical significance within the analysis of the PRJNA719796 dataset despite a clear trend highlights the inherent challenges in studying genes with biological variability in limited sample sets.

4.6 XIST as a Marker of *TACR1*-High PDAC: Evidence for X-Chromosome Regulation

A striking and unexpected finding from my analysis of the PRJNA1133919 dataset was the strong association between *TACR1* expression and patient sex. Female PDAC samples consistently exhibited higher *TACR1* expression compared to male samples, with four out of five female samples clustering in the high-expression group while five out of six male samples showed minimal expression. This sex-specific pattern suggests potential hormonal or chromosomal regulation of *TACR1* expression that has not been previously reported in PDAC.

The dramatic upregulation of *XIST* in *TACR1*-high samples from the PRJNA719796 dataset provided further evidence for sex-specific regulatory mechanisms. *XIST*, a long non-coding RNA responsible for X-chromosome inactivation in females, showed minimal expression in *TACR1*-low samples but extremely high levels in *TACR1*-high samples. While this pattern was not as pronounced in the PRJNA1133919 dataset, the trend toward higher *XIST* expression in female *TACR1*-high samples persisted.

These observations raise intriguing possibilities regarding the regulation of *TACR1* in PDAC. While *TACR1* is located on chromosome 2, its expression may be influenced by X-linked transcription factors or regulatory elements that escape X-inactivation in females, resulting in sex-specific expression patterns. Additionally, sex hormones such as estrogen may differentially modulate *TACR1* transcription, potentially through hormone-responsive elements in the promoter region. Previous studies have shown that estrogen can influence NK1R expression in other tissues (189). Moreover, sex-specific epigenetic patterns established during development may contribute to differential *TACR1* expression between males and females. The correlation with *XIST* suggests potential involvement of X-chromosome-related epigenetic regulators in this process, and therefore provides a rationale for further investigation into sex-specific regulatory mechanisms in PDAC. These findings may support sex-based patient stratification and may contribute to the development of targeted therapeutic strategies tailored by sex.

The distinct molecular signatures associated with *TACR1*-high/female and *TACR1*-low/male samples further support the biological significance of these patterns. The enrichment of immune-related pathways, particularly B-cell activation and immunoglobulin production, in *TACR1*-high samples, which are discussed in the following chapter, suggests a potential intersection between NK1R signalling, sex-specific immunity, and tumour biology that warrants further investigation.

4.7 Enrichment of Immune Signatures in *TACR1*-High Tumours

The enrichment of immune-related pathways in *TACR1*-high tumours represents another unexpected finding and bridges neuroimmune interactions and cancer biology. My Gene Ontology analysis of the PRJNA1133919 dataset revealed significant enrichment of immunoglobulin complex, adaptive immune response, B cell activation, antigen binding, immunoglobulin production, B cell proliferation, external side of plasma membrane, and signalling receptor activity. These enriched terms confirm a strong B-cell-mediated immune signature in *TACR1*-high samples.

In *TACR1*-low samples, significantly enriched GO terms included intracellular membrane-bounded organelle, nucleus, intracellular organelle, and intracellular anatomical structure.

My analysis further revealed several significantly upregulated genes in the *TACR1*-high group. These include multiple immunoglobulin-related genes -

IGKV1D-39, *IGGL5*, and *CD79A* - which have been extensively documented for their roles in immune function and B-cell development (162–164). Additionally, I observed upregulation of *SHISA8* and *CBLN1*, both of which are thought to participate in neuronal synaptic plasticity regulation according to recent research (165,166). Other notable upregulated genes include *GFRA1*, which has been implicated in osteosarcoma chemoresistance mechanisms (167), and *ITIH5*, previously identified as a metastasis suppressor gene in pancreatic ductal adenocarcinoma (168).

This association between *TACR1* expression and B cell-mediated immunity suggests novel dimensions to neurokinin signalling in the tumour microenvironment that extend beyond its canonical roles (190,191). This immune signature could reflect either a reactive phenomenon, where immune infiltration might be associated with *TACR1* expression, or alternatively, *TACR1*-expressing tumour cells might actively modulate the immune microenvironment. The clinical implications of this association are particularly relevant given increasing interest in immunotherapeutic approaches for PDAC. If *TACR1* expression indeed correlates with specific immune microenvironmental states, it might serve as a potential biomarker for immunotherapy response.

Furthermore, the co-occurrence of B cell-related immune signatures with *XIST* upregulation and downregulation of Y-chromosome-linked genes in *TACR1*-high tumours raises the possibility of sex-specific transcriptional or immune modulation. It is well established that females generally exhibit stronger humoral and cellular immune responses than males, leading to more robust vaccine responses but also a higher prevalence of autoimmune diseases (192). These differences are attributed to a combination of hormonal influences, X-linked gene dosage, and epigenetic regulation (193), including the role of *XIST* in X-chromosome inactivation (194). While sex was not a stratification variable in this study, these findings highlight the importance of considering biological sex as a factor in tumour-immune dynamics and in the development of personalised immunotherapeutic strategies in PDAC.

4.8 Clinical Implications and Therapeutic Potential

The integration of my in vitro findings with bioinformatic analyses has significant implications for PDAC classification and therapeutic stratification. The observation that *TACR1* expression declines with tumour progression, coupled with the association between low *TACR1* levels and poor survival, suggests that *TACR1*

expression could serve as a prognostic biomarker in PDAC. Moreover, the differential sensitivity to NK1R antagonism observed across cell lines with varying *TACR1*-tr expression levels indicates that isoform-specific profiling might identify patient subgroups most likely to benefit from NK1R-targeted therapy.

The decreased sensitivity of pancreatic stellate cells (PSCs) to AP treatment compared to cancer cells presents another potential therapeutic advantage. PSCs contribute substantially to aggressive stromal fibrosis and interact closely with cancer cells, thereby promoting pancreatic tumour growth and limiting drug delivery (195,196). Research has also linked PSCs to genomic instability and epithelial-mesenchymal transition (EMT) induction (195). A therapeutic approach that preferentially targets cancer cells while sparing stromal components might achieve tumour control without exacerbating the stromal barrier to drug penetration (197). The potential to disrupt signalling in these cells could also significantly improve patient outcomes by inhibiting tumour recurrence following surgical intervention.

The potential efficacy of NK1R antagonists against cancer stem cell-like populations is particularly promising for preventing recurrence and metastasis. Current therapeutic regimens for PDAC often fail to eradicate CSCs, leading to disease relapse (198). The ability of AP to inhibit spheroid and colony formation at lower concentrations than required for bulk tumour cell growth suggests that NK1R antagonists might complement conventional cytotoxic agents by targeting therapy-resistant subpopulations.

The observed differences in *TACR1* expression between male and female patients in my analyses raise important considerations for personalized treatment approaches. The elevated expression of *TACR1* in female PDAC patients indicates potential for improved responsiveness to NK1R-targeted therapies in this group. This hypothesis aligns with the growing recognition of sex-based differences in cancer biology and treatment response (199).

4.9 Critical Analysis of Conflicting Evidence on *TACR1* Expression Levels in PDAC

4.9.1 Transcriptomic Discrepancies

The transcriptomic analysis of *TACR1* expression in PDAC has yielded notably contradictory results across different studies. These discrepancies warrant careful examination to accurately characterize the expression profile of this receptor in pancreatic cancer.

My comprehensive analysis utilizing multiple independent transcriptomic datasets (CCLE, TCGA, GSE62165, GSE15471, and GSE16515) consistently demonstrate significant downregulation of *TACR1* in PDAC tissue compared to normal pancreatic cells (Figure 6a). Specifically, the PRJNA719796 dataset also revealed *TACR1* downregulation with a log2FC of -0.73, though this did not reach statistical significance (padj = 0.58). Further supporting this downregulation pattern, GEO microarray data analysis indicates a trend toward decreasing total *TACR1* expression with advancing tumour stages (Figure 6b).

In direct contradiction to my findings, earlier research by Friess et al. (53) reported elevated NK1R expression in tumour samples compared to normal tissue. Their study suggests increasing *TACR1* levels correlating with disease progression and reduced survival rates. This represents a fundamental inconsistency with observations from larger, more recent datasets.

Several factors may contribute to these conflicting reports on *TACR1* expression levels. Different research approaches represent a key factor to consider, as the Friess et al. study employed different analytical techniques compared to my multiplatform approach. My bioinformatic evaluation incorporated substantially larger sample sizes (193 tumour patients and 68 normal controls from GEO, plus 86 additional patients through OncoLnc), potentially providing a more representative picture of *TACR1* expression across PDAC populations.

Additionally, primer selection for detection can affect results. Friess et al. used primers that target the first exon, allowing them to detect both variants simultaneously. In contrast, my research used primers specifically designed to distinguish between NK1R isoforms, which might result in measuring lower expression levels compared to assessments of total NK1R mRNA (which includes both full-length and truncated forms). RT-qPCR techniques can yield varying results, sometimes causing differences in standard error calculations. (200).

The literature beyond PDAC presents a similarly mixed picture. While published literature mostly reports on *TACR1* overexpression in various cancers (69), my findings align with emerging evidence that its expression can be heterogeneous and even suppressed in certain malignant contexts (74–78).

A particularly notable finding from the analysis of the PRJNA1133919 dataset was the striking sex-specific pattern of *TACR1* expression. Female samples exhibited substantially higher *TACR1* expression (range: 70-150 feature counts) compared to male samples (range: 0-138 feature counts, with most male samples showing very low expression). This sex-based variability represents another dimension that could potentially explain inconsistencies between studies with different sex distributions in their cohorts.

The contradictory transcriptomic evidence regarding *TACR1* expression in PDAC suggests that this receptor's expression pattern is more complex than initially appreciated. The difference between my large-scale analysis, indicating downregulation, and previous reports describing upregulation highlights the need for further research that employs standardized methodologies and clearly defined patient cohorts. These inconsistencies emphasize the necessity of accounting for factors such as tumour heterogeneity, analytical techniques, cohort size, and biological variables, including sex, when interpreting transcriptomic data. *TACR1* expression in PDAC appears to be highly context-dependent, influenced by multiple factors beyond tumour status alone, which has significant implications for its reliability as a diagnostic biomarker or therapeutic target.

4.9.2 Post-transcriptional Regulation

Although discrepancies between mRNA expression and corresponding protein levels are commonly encountered (201,202), the discrepancies particularly in Capan-1 cells where NK1R-tr protein was detected despite undetectable *TACR1*-tr mRNA warrant further discussion. Other publications reported to detect *TACR1* in Capan-1 via RT-qPCR and Western blot (53,203), which suggests varying sensitivity between the methods employed.

Furthermore, the truncated isoform may undergo enhanced translational efficiency or exhibit increased protein stability compared to the full-length variant, resulting in detectable protein levels despite low mRNA expression (204). Additionally, transcriptional analysis provides a snapshot of gene expression at a specific time point, while protein accumulation reflects longer-term expression patterns. Fluctuations in *TACR1* transcription that occur during tumour progression may not be captured in single-point analyses (205). Moreover, the internalization-

defective nature of NK1R-tr resulting in sustained signalling and potential negative feedback on *TACR1* transcription, which might explain the observed low mRNA levels despite functional protein presence (96).

4.9.3 *TACR1* Downregulation with Poor Prognosis

The association between *TACR1* downregulation and unfavourable outcomes, as demonstrated in survival analysis (Figure 6c), presents an apparent contradiction: if NK1R promotes tumour growth, why would its decreased expression correlate with worse outcomes? Several mechanisms may explain this phenomenon. Advanced tumours may evolve independence from NK1R signalling as they acquire additional oncogenic alterations, allowing them to bypass this pathway while maintaining aggressive behaviour. Moreover, the balance between full-length and truncated isoforms, rather than total *TACR1* expression, may be critical for tumour behaviour. The truncated variant lacks β-arrestin binding sites, resulting in sustained signalling and potential enhancement of oncogenic pathways despite lower overall receptor expression (105). As evidenced by the positive correlation between *TAC1* and *ZEB1* expression, and the clustering of *TAC1* with mesenchymal markers, increased ligand production may compensate for reduced receptor levels, maintaining pathway activation through a concentration-dependent mechanism.

4.10 Limitations and Future Directions

Several limitations of my study should be discussed. First, the relative overall mRNA expression patterns of *TACR1* splice variants raise questions about how AP displays significant anti-proliferative activity in pancreatic cancer cells, which I hypothesized would be driven by the SP/NK1R signalling axis. Although AP binds strongly to NK1R, it also exhibits minimal affinity for corticosteroid receptors, serotonin, or dopamine. An interesting direction for future research would be to determine whether AP might exhibit anti-tumour effects through interaction with these alternative receptors in contexts where NK1R is absent.

Second, as discussed in chapter 4.10, the discrepancies between transcriptional and protein expression data for NK1R isoforms highlight the technical challenges in accurately quantifying splice variants. Future studies should employ isoform-specific antibodies or targeted proteomics approaches to more precisely characterize NK1R isoform distribution in PDAC tissues. Furthermore, while my cell line-based functional studies provided valuable mechanistic insights, they may not fully recapitulate the complex tumour microenvironment of PDAC. Patient-derived

organoid-based experiments, particularly those involving co-culture with stromal and immune components, would provide a more physiologically relevant model system.

Third, the strong association between *TACR1* expression and patient sex warrants further investigation in larger cohorts with detailed clinical annotation. Validation of sex-specific expression patterns in independent datasets and exploration of potential hormonal or epigenetic regulatory mechanisms would enhance the translational relevance of these findings.

Future research directions should include targeted knockdown or overexpression of NK1R-fl and NK1R-tr in isogenic cell lines. This may allow for accurate identification of their individual roles in PDAC progression and treatment response. Furthermore, preclinical testing of NK1R antagonists in patient-derived models, stratified by *TACR1* expression and isoform distribution, would provide stronger evidence for their therapeutic potential.

Additionally, evaluation of NK1R antagonists in combination with conventional chemotherapeutic agents, immunomodulatory compounds, or molecular-targeted therapies may reveal synergistic interactions that potentiate therapeutic efficacy. Of greater significance, prospective validation of *TACR1* expression patterns and isoform distribution as predictive biomarkers for NK1R-targeted interventions would enable facilitate patient stratification in clinical trials. Finally, systematic investigation of the molecular mechanisms underlying sex-specific differences in *TACR1* expression and their consequent impact on therapeutic response would advance the development of sex-tailored treatment strategies.

Lastly, the interpretative scope of my findings should be considered within the context of several methodological limitations. The modest sample sizes in both analysed datasets (n=12 for PRJNA719796 and n=10 for PRJNA1133919, with one sample excluded as an outlier) necessitate cautious interpretation of statistical findings, particularly for genes with biological variability like *TACR1*. Power calculations suggest that detecting subtle expression differences or splicing events with high confidence would require substantially larger cohorts. This limitation is particularly relevant for the sex-specific findings, where subdividing already small sample groups further reduces statistical power. The use of bulk RNA sequencing introduces additional complexity through cellular heterogeneity. PDAC is characterized by extensive desmoplasia, with stromal cells often comprising the majority of tumour mass (206,207). Consequently, bulk transcriptomic profiles represent aggregate signals from diverse cell populations, potentially masking cell type-specific expression patterns (208). The observed heterogeneity

is particularly relevant to *TACR1*, which may be expressed in both epithelial tumour cells and the neural components of the tumour microenvironment. The unique immune signature associated with *TACR1*-high samples raises important questions about the source of *TACR1* expression. Specifically, it is important to determine whether this expression primarily comes from malignant epithelial cells or from infiltrating immune cell populations.

5. Conclusion

My comprehensive investigation of the SP/NK1R system in PDAC has revealed complex patterns of isoform expression, sex-specific regulation, and functional significance in tumour biology. The predominance of NK1R-tr in PDAC cells, coupled with the antiproliferative effects of NK1R antagonism, particularly in cancer stem cell-like populations, supports the therapeutic potential of targeting this pathway. The inverse correlation between *TACR1* expression and tumour progression, as well as the distinct molecular signatures associated with high versus low *TACR1* expression, suggests that receptor expression might serve as both a prognostic biomarker and a predictive indicator for response to NK1R-targeted therapy.

The identification of differential isoform expression across tumour cell lines provides a mechanistic basis for the variable responsiveness to NK1R antagonists, with cells expressing higher levels of NK1R-tr showing enhanced sensitivity to aprepitant. My functional studies demonstrated that NK1R antagonism primarily exerts its effects through cell cycle modulation rather than classical apoptosis, with significant effects on ERK signalling pathways that drive cellular proliferation.

Bioinformatic analyses revealed significant sex-specific differences in the expression of *TACR1*. Female PDAC samples consistently showed higher levels of this receptor compared to male samples. Furthermore, the correlation between *TACR1* expression and immune-related gene signatures suggests a potential interaction between neurokinin signalling and the tumour immune microenvironment. These findings highlight the need for further investigation to better understand the functional implications of this interaction.

These findings lay the groundwork for developing personalized therapeutic strategies that target the substance P/neurokinin-1 receptor (SP/NK1R) system in PDAC, which could have significant implications for improving outcomes in this challenging malignancy. The integration of receptor expression profiling with sex-specific considerations may represent a significant step toward more effective patient stratification and individualized treatment approaches for pancreatic cancer.

References

1. Beirith I, Renz BW, Mudusetti S, Ring NS, Kolorz J, Koch D, et al. Identification of the Neurokinin-1 Receptor as Targetable Stratification Factor for Drug Repurposing in Pancreatic Cancer. Cancers (Basel) [Internet]. 2021 Jun 1 [cited 2023 Jun 1];13(11). Available from: /pmc/articles/PMC8198055/

2. Sarantis P, Koustas E, Papadimitropoulou A, Papavassiliou AG, Karamouzis M V. Pancreatic ductal adenocarcinoma: Treatment hurdles, tumor microenvironment and immunotherapy [Internet]. Vol. 12, World Journal of Gastrointestinal Oncology. Baishideng Publishing Group Co; 2020 [cited 2023 Sep 5]. p. 173–81. Available from: /pmc/articles/PMC7031151/

3. Rahib L, Smith BD, Aizenberg R, Rosenzweig AB, Fleshman JM, Matrisian LM. Projecting cancer incidence and deaths to 2030: the unexpected burden of thyroid, liver, and pancreas cancers in the United States. Cancer Res [Internet]. 2014 Jun 1 [cited 2024 Dec 2];74(11):2913–21. Available from: https://pubmed.ncbi.nlm.nih.gov/24840647/

4. Bray F, Laversanne M, Sung H, Ferlay J, Siegel RL, Soerjomataram I, et al. Global cancer statistics 2022: GLOBOCAN estimates of incidence and mortality worldwide for 36 cancers in 185 countries. CA Cancer J Clin [Internet]. 2024 May [cited 2024 Dec 2];74(3):229–63. Available from: https://pubmed.ncbi.nlm.nih.gov/38572751/

5. Ferlay J, Soerjomataram I, Dikshit R, Eser S, Mathers C, Rebelo M, et al. Cancer incidence and mortality worldwide: Sources, methods and major patterns in GLOBOCAN 2012. Int J Cancer [Internet]. 2015 Mar 1 [cited 2024 Dec 2];136(5):E359–86. Available from: https://onlinelibrary.wiley.com/doi/full/10.1002/ijc.29210

6. Park W, Chawla A, O'Reilly EM. Pancreatic Cancer: A Review. JAMA [Internet]. 2021 Sep 7 [cited 2024 Dec 2];326(9):851. Available from: https://pmc.ncbi.nlm.nih.gov/articles/PMC9363152/

7. Hernandez D, Wagner F, Hernandez-Villafuerte K, Schlander M. Economic Burden of Pancreatic Cancer in Europe: a Literature Review. J Gastrointest Cancer [Internet]. 2023 Jun 1 [cited 2024 Dec 2];54(2):391–407. Available from: https://pubmed.ncbi.nlm.nih.gov/35474568/

8. Yuan C, Kim J, Wang QL, Lee AA, Babic A, Amundadottir LT, et al. The age-dependent association of risk factors with pancreatic cancer. Ann Oncol [Internet]. 2022 Jul 1 [cited 2024 Dec 2];33(7):693–701. Available from: https://pubmed.ncbi.nlm.nih.gov/35398288/

9. Bryant JM, Palm RF, Herrera R, Rubens M, Hoffe SE, Kim DW, et al. Multi-Institutional Outcomes of Patients Aged 75 years and Older With Pancreatic Ductal Adenocarcinoma Treated With 5-Fraction Ablative Stereotactic Magnetic Resonance Image-Guided Adaptive Radiation Therapy (A-SMART). Cancer Control [Internet]. 2023 Jan 1 [cited 2024 Dec 2];30. Available from: https://pubmed.ncbi.nlm.nih.gov/36598464/

10. O'Neill CB, Atoria CL, O'Reilly EM, Lafemina J, Henman MC, Elkin EB. Costs and trends in pancreatic cancer treatment. Cancer [Internet]. 2012 Oct 15 [cited 2024 Dec 2];118(20):5132–9. Available from: https://pubmed.ncbi.nlm.nih.gov/22415469/

11. Stukalin I, Ahmed NS, Fundytus AM, Qian AS, Coward S, Kaplan GG, et al. Trends and Projections in National United States Health Care Spending for Gastrointestinal Malignancies (1996-2030). Gastroenterology [Internet]. 2022 Apr 1 [cited 2024 Dec 2];162(4):1098-1110.e2. Available from: https://pubmed.ncbi.nlm.nih.gov/34922947/

12. Cipora E, Partyka O, Pajewska M, Czerw A, Sygit K, Sygit M, et al. Treatment Costs and Social Burden of Pancreatic Cancer. Cancers (Basel) [Internet]. 2023 Mar 1 [cited 2024 Dec 2];15(6):1911. Available from: https://pmc.ncbi.nlm.nih.gov/articles/PMC10047484/

13. Sikdar N, Saha G, Dutta A, Ghosh S, Shrikhande S V., Banerjee S. Genetic Alterations of Periampullary and Pancreatic Ductal Adenocarcinoma: An Overview. Curr Genomics [Internet]. 2018 Feb 21 [cited 2024 Dec 2];19(6):444. Available from: https://pmc.ncbi.nlm.nih.gov/articles/PMC6128383/

14. Grant TJ, Hua K, Singh A. Molecular Pathogenesis of Pancreatic Cancer. Prog Mol Biol Transl Sci [Internet]. 2016 [cited 2024 Dec 2];144:241. Available from: https://pmc.ncbi.nlm.nih.gov/articles/PMC6260831/

15. Takai E, Yachida S. Genomic alterations in pancreatic cancer and their relevance to therapy. World J Gastrointest Oncol [Internet]. 2015 Oct 15 [cited 2024 Dec 2];7(10):250. Available from: https://pmc.ncbi.nlm.nih.gov/articles/PMC4606179/

16. Palma AM, Vudatha V, Peixoto ML, Madan E. Tumor heterogeneity: An oncogenic driver of PDAC progression and therapy resistance under stress conditions. Adv Cancer Res [Internet]. 2023 Jan 1 [cited 2024 Dec 3];159:203–49. Available from: https://pubmed.ncbi.nlm.nih.gov/37268397/

17. Shou S, Li Y, Chen J, Zhang X, Zhang C, Jiang X, et al. Understanding, diagnosing, and treating pancreatic cancer from the perspective of telomeres and telomerase. Cancer Gene Ther [Internet]. 2024 Sep 1 [cited 2025 Apr 20];31(9):1292. Available from: https://pmc.ncbi.nlm.nih.gov/articles/PMC11405285/

18. Johnson C, Burkhart DL, Haigis KM. Classification of KRAS activating mutations and the implications for therapeutic intervention. Cancer Discov [Internet]. 2022 Apr 1 [cited 2024 Dec 3];12(4):913. Available from: https://pmc.ncbi.nlm.nih.gov/articles/PMC8988514/

19. Mccleary-Wheeler AL, Mcwilliams R, Fernandez-Zapico ME. Aberrant signaling pathways in pancreatic cancer: A two compartment view. Mol Carcinog [Internet]. 2012 Jan [cited 2024 Dec 3];51(1):25. Available from: https://pmc.ncbi.nlm.nih.gov/articles/PMC3253704/

20. Racu ML, Lebrun L, Schiavo AA, Van Campenhout C, De Clercq S, Absil L, et al. The Role of SMAD4 Inactivation in Epithelial–Mesenchymal Plasticity of Pancreatic Ductal Adenocarcinoma: The Missing Link? Cancers (Basel) [Internet]. 2022 Feb 1 [cited 2024 Dec 3];14(4):973. Available from: https://pmc.ncbi.nlm.nih.gov/articles/PMC8870198/

21. Sousa CM, Kimmelman AC. The complex landscape of pancreatic cancer metabolism. Carcinogenesis [Internet]. 2014 [cited 2024 Dec 3];35(7):1441. Available from: https://pmc.ncbi.nlm.nih.gov/articles/PMC4076815/

22. Shi M, Cui J, Du J, Wei D, Jia Z, Zhang J, et al. A novel KLF4/LDHA signaling pathway regulates aerobic glycolysis in and progression of pancreatic cancer. Clinical Cancer Research [Internet]. 2014 Aug 15 [cited 2025 Apr 20];20(16):4370–80. Available from: /clincancerres/article/20/16/4370/13182/A-Novel-KLF4-LDHA-Signaling-Pathway-Regulates

23. Gao J, Long B, Wang Z. Role of Notch signaling pathway in pancreatic cancer. Am J Cancer Res [Internet]. 2017 [cited 2024 Dec 3];7(2):173. Available from: https://pmc.ncbi.nlm.nih.gov/articles/PMC5336494/

24. Neureiter D, Jäger T, Ocker M, Kiesslich T. Epigenetics and pancreatic cancer: Pathophysiology and novel treatment aspects. World Journal of

Gastroenterology : WJG [Internet]. 2014 [cited 2024 Dec 3];20(24):7830. Available from: https://pmc.ncbi.nlm.nih.gov/articles/PMC4069312/

25. Orth M, Metzger P, Gerum S, Mayerle J, Schneider G, Belka C, et al. Pancreatic ductal adenocarcinoma: biological hallmarks, current status, and future perspectives of combined modality treatment approaches. Radiation Oncology 2019 14:1 [Internet]. 2019 Aug 8 [cited 2023 May 17];14(1):1–20. Available from: https://ro-journal.biomedcentral.com/articles/10.1186/s13014-019-1345-6

26. Brezgyte G, Shah V, Jach D, Crnogorac-jurcevic T. Non-Invasive Biomarkers for Earlier Detection of Pancreatic Cancer—A Comprehensive Review. Cancers (Basel) [Internet]. 2021 Jun 1 [cited 2024 Dec 3];13(11):2722. Available from: https://pmc.ncbi.nlm.nih.gov/articles/PMC8198035/

27. Chrystoja CC, Diamandis EP, Brand R, Rückert F, Haun R, Molina R. Pancreatic cancer. Clin Chem [Internet]. 2013 Jan [cited 2024 Dec 3];59(1):41–6. Available from: https://pubmed.ncbi.nlm.nih.gov/23136253/

28. Ansari D, Gustafsson A, Andersson R. Update on the management of pancreatic cancer: surgery is not enough. World J Gastroenterol [Internet]. 2015 Mar 21 [cited 2024 Dec 3];21(11):3157–65. Available from: https://pubmed.ncbi.nlm.nih.gov/25805920/

29. Groot VP, Gemenetzis G, Blair AB, Ding D, Javed AA, Burkhart RA, et al. Implications of the Pattern of Disease Recurrence on Survival Following Pancreatectomy for Pancreatic Ductal Adenocarcinoma. Ann Surg Oncol [Internet]. 2018 Aug 1 [cited 2024 Dec 3];25(8):2475. Available from: https://pmc.ncbi.nlm.nih.gov/articles/PMC6220676/

30. Herreros-Villanueva M, Gironella M, Castells A, Bujanda L. Molecular markers in pancreatic cancer diagnosis. Clinica Chimica Acta. 2013 Mar 15;418:22–9.

31. Neuzillet C, Tijeras-Raballand A, Bourget P, Cros J, Couvelard A, Sauvanet A, et al. State of the art and future directions of pancreatic ductal adenocarcinoma therapy. Pharmacol Ther [Internet]. 2015 Nov 1 [cited 2024 Dec 3];155:80–104. Available from: https://pubmed.ncbi.nlm.nih.gov/26299994/

32. Shankar K, Huffman D, Peterson C, Alhamad K, Jayakrishnan TT, Attah AA, et al. An internal review of chemotherapy toxicities in patients with pancreatic cancer. Journal of Clinical Oncology [Internet]. 2021 May 20 [cited 2024 Dec 3];39(15_suppl):e16258–e16258. Available from: https://ascopubs.org/doi/10.1200/JCO.2021.39.15_suppl.e16258

33. Ghosn M, Ibrahim T, Assi T, El Rassy E, Kourie HR, Kattan J. Dilemma of first line regimens in metastatic pancreatic adenocarcinoma. World J Gastroenterol [Internet]. 2016 Dec 14 [cited 2024 Dec 3];22(46):10124. Available from: https://pmc.ncbi.nlm.nih.gov/articles/PMC5155171/

34. Olaoba OT, Yang M, Adelusi TI, Maidens T, Kimchi ET, Staveley-O'Carroll KF, et al. Targeted Therapy for Highly Desmoplastic and Immunosuppressive Tumor Microenvironment of Pancreatic Ductal Adenocarcinoma. Cancers 2024, Vol 16, Page 1470 [Internet]. 2024 Apr 11 [cited 2024 Dec 3];16(8):1470. Available from: https://www.mdpi.com/2072-6694/16/8/1470/htm

35. Martinez-Bosch N, Vinaixa J, Navarro P. Immune Evasion in Pancreatic Cancer: From Mechanisms to Therapy. Cancers (Basel) [Internet]. 2018 Jan 1 [cited 2024 Dec 3];10(1):6. Available from: https://pmc.ncbi.nlm.nih.gov/articles/PMC5789356/

36. Kemp SB, Pasca di Magliano M, Crawford HC. Myeloid Cell Mediated IImmune Suppression in Pancreatic Cancer. Cell Mol Gastroenterol Hepatol [Internet]. 2021 Jan 1 [cited 2024 Dec 3];12(5):1531. Available from: https://pmc.ncbi.nlm.nih.gov/articles/PMC8529393/

37. Skelton RA, Javed A, Zheng L, He J. Overcoming the resistance of pancreatic cancer to immune checkpoint inhibitors. J Surg Oncol [Internet]. 2017 Jul 1 [cited 2024 Dec 3];116(1):55–62. Available from: https://pubmed.ncbi.nlm.nih.gov/28628715/

38. Evan T, Wang VMY, Behrens A. The roles of intratumour heterogeneity in the biology and treatment of pancreatic ductal adenocarcinoma. Oncogene [Internet]. 2022 Oct 14 [cited 2025 Apr 20];41(42):4686. Available from: https://pmc.ncbi.nlm.nih.gov/articles/PMC9568427/

39. Marusyk A, Janiszewska M, Polyak K. Intratumor heterogeneity: the Rosetta stone of therapy resistance. Cancer Cell [Internet]. 2020 Apr 13 [cited 2024 Dec 3];37(4):471. Available from: https://pmc.ncbi.nlm.nih.gov/articles/PMC7181408/

40. Perelló-Reus CM, Rubio-Tomás T, Cisneros-Barroso E, Ibargüen-González L, Segura-Sampedro JJ, Morales-Soriano R, et al. Challenges in precision medicine in pancreatic cancer: A focus in cancer stem cells and microbiota. Front Oncol [Internet]. 2022 Dec 1 [cited 2024 Dec 3];12:995357. Available from: https://pmc.ncbi.nlm.nih.gov/articles/PMC9751445/

41. Krantz BA, O'Reilly EM. Biomarker-Based Therapy in Pancreatic Ductal Adenocarcinoma: An Emerging Reality? Clin Cancer Res [Internet]. 2017 May 15 [cited 2024 Dec 4];24(10):2241. Available from: https://pmc.ncbi.nlm.nih.gov/articles/PMC5955785/

42. Ying H, Dey P, Yao W, Kimmelman AC, Draetta GF, Maitra A, et al. Genetics and biology of pancreatic ductal adenocarcinoma. Genes Dev [Internet]. 2016 Feb 15 [cited 2025 May 20];30(4):355. Available from: https://pmc.ncbi.nlm.nih.gov/articles/PMC4762423/

43. Akhoundova D, Rubin MA. Clinical application of advanced multi-omics tumor profiling: Shaping precision oncology of the future. Cancer Cell [Internet]. 2022 Sep 12 [cited 2024 Dec 4];40(9):920–38. Available from: https://pubmed.ncbi.nlm.nih.gov/36055231/

44. Torres C, Grippo PJ. Pancreatic Cancer Subtypes: A Roadmap for Precision Medicine. Ann Med [Internet]. 2018 May 19 [cited 2024 Dec 4];50(4):277. Available from: https://pmc.ncbi.nlm.nih.gov/articles/PMC6151873/

45. Real FX, Siveke JT. Pancreatic cancer transcriptomes: molecular stratification in the adjuvant setting. Annals of Oncology [Internet]. 2021 Feb 1 [cited 2024 Dec 4];32(2):133–5. Available from: http://www.annalsofoncology.org/article/S0923753420431679/fulltext

46. Tesfaye AA, Kamgar M, Azmi A, Philip PA. The evolution into personalized therapies in pancreatic ductal adenocarcinoma: challenges and opportunities. Expert Rev Anticancer Ther [Internet]. 2018 [cited 2024 Dec 4];18(2):131–48. Available from: https://pubmed.ncbi.nlm.nih.gov/29254387/

47. Pervin J, Asad M, Cao S, Jang GH, Feizi N, Haibe-Kains B, et al. Clinically impactful metabolic subtypes of pancreatic ductal adenocarcinoma (PDAC). Front Genet [Internet]. 2023 [cited 2024 Dec 4];14:1282824. Available from: https://pmc.ncbi.nlm.nih.gov/articles/PMC10643182/

48. Espinet E, Klein L, Puré E, Singh SK. Mechanisms of PDAC subtype heterogeneity and therapy response. Trends Cancer [Internet]. 2022 Dec 1

[cited 2024 Dec 4];8(12):1060–71. Available from: https://pubmed.ncbi.nlm.nih.gov/36117109/

49. Bailey P, Chang DK, Nones K, Johns AL, Patch AM, Gingras MC, et al. Genomic analyses identify molecular subtypes of pancreatic cancer. Nature [Internet]. 2016 Mar 3 [cited 2024 Dec 4];531(7592):47–52. Available from: https://pubmed.ncbi.nlm.nih.gov/26909576/

50. Lee JJ, Bernard V, Semaan A, Monberg ME, Huang J, Stephens BM, et al. Elucidation of Tumor-Stromal Heterogeneity and the Ligand-Receptor Interactome by Single-Cell Transcriptomics in Real-world Pancreatic Cancer Biopsies. Clin Cancer Res [Internet]. 2021 Nov 15 [cited 2024 Dec 4];27(21):5912–21. Available from: https://pubmed.ncbi.nlm.nih.gov/34426439/

51. Suzuki SR, Kuno A, Ozaki H. Cell-to-cell interaction analysis of prognostic ligand-receptor pairs in human pancreatic ductal adenocarcinoma. Biochem Biophys Rep [Internet]. 2021 Dec 1 [cited 2024 Dec 4];28. Available from: https://pubmed.ncbi.nlm.nih.gov/34522794/

52. Chiramel J, Backen AC, Pihlak R, Lamarca A, Frizziero M, Tariq NUA, et al. Targeting the Epidermal Growth Factor Receptor in Addition to Chemotherapy in Patients with Advanced Pancreatic Cancer: A Systematic Review and Meta-Analysis. Int J Mol Sci [Internet]. 2017 May 1 [cited 2024 Dec 4];18(5):909. Available from: https://pmc.ncbi.nlm.nih.gov/articles/PMC5454822/

53. Friess H, Zhu Z, Liard V, Shi X, Shrikhande S V., Wang L, et al. Neurokinin-1 Receptor Expression and Its Potential Effects on Tumor Growth in Human Pancreatic Cancer. Laboratory Investigation 2003 83:5 [Internet]. 2003 May 1 [cited 2024 Dec 4];83(5):731–42. Available from: https://www.nature.com/articles/3780660

54. Kocher F, Puccini A, Untergasser G, Martowicz A, Zimmer K, Pircher A, et al. Multi-omic Characterization of Pancreatic Ductal Adenocarcinoma Relates CXCR4 mRNA Expression Levels to Potential Clinical Targets. Clinical Cancer Research [Internet]. 2022 Nov 15 [cited 2024 Dec 4];28(22):4957. Available from: https://pmc.ncbi.nlm.nih.gov/articles/PMC9660543/

55. Sivapalan L, Kocher HM, Ross-Adams H, Chelala C. The molecular landscape of pancreatic ductal adenocarcinoma. Pancreatology [Internet]. 2022

Nov 1 [cited 2024 Dec 4];22(7):925–36. Available from: https://pubmed.ncbi.nlm.nih.gov/35927150/

56. Chen K, Wang Q, Li M, Guo H, Liu W, Wang F, et al. Single-cell RNA-seq reveals dynamic change in tumor microenvironment during pancreatic ductal adenocarcinoma malignant progression. EBioMedicine [Internet]. 2021 Apr 1 [cited 2024 Dec 4];66. Available from: http://www.thelancet.com/article/S2352396421001080/fulltext

57. Karczewski KJ, Snyder MP. Integrative omics for health and disease. Nature Reviews Genetics 2018 19:5 [Internet]. 2018 Feb 26 [cited 2024 Dec 4];19(5):299–310. Available from: https://www.nature.com/articles/nrg.2018.4

58. Renz BW, Takahashi R, Tanaka T, Macchini M, Hayakawa Y, Dantes Z, et al. β2 adrenergic-neurotrophin feed-forward loop promotes pancreatic cancer. Cancer Cell [Internet]. 2018 Jan 1 [cited 2023 Sep 28];33(1):75. Available from: /pmc/articles/PMC5760435/

59. Huang FF, Cui WH, Ma LY, Chen Q, Liu Y. Crosstalk of nervous and immune systems in pancreatic cancer. Front Cell Dev Biol [Internet]. 2023 [cited 2024 Dec 16];11:1309738. Available from: https://pmc.ncbi.nlm.nih.gov/articles/PMC10720593/

60. Bockman DE. Nerves in the pancreas: what are they for? The American Journal of Surgery. 2007 Oct 1;194(4):S61–4.

61. Babic T, Travagli RA. Neural Control of the Pancreas. Pancreapedia: The Exocrine Pancreas Knowledge Base [Internet]. 2016 [cited 2025 Apr 20]; Available from: http://pancreapedia.org/?q=node/9486

62. Iyengar S, Ossipov MH, Johnson KW. The role of calcitonin gene–related peptide in peripheral and central pain mechanisms including migraine. Pain [Internet]. 2017 Apr 1 [cited 2025 Apr 20];158(4):543. Available from: https://pmc.ncbi.nlm.nih.gov/articles/PMC5359791/

63. Weitz J, Garg B, Tiriac H, Martsinkovskiy A, Patel S, Lowy A. Pancreatic Ductal Adenocarcinoma Induces Neural Injury that Promotes a Transcriptomic and Functional Repair Signature by Peripheral Neuroglia. Res Sq [Internet]. 2023 Mar 28 [cited 2025 Apr 19]; Available from: https://pubmed.ncbi.nlm.nih.gov/37034696/

64. Stopczynski RE, Normolle DP, Hartman DJ, Ying H, DeBerry JJ, Bielefeldt K, et al. Neuroplastic changes occur early in the development of pancreatic

ductal adenocarcinoma. Cancer Res [Internet]. 2014 Mar 15 [cited 2025 Apr 19];74(6):1718. Available from: https://pmc.ncbi.nlm.nih.gov/articles/PMC4036226/

65. Demir IE, Friess H, Ceyhan GO. Neural plasticity in pancreatitis and pancreatic cancer. Nature Reviews Gastroenterology & Hepatology 2015 12:11 [Internet]. 2015 Oct 13 [cited 2024 Dec 4];12(11):649–59. Available from: https://www.nature.com/articles/nrgastro.2015.166

66. Jurcak N, Zheng L. Signaling in the Microenvironment of Pancreatic Cancer: Transmitting Along the Nerve. Pharmacol Ther [Internet]. 2019 Aug 1 [cited 2024 Dec 16];200:126. Available from: https://pmc.ncbi.nlm.nih.gov/articles/PMC6626552/

67. Bapat AA, Hostetter G, Von Hoff DD, Han H. Perineural invasion and associated pain in pancreatic cancer. Nature Reviews Cancer 2011 11:10 [Internet]. 2011 Sep 23 [cited 2025 Apr 19];11(10):695–707. Available from: https://www.nature.com/articles/nrc3131

68. Chaudhary PK, Kim S. An Insight into GPCR and G-Proteins as Cancer Drivers. Cells [Internet]. 2021 Dec 1 [cited 2024 Dec 4];10(12):3288. Available from: https://pmc.ncbi.nlm.nih.gov/articles/PMC8699078/

69. Muñoz M, Coveñas R. Neurokinin-1 Receptor: A New Promising Target in the Treatment of Cancer. Discov Med. 2010 Oct 8;10(53):305–13.

70. Rosso M, Muñoz M, Berger M. The Role of Neurokinin-1 Receptor in the Microenvironment of Inflammation and Cancer. The Scientific World Journal [Internet]. 2012 [cited 2024 Dec 4];2012:381434. Available from: https://pmc.ncbi.nlm.nih.gov/articles/PMC3322385/

71. Douglas SD, Leeman SE. Neurokinin-1 receptor: functional significance in the immune system in reference to selected infections and inflammation. Ann N Y Acad Sci [Internet]. 2011 [cited 2024 Dec 4];1217(1):83–95. Available from: https://pubmed.ncbi.nlm.nih.gov/21091716/

72. Coveñas R, Muñoz M. Cancer progression and substance P. Histol Histopathol [Internet]. 2014 [cited 2024 Dec 4];29(7):881–90. Available from: https://pubmed.ncbi.nlm.nih.gov/24535838/

73. Zhu Z, Friess H, diMola FF, Zimmermann A, Graber HU, Korc M, et al. Nerve growth factor expression correlates with perineural invasion and pain in human pancreatic cancer. J Clin Oncol [Internet]. 1999 [cited 2024 Dec

4];17(8):2419–28. Available from: https://pubmed.ncbi.nlm.nih.gov/10561305/

74. Berger M, Neth O, Ilmer M, Garnier A, Salinas-Martín MV, De Agustín Asencio JC, et al. Hepatoblastoma cells express truncated neurokinin-1 receptor and can be growth inhibited by aprepitant in vitro and in vivo. J Hepatol [Internet]. 2014 May 1 [cited 2023 Jun 9];60(5):985–94. Available from: http://www.journal-of-hepatology.eu/article/S016882781400004X/fulltext

75. Navarro P, Ramkissoon SH, Shah S, Park JM, Murthy RG, Patel SA, et al. An indirect role for the oncomir-519b in the expression of truncated neurokinin-1 in breast cancer cells. Exp Cell Res [Internet]. 2012;318(20):2604–15. Available from: http://dx.doi.org/10.1016/j.yexcr.2012.09.002

76. Liu X, Zhang L, Tong Y, Yu M, Wang M, Dong D, et al. MicroRNA-22 inhibits proliferation, invasion and metastasis of breast cancer cells through targeting truncated neurokinin-1 receptor and ERα. Life Sci. 2019;217(November 2018):57–69.

77. Zhou Y, Zhao L, Xiong T, Chen X, Zhang Y, Yu M, et al. Roles of full-length and truncated neurokinin-1 receptors on tumor progression and distant metastasis in human breast cancer. Breast Cancer Res Treat [Internet]. 2013 Jul [cited 2024 Dec 13];140(1):49–61. Available from: https://pubmed.ncbi.nlm.nih.gov/23807418/

78. Garnier A, Ilmer M, Becker K, Häberle B, Von Schweinitz D, Kappler R, et al. Truncated neurokinin-1 receptor is an ubiquitous antitumor target in hepatoblastoma, and its expression is independent of tumor biology and stage. Oncol Lett [Internet]. 2016 Jan 1 [cited 2023 Jun 9];11(1):870. Available from: /pmc/articles/PMC4726931/

79. Wang Y, O'Harte F, Conlon JM. Structural characterization of tachykinins (neuropeptide gamma, neurokinin A, and substance P) from a reptile, Alligator mississipiensis. Gen Comp Endocrinol [Internet]. 1992 [cited 2024 Dec 5];88(2):277–86. Available from: https://pubmed.ncbi.nlm.nih.gov/1282482/

80. Conlon JM. The Tachykinin Peptide Family, with Particular Emphasis on Mammalian Tachykinins and Tachykinin Receptor Agonists. 2004 [cited 2024 Dec 5];25–61. Available from: https://link.springer.com/chapter/10.1007/978-3-642-18891-6_2

81. Suvas S. Role of Substance P Neuropeptide in Inflammation, Wound Healing, and Tissue Homeostasis. J Immunol [Internet]. 2017 Sep 1 [cited 2024

Dec 5];199(5):1543–52. Available from: https://pubmed.ncbi.nlm.nih.gov/28827386/

82. Kellstein DE, Price DD, Hayes RL, Mayer DJ. Evidence that substance P selectively modulates C-fiber-evoked discharges of dorsal horn nociceptive neurons. Brain Res [Internet]. 1990 Sep 3 [cited 2024 Dec 5];526(2):291–8. Available from: https://pubmed.ncbi.nlm.nih.gov/1701684/

83. Cao YQ, Mantyh PW, Carlson EJ, Gillespie AM, Epstein CJ, Basbaum AI. Primary afferent tachykinins are required to experience moderate to intense pain. Nature 1998 392:6674 [Internet]. 1998 Mar 26 [cited 2024 Dec 5];392(6674):390–4. Available from: https://www.nature.com/articles/32897

84. Birklein F, Schmelz M. Neuropeptides, neurogenic inflammation and complex regional pain syndrome (CRPS). Neurosci Lett. 2008 Jun 6;437(3):199–202.

85. Hon WK, Pothoulakis C. Immunomodulatory Properties of Substance P. Ann N Y Acad Sci [Internet]. 2006 Nov 1 [cited 2024 Dec 5];1088(1):23–40. Available from: https://onlinelibrary.wiley.com/doi/full/10.1196/annals.1366.024

86. Sanders KM, Koh SD, Ro S, Ward SM. Regulation of gastrointestinal motility--insights from smooth muscle biology. Nat Rev Gastroenterol Hepatol [Internet]. 2012 Nov [cited 2024 Dec 5];9(11):633–45. Available from: https://pubmed.ncbi.nlm.nih.gov/22965426/

87. Humes C, Sic A, Knezevic NN. Substance P's Impact on Chronic Pain and Psychiatric Conditions—A Narrative Review. Int J Mol Sci [Internet]. 2024 Jun 1 [cited 2024 Dec 5];25(11):5905. Available from: https://pmc.ncbi.nlm.nih.gov/articles/PMC11172719/

88. Li M, Zhong X, Xu WT. Substance P promotes the progression of bronchial asthma through activating the PI3K/AKT/NF-κB pathway mediated cellular inflammation and pyroptotic cell death in bronchial epithelial cells. Cell Cycle [Internet]. 2022 [cited 2024 Dec 5];21(20):2179–91. Available from: https://pubmed.ncbi.nlm.nih.gov/35726575/

89. Patel M, Subas SV, Ghani MR, Busa V, Dardeir A, Marudhai S, et al. Role of Substance P in the Pathophysiology of Inflammatory Bowel Disease and Its Correlation With the Degree of Inflammation. Cureus [Internet]. 2020 Oct 18 [cited 2024 Dec 5];12(10):e11027. Available from: https://pmc.ncbi.nlm.nih.gov/articles/PMC7671294/

90. Onaga T. Tachykinin: Recent developments and novel roles in health and disease. Biomol Concepts [Internet]. 2014 Jun 1 [cited 2024 Dec 5];5(3):225–43. Available from: https://www.degruyter.com/document/doi/10.1515/bmc-2014-0008/html?srsltid=AfmBOoqZgPxlnLO8_0AFlFUImGKhid8N6Nopw28LSv5hasrIufw5Dbi2

91. Kriska T, Natarajan J, Herrnreiter A, Park SK, Pfister SL, Thomas MJ, et al. Cellular metabolism of substance P produces neurokinin-1 receptor peptide agonists with diminished cyclic AMP signaling. Am J Physiol Cell Physiol [Internet]. 2024 Jul 1 [cited 2024 Dec 5];327(1):C151–67. Available from: https://pubmed.ncbi.nlm.nih.gov/38798270/

92. Gayen A, Goswami SK, Mukhopadhyay C. NMR evidence of GM1-induced conformational change of Substance P using isotropic bicelles. Biochimica et Biophysica Acta (BBA) - Biomembranes. 2011 Jan 1;1808(1):127–39.

93. McIntire WE. Structural determinants involved in the formation and activation of G protein betagamma dimers. Neurosignals [Internet]. 2009 Feb [cited 2024 Dec 5];17(1):82–99. Available from: https://pubmed.ncbi.nlm.nih.gov/19212142/

94. Rozengurt E. Neurokinin 1 receptor desensitization and resensitization: is it all happening at the membrane? Focus on “Protein phosphatase 2A mediates resensitization of the neurokinin 1 receptor.” Am J Physiol Cell Physiol [Internet]. 2011 Oct [cited 2025 Apr 20];301(4). Available from: https://pubmed.ncbi.nlm.nih.gov/21832247/

95. DeWire SM, Ahn S, Lefkowitz RJ, Shenoy SK. Beta-arrestins and cell signaling. Annu Rev Physiol [Internet]. 2007 [cited 2025 Apr 19];69:483–510. Available from: https://pubmed.ncbi.nlm.nih.gov/17305471/

96. Lai JP, Lai S, Tuluc F, Tansky MF, Kilpatrick LE, Leeman SE, et al. Differences in the length of the carboxyl terminus mediate functional properties of neurokinin-1 receptor. Proc Natl Acad Sci U S A [Internet]. 2008 Aug 26 [cited 2024 Dec 4];105(34):12605–10. Available from: https://pubmed.ncbi.nlm.nih.gov/18713853/

97. Rodríguez FD, Coveñas R. The Neurokinin-1 Receptor: Structure Dynamics and Signaling. Receptors 2022, Vol 1, Pages 54-71 [Internet]. 2022 Oct 8 [cited 2024 Dec 4];1(1):54–71. Available from: https://www.mdpi.com/2813-2564/1/1/4/htm

98. Maggi CA. The mammalian tachykinin receptors. General Pharmacology: The Vascular System. 1995 Sep 1;26(5):911–44.

99. Pennefather JN, Lecci A, Candenas ML, Patak E, Pinto FM, Maggi CA. Tachykinins and tachykinin receptors: a growing family. Life Sci. 2004 Feb 6;74(12):1445–63.

100. Woolley MJ, Conner AC. Understanding the common themes and diverse roles of the second extracellular loop (ECL2) of the GPCR super-family. Mol Cell Endocrinol [Internet]. 2017 Jul 5 [cited 2024 Dec 4];449:3–11. Available from: https://pubmed.ncbi.nlm.nih.gov/27899324/

101. Lindström E, Von Mentzer B, Påhlman I, Ahlstedt I, Uvebrant A, Kristensson E, et al. Neurokinin 1 receptor antagonists: correlation between in vitro receptor interaction and in vivo efficacy. J Pharmacol Exp Ther [Internet]. 2007 Sep [cited 2025 May 15];322(3):1286–93. Available from: https://pubmed.ncbi.nlm.nih.gov/17575073/

102. Chen S, Lu M, Liu D, Yang L, Yi C, Ma L, et al. Human substance P receptor binding mode of the antagonist drug aprepitant by NMR and crystallography. Nat Commun [Internet]. 2019 Dec 1 [cited 2025 May 15];10(1). Available from: https://pubmed.ncbi.nlm.nih.gov/30733446/

103. RCSB PDB: Homepage [Internet]. [cited 2025 Apr 21]. Available from: https://www.rcsb.org/

104. Schöppe J, Ehrenmann J, Klenk C, Rucktooa P, Schütz M, Doré AS, et al. Crystal structures of the human neurokinin 1 receptor in complex with clinically used antagonists. Nature Communications 2019 10:1 [Internet]. 2019 Jan 3 [cited 2025 May 21];10(1):1–11. Available from: https://www.nature.com/articles/s41467-018-07939-8

105. Spitsin S, Pappa V, Douglas SD. Truncation of neurokinin-1 receptor-Negative regulation of substance P signaling. J Leukoc Biol [Internet]. 2018 Jun 1 [cited 2024 Dec 4];103(6):1043–51. Available from: https://pubmed.ncbi.nlm.nih.gov/29345372/

106. Meza U, Thapliyal A, Bannister RA, Adams BA. Neurokinin 1 receptors trigger overlapping stimulation and inhibition of CaV2.3 (R-type) calcium channels. Mol Pharmacol [Internet]. 2007 [cited 2024 Dec 4];71(1):284–93. Available from: https://pubmed.ncbi.nlm.nih.gov/17050807/

107. Grady EF, Garland AM, Gamp PD, Lovett M, Payan DG, Bunnett NW. Delineation of the endocytic pathway of substance P and its seven-transmembrane domain NK1 receptor. Mol Biol Cell [Internet]. 1995 [cited 2025 Apr 19];6(5):509. Available from: https://pmc.ncbi.nlm.nih.gov/articles/PMC301212/

108. Guo Y, Pan W, Liu S, Shen Z, Xu Y, Hu L. ERK/MAPK signalling pathway and tumorigenesis. Exp Ther Med [Internet]. 2020 Jan 15 [cited 2024 Dec 4];19(3). Available from: https://pubmed.ncbi.nlm.nih.gov/32104259/

109. Caberlotto L, Hurd YL, Murdock P, Wahlin JP, Melotto S, Corsi M, et al. Neurokinin 1 receptor and relative abundance of the short and long isoforms in the human brain. Eur J Neurosci [Internet]. 2003 May [cited 2024 Dec 4];17(9):1736–46. Available from: https://pubmed.ncbi.nlm.nih.gov/12752772/

110. Kanduluru AK, Low PS. Development of a Ligand-Targeted Therapeutic Agent for Neurokinin-1 Receptor Expressing Cancers. Mol Pharm [Internet]. 2017 Nov 6 [cited 2024 Dec 4];14(11):3859–65. Available from: https://pubmed.ncbi.nlm.nih.gov/28969417/

111. Berger M, Von Schweinitz D. Therapeutic Innovations for Targeting Childhood Neuroblastoma: Implications of the Neurokinin-1 Receptor System. Anticancer Res [Internet]. 2017 Nov 1 [cited 2024 Dec 4];37(11):5911–8. Available from: https://pubmed.ncbi.nlm.nih.gov/29061769/

112. Lappano R, Maggiolini M. GPCRs and cancer. Acta Pharmacologica Sinica 2012 33:3 [Internet]. 2012 Jan 23 [cited 2024 Dec 13];33(3):351–62. Available from: https://www.nature.com/articles/aps2011183

113. Garnier A, Vykoukal J, Hubertus J, Alt E, Von Schweinitz D, Kappler R, et al. Targeting the neurokinin-1 receptor inhibits growth of human colon cancer cells. Int J Oncol [Internet]. 2015 Jul 1 [cited 2024 Dec 13];47(1):151–60. Available from: http://www.spandidos-publications.com/10.3892/ijo.2015.3016/abstract

114. Muñoz MF, Argüelles S, Rosso M, Medina R, Coveñas R, Ayala A, et al. The Neurokinin-1 Receptor Is Essential for the Viability of Human Glioma Cells: A Possible Target for Treating Glioblastoma. Biomed Res Int [Internet]. 2022 [cited 2024 Dec 13];2022:6291504. Available from: https://pmc.ncbi.nlm.nih.gov/articles/PMC9006081/

115. Zhang XW, Li L, Hu WQ, Hu MN, Tao Y, Hu H, et al. Neurokinin-1 receptor promotes non-small cell lung cancer progression through transactivation of EGFR. Cell Death Dis [Internet]. 2022 Jan 1 [cited 2024 Dec 13];13(1):41. Available from: https://pmc.ncbi.nlm.nih.gov/articles/PMC8748918/

116. Coveñas R, Rodríguez FD, Robinson P, Muñoz M. The Repurposing of Non-Peptide Neurokinin-1 Receptor Antagonists as Antitumor Drugs: An Urgent Challenge for Aprepitant. Int J Mol Sci [Internet]. 2023 Nov 1 [cited

2025 Apr 18];24(21). Available from: https://pubmed.ncbi.nlm.nih.gov/37958914/

117. Ilmer M, Boiles AR, Regel I, Yokoi K, Michalski CW, Wistuba II, et al. RSPO2 Enhances Canonical Wnt Signaling to Confer Stemness-Associated Traits to Susceptible Pancreatic Cancer Cells. Cancer Res [Internet]. 2015 May 1 [cited 2025 Apr 19];75(9):1883–96. Available from: https://pubmed.ncbi.nlm.nih.gov/25769727/

118. Primer designing tool [Internet]. [cited 2025 May 20]. Available from: https://www.ncbi.nlm.nih.gov/tools/primer-blast/

119. Kolorz J, Demir S, Gottschlich A, Beirith I, Ilmer M, Lüthy D, et al. The Neurokinin-1 Receptor Is a Target in Pediatric Rhabdoid Tumors. Curr Oncol [Internet]. 2021 Jan 1 [cited 2023 Jun 1];29(1):94–110. Available from: https://pubmed.ncbi.nlm.nih.gov/35049682/

120. Galaxy [Internet]. [cited 2025 Apr 18]. Available from: https://usegalaxy.eu/

121. Afgan E, Baker D, Batut B, Van Den Beek M, Bouvier D, Ech M, et al. The Galaxy platform for accessible, reproducible and collaborative biomedical analyses: 2018 update. Nucleic Acids Res [Internet]. 2018 Jul 2 [cited 2025 May 15];46(W1):W537–44. Available from: https://pubmed.ncbi.nlm.nih.gov/29790989/

122. Home - SRA - NCBI [Internet]. [cited 2025 Apr 18]. Available from: https://www.ncbi.nlm.nih.gov/sra

123. Batut B, Freeberg M, Heydarian M, Erxleben A, Videm P, Blank C, et al. Hands-on: Reference-based RNA-Seq data analysis [Internet]. 2025 [cited 2025 Apr 18]. Available from: https://training.galaxyproject.org/training-material/topics/transcriptomics/tutorials/ref-based/tutorial.html

124. Chen S, Zhou Y, Chen Y, Gu J, Biotechnology H. fastp: an ultra-fast all-in-one FASTQ preprocessor. bioRxiv [Internet]. 2018 Apr 9 [cited 2025 Apr 18];274100. Available from: https://www.biorxiv.org/content/10.1101/274100v2

125. Gallardo C, Delisle L, Videm P. Genome-wide alternative splicing analysis [Internet]. 2025 [cited 2025 Apr 21]. Available from: https://training.galaxyproject.org/training-material/topics/transcriptomics/tutorials/differential-isoform-expression/tutorial.html

126. Turner JP, Smith BJ. Letter codes, structures, masses, and derivatives of amino acids. Applied Biochemistry and Biotechnology - Part B Molecular

Biotechnology [Internet]. 1997 [cited 2025 May 15];8(3):233–47. Available from: https://link.springer.com/article/10.1007/BF02760777

127. Monkman JH, Thompson EW, Nagaraj SH. Targeting Epithelial Mesenchymal Plasticity in Pancreatic Cancer: A Compendium of Preclinical Discovery in a Heterogeneous Disease. Cancers (Basel) [Internet]. 2019 Nov 1 [cited 2025 Apr 19];11(11). Available from: https://pubmed.ncbi.nlm.nih.gov/31703358/

128. Dardare J, Witz A, Merlin JL, Bochnakian A, Toussaint P, Gilson P, et al. Epithelial to Mesenchymal Transition in Patients with Pancreatic Ductal Adenocarcinoma: State-of-the-Art and Therapeutic Opportunities. Pharmaceuticals [Internet]. 2021 Aug 1 [cited 2025 May 19];14(8):740. Available from: https://pmc.ncbi.nlm.nih.gov/articles/PMC8399337/

129. Dijk F, Veenstra VL, Soer EC, Dings MPG, Zhao L, Halfwerk JB, et al. Unsupervised class discovery in pancreatic ductal adenocarcinoma reveals cell-intrinsic mesenchymal features and high concordance between existing classification systems. Scientific Reports 2020 10:1 [Internet]. 2020 Jan 15 [cited 2025 Apr 19];10(1):1–12. Available from: https://www.nature.com/articles/s41598-019-56826-9

130. Sinha A, Cherba D, Bartlam H, Lenkiewicz E, Evers L, Barrett MT, et al. Mesenchymal-like pancreatic cancer cells harbor specific genomic alterations more frequently than their epithelial-like counterparts. Mol Oncol [Internet]. 2014 Oct 1 [cited 2025 May 15];8(7):1253. Available from: https://pmc.ncbi.nlm.nih.gov/articles/PMC4198499/

131. Muñoz M, Rosso M. The NK-1 receptor antagonist aprepitant as a broad spectrum antitumor drug. Invest New Drugs [Internet]. 2010 Apr [cited 2025 Apr 19];28(2):187–93. Available from: https://pubmed.ncbi.nlm.nih.gov/19148578/

132. Sousa CM, Biancur DE, Wang X, Halbrook CJ, Sherman MH, Zhang L, et al. Pancreatic stellate cells support tumour metabolism through autophagic alanine secretion. Nature [Internet]. 2016 Aug 10 [cited 2025 Apr 19];536(7617):479–83. Available from: https://pubmed.ncbi.nlm.nih.gov/27509858/

133. Ishiguro T, Ohata H, Sato A, Yamawaki K, Enomoto T, Okamoto K. Tumor-derived spheroids: Relevance to cancer stem cells and clinical applications. Cancer Sci [Internet]. 2017 Mar 1 [cited 2025 Apr 19];108(3):283–9. Available from: https://pubmed.ncbi.nlm.nih.gov/28064442/

134. Rajendran V, Jain MV. In Vitro Tumorigenic Assay: Colony Forming Assay for Cancer Stem Cells. Methods Mol Biol [Internet]. 2018 [cited 2025 Apr 19];1692:89–95. Available from: https://pubmed.ncbi.nlm.nih.gov/28986889/

135. Al-Ghamdi S, Cachat J, Albasri A, Ahmed M, Jackson D, Zaitoun A, et al. C-terminal tensin-like gene functions as an oncogene and promotes cell motility in pancreatic cancer. Pancreas [Internet]. 2013 Jan [cited 2025 May 16];42(1):135–40. Available from: https://pubmed.ncbi.nlm.nih.gov/22750970/

136. Kashiwagi R, Funayama R, Aoki S, Matsui A, Klein S, Sato Y, et al. Collagen XVII regulates tumor growth in pancreatic cancer through interaction with the tumor microenvironment. Cancer Sci [Internet]. 2023 Nov 1 [cited 2025 May 16];114(11):4286. Available from: https://pmc.ncbi.nlm.nih.gov/articles/PMC10637054/

137. Le K, Wang J, Zhang T, Guo Y, Chang H, Wang S, et al. Overexpression of Mesothelin in Pancreatic Ductal Adenocarcinoma (PDAC). Int J Med Sci [Internet]. 2020 [cited 2025 May 16];17(4):422. Available from: https://pmc.ncbi.nlm.nih.gov/articles/PMC7053310/

138. Bhasin MK, Ndebele K, Bucur O, Yee EU, Otu HH, Plati J, et al. Meta-analysis of transcriptome data identifies a novel 5-gene pancreatic adenocarcinoma classifier. Oncotarget [Internet]. 2016 Apr 26 [cited 2025 May 16];7(17):23263–81. Available from: https://pubmed.ncbi.nlm.nih.gov/26993610/

139. Long J, Zhang Z, Liu Z, Xu Y, Ge C. Identification of genes and pathways associated with pancreatic ductal adenocarcinoma by bioinformatics analyses. Oncol Lett [Internet]. 2015 Feb 1 [cited 2025 May 14];11(2):1391. Available from: https://pmc.ncbi.nlm.nih.gov/articles/PMC4734321/

140. Nwosu ZC, Giza HM, Nassif M, Charlestin V, Menjivar RE, Kim D, et al. Multidimensional analyses identify genes of high priority for pancreatic cancer research. JCI Insight [Internet]. 2025 Feb 24 [cited 2025 May 14];10(4):e174264. Available from: https://pmc.ncbi.nlm.nih.gov/articles/PMC11949049/

141. Lv K, Yang J, Sun J, Guan J. Identification of key candidate genes for pancreatic cancer by bioinformatics analysis. Exp Ther Med [Internet]. 2019 May 28 [cited 2025 May 14];18(1):451. Available from: https://pmc.ncbi.nlm.nih.gov/articles/PMC6580103/

142. Lottaz C, Toedling J, Spang R. Annotation-based distance measures for patient subgroup discovery in clinical microarray studies. Bioinformatics [Internet]. 2007 Sep 1 [cited 2025 May 14];23(17):2256–64. Available from: https://pubmed.ncbi.nlm.nih.gov/17586546/

143. Wright G, Tan B, Rosenwald A, Hurt EH, Wiestner A, Staudt LM. A gene expression-based method to diagnose clinically distinct subgroups of diffuse large B cell lymphoma. Proc Natl Acad Sci U S A [Internet]. 2003 Aug 19 [cited 2025 May 14];100(17):9991–6. Available from: https://www.pnas.org/doi/abs/10.1073/pnas.1732008100

144. Lusa L, McShane LM, Reid JF, De Cecco L, Ambrogi F, Biganzoli E, et al. Challenges in projecting clustering results across gene expression-profiling datasets. J Natl Cancer Inst [Internet]. 2007 Nov [cited 2025 May 14];99(22):1715–23. Available from: https://pubmed.ncbi.nlm.nih.gov/18000217/

145. Sun H, Dai X, Han B. TRIM29 as a Novel Biomarker in Pancreatic Adenocarcinoma. Dis Markers [Internet]. 2014 [cited 2025 May 16];2014:317817. Available from: https://pmc.ncbi.nlm.nih.gov/articles/PMC4016900/

146. Wang L, Yang H, Palmbos PL, Ney G, Detzler TA, Coleman D, et al. ATDC/TRIM29 phosphorylation by ATM/MAPKAP kinase 2 mediates radioresistance in pancreatic cancer cells. Cancer Res [Internet]. 2014 Mar 15 [cited 2025 May 16];74(6):1778. Available from: https://pmc.ncbi.nlm.nih.gov/articles/PMC3961828/

147. Chen G, Song H, Yang Z, Du T, Zheng Y, Lu Z, et al. AQP5 Is a Novel Prognostic Biomarker in Pancreatic Adenocarcinoma. Front Oncol [Internet]. 2022 May 10 [cited 2025 May 16];12:890193. Available from: https://pmc.ncbi.nlm.nih.gov/articles/PMC9128544/

148. Wu W, Li Q, Zhu Z, Li C, Lu P, Zhou X, et al. HTR1D functions as a key target of HOXA10-AS/miR-340-3p axis to promote the malignant outcome of pancreatic cancer via PI3K-AKT signaling pathway. Int J Biol Sci [Internet]. 2022 [cited 2025 May 16];18(9):3777–94. Available from: https://pubmed.ncbi.nlm.nih.gov/35813473/

149. Chang DZ, Ma Y, Ji B, Liu Y, Hwu P, Abbruzzese JL, et al. Increased CDC20 expression is associated with pancreatic ductal adenocarcinoma differentiation and progression. J Hematol Oncol [Internet]. 2012 [cited 2025 May 16];5:15. Available from: https://pmc.ncbi.nlm.nih.gov/articles/PMC3350393/

150. Xiong Y, Kong X, Tu S, Xin W, Wei Y, Yi S, et al. LINC02086 inhibits ferroptosis and promotes malignant phenotypes of pancreatic cancer via miR-342-3p/CA9 axis. Funct Integr Genomics [Internet]. 2024 Apr 1 [cited 2025 May 16];24(2). Available from: https://pubmed.ncbi.nlm.nih.gov/38438595/

151. Xiao S, Yang C, Zhang Y, Lai C. Downregulation of B3GNT6 is a predictor of poor outcomes in patients with colorectal cancer. World J Surg Oncol [Internet]. 2022 Dec 1 [cited 2025 May 16];20(1):110. Available from: https://pmc.ncbi.nlm.nih.gov/articles/PMC8988341/

152. Cao P, Wu Y, Sun D, Zhang W, Qiu J, Tang Z, et al. IGF2BP2 promotes pancreatic carcinoma progression by enhancing the stability of B3GNT6 mRNA via m6A methylation. Cancer Med [Internet]. 2022 Feb 1 [cited 2025 May 16];12(4):4405. Available from: https://pmc.ncbi.nlm.nih.gov/articles/PMC9972174/

153. Coothankandaswamy V, Cao S, Xu Y, Prasad PD, Singh PK, Reynolds CP, et al. Amino acid transporter SLC6A14 is a novel and effective drug target for pancreatic cancer. Br J Pharmacol [Internet]. 2016 [cited 2025 May 16];173(23):3292–306. Available from: https://pubmed.ncbi.nlm.nih.gov/27747870/

154. Wei W, Liu Y, Lu Y, Yang B, Tang L. LncRNA XIST Promotes Pancreatic Cancer Proliferation Through miR-133a/EGFR. J Cell Biochem [Internet]. 2017 Oct 1 [cited 2025 May 16];118(10):3349–58. Available from: https://pubmed.ncbi.nlm.nih.gov/28295543/

155. Cheng K, Pan J, Liu Q, Ji Y, Liu L, Guo X, et al. Exosomal lncRNA XIST promotes perineural invasion of pancreatic cancer cells via miR-211-5p/GDNF. Oncogene [Internet]. 2024 May 2 [cited 2025 May 16];43(18):1341–52. Available from: https://pubmed.ncbi.nlm.nih.gov/38454138/

156. Zhang R, Liu Q, Peng J, Wang M, Li T, Liu J, et al. CXCL5 overexpression predicts a poor prognosis in pancreatic ductal adenocarcinoma and is correlated with immune cell infiltration. J Cancer [Internet]. 2020 [cited 2025 May 16];11(9):2371. Available from: https://pmc.ncbi.nlm.nih.gov/articles/PMC7065995/

157. Cunningham CM, Li M, Ruffenach G, Doshi M, Aryan L, Hong J, et al. Y-Chromosome Gene, Uty, Protects Against Pulmonary Hypertension by Reducing Proinflammatory Chemokines. Am J Respir Crit Care Med [Internet].

2022 Jul 15 [cited 2025 May 16];206(2):186–96. Available from: https://pubmed.ncbi.nlm.nih.gov/35504005/

158. Khani F, Nafian S, Mollamohammadi S, Nemati S, Shokoohian B, Hassani SN, et al. Y Chromosome Genes May Play Roles in the Development of Neural Rosettes from Human Embryonic Stem Cells. Stem Cell Rev Rep [Internet]. 2022 Dec 1 [cited 2025 May 16];18(8):3008–20. Available from: https://pubmed.ncbi.nlm.nih.gov/35661078/

159. Godfre AK, Naqvi S, Chmátal L, Chic JM, Mitchel RN, Gyg SP, et al. Quantitative analysis of Y-Chromosome gene expression across 36 human tissues. Genome Res [Internet]. 2020 Jun 1 [cited 2025 May 16];30(6):860–73. Available from: https://pubmed.ncbi.nlm.nih.gov/32461223/

160. Wu H, Tian W, Tai X, Li X, Li Z, Shui J, et al. Identification and functional analysis of novel oncogene DDX60L in pancreatic ductal adenocarcinoma. BMC Genomics [Internet]. 2021 Dec 1 [cited 2025 May 16];22(1):1–14. Available from: https://bmcgenomics.biomedcentral.com/articles/10.1186/s12864-021-08137-5

161. Gendrel AV, Heard E. Noncoding RNAs and epigenetic mechanisms during X-chromosome inactivation. Annu Rev Cell Dev Biol [Internet]. 2014 [cited 2025 May 14];30:561–80. Available from: https://pubmed.ncbi.nlm.nih.gov/25000994/

162. Xia ZN, Wang XY, Cai LC, Jian WG, Zhang C. IGLL5 is correlated with tumor-infiltrating immune cells in clear cell renal cell carcinoma. FEBS Open Bio [Internet]. 2021 Mar 1 [cited 2025 May 16];11(3):898–910. Available from: https://pubmed.ncbi.nlm.nih.gov/33449444/

163. Smilevska T, Tsakou E, Hadzidimitriou A, Bikos V, Stavroyianni N, Laoutaris N, et al. Immunoglobulin kappa gene repertoire and somatic hypermutation patterns in follicular lymphoma. Blood Cells Mol Dis [Internet]. 2008 Sep [cited 2025 May 16];41(2):215–8. Available from: https://pubmed.ncbi.nlm.nih.gov/18640859/

164. Mason DY, Cordell JL, Brown MH, Borst J, Jones M, Pulford K, et al. CD79a: A Novel Marker for B-Cell Neoplasms in Routinely Processed Tissue Samples. Blood. 1995 Aug 15;86(4):1453–9.

165. SHISA8 shisa family member 8 [Homo sapiens (human)] - Gene - NCBI [Internet]. 2025 [cited 2025 May 16]. Available from: https://www.ncbi.nlm.nih.gov/gene/440829

166. Hirai H, Pang Z, Bao D, Miyazaki T, Li L, Miura E, et al. Cbln1 is essential for synaptic integrity and plasticity in the cerebellum. Nat Neurosci [Internet]. 2005 Nov [cited 2025 May 16];8(11):1534–41. Available from: https://pubmed.ncbi.nlm.nih.gov/16234806/

167. Kim M, Kim DJ. GFRA1: A Novel Molecular Target for the Prevention of Osteosarcoma Chemoresistance. Int J Mol Sci [Internet]. 2018 Apr 4 [cited 2025 May 16];19(4). Available from: https://pubmed.ncbi.nlm.nih.gov/29617307/

168. Sasaki K, Kurahara H, Young ED, Natsugoe S, Ijichi A, Iwakuma T, et al. Genome-wide in vivo RNAi screen identifies ITIH5 as a metastasis suppressor in pancreatic cancer. Clin Exp Metastasis [Internet]. 2017 Apr 1 [cited 2025 May 16];34(3–4):229–39. Available from: https://pubmed.ncbi.nlm.nih.gov/28289921/

169. Satoh K, Hamada S, Shimosegawa T. Involvement of epithelial to mesenchymal transition in the development of pancreatic ductal adenocarcinoma. J Gastroenterol [Internet]. 2015 Feb 1 [cited 2025 May 21];50(2):140–6. Available from: https://pubmed.ncbi.nlm.nih.gov/25216997/

170. Terry S, Savagner P, Ortiz-Cuaran S, Mahjoubi L, Saintigny P, Thiery JP, et al. New insights into the role of EMT in tumor immune escape. Mol Oncol [Internet]. 2017 Jul 1 [cited 2025 May 21];11(7):824–46. Available from: https://pubmed.ncbi.nlm.nih.gov/28614624/

171. Thangavelu PU, Krenács T, Dray E, Duijf PHG. In epithelial cancers, aberrant COL17A1 promoter methylation predicts its misexpression and increased invasion. Clin Epigenetics [Internet]. 2016 Nov 18 [cited 2025 May 21];8(1). Available from: https://pubmed.ncbi.nlm.nih.gov/27891193/

172. Watanabe M, Kosumi H, Osada SI, Takashima S, Wang Y, Nishie W, et al. Type XVII collagen interacts with the aPKC-PAR complex and maintains epidermal cell polarity. Exp Dermatol [Internet]. 2021 Jan 1 [cited 2025 May 21];30(1):62–7. Available from: https://pubmed.ncbi.nlm.nih.gov/32970880/

173. Liu Y, Ho C, Wen D, Sun J, Huang L, Gao Y, et al. Targeting the stem cell niche: role of collagen XVII in skin aging and wound repair. Theranostics [Internet]. 2022 [cited 2025 May 21];12(15):6446–54. Available from: https://pubmed.ncbi.nlm.nih.gov/36185608/

174. Jones VA, Patel PM, Gibson FT, Cordova A, Amber KT. The Role of Collagen XVII in Cancer: Squamous Cell Carcinoma and Beyond. Front Oncol

[Internet]. 2020 Mar 19 [cited 2025 May 21];10. Available from: https://pubmed.ncbi.nlm.nih.gov/32266137/

175. Chae YK, Woo J, Kim MJ, Kang SK, Kim MS, Lee J, et al. Expression of aquaporin 5 (AQP5) promotes tumor invasion in human non small cell lung cancer. PLoS One [Internet]. 2008 May 14 [cited 2025 May 21];3(5). Available from: https://pubmed.ncbi.nlm.nih.gov/18478076/

176. Jensen HH, Login FH, Koffman JS, Kwon TH, Nejsum LN. The role of aquaporin-5 in cancer cell migration: A potential active participant. Int J Biochem Cell Biol [Internet]. 2016 Oct 1 [cited 2025 May 21];79:271–6. Available from: https://pubmed.ncbi.nlm.nih.gov/27609140/

177. Bruno S, Ghelli Luserna di Rorà A, Napolitano R, Soverini S, Martinelli G, Simonetti G. CDC20 in and out of mitosis: a prognostic factor and therapeutic target in hematological malignancies. J Exp Clin Cancer Res [Internet]. 2022 Dec 1 [cited 2025 May 21];41(1). Available from: https://pubmed.ncbi.nlm.nih.gov/35490245/

178. Albasri A, Seth R, Jackson D, Benhasouna A, Crook S, Nateri AS, et al. C-terminal Tensin-like (CTEN) is an oncogene which alters cell motility possibly through repression of E-cadherin in colorectal cancer. J Pathol [Internet]. 2009 May [cited 2025 May 21];218(1):57–65. Available from: https://pubmed.ncbi.nlm.nih.gov/19214987/

179. Ishiwata T, Matsuda Y, Yoshimura H, Sasaki N, Ishiwata S, Ishikawa N, et al. Pancreatic cancer stem cells: features and detection methods. Pathol Oncol Res [Internet]. 2018 Oct 1 [cited 2025 May 21];24(4):797–805. Available from: https://pubmed.ncbi.nlm.nih.gov/29948612/

180. Frappart PO, Hofmann TG. Pancreatic Ductal Adenocarcinoma (PDAC) Organoids: The Shining Light at the End of the Tunnel for Drug Response Prediction and Personalized Medicine. Cancers (Basel) [Internet]. 2020 Oct 1 [cited 2023 May 17];12(10):1–18. Available from: /pmc/articles/PMC7598647/

181. Frappart PO, Walter K, Gout J, Beutel AK, Morawe M, Arnold F, et al. Pancreatic cancer-derived organoids - a disease modeling tool to predict drug response. United European Gastroenterol J [Internet]. 2020 Jun 1 [cited 2025 May 17];8(5):594–606. Available from: https://pubmed.ncbi.nlm.nih.gov/32213029/

182. Rezaei S, Javid H, Iranpour S, Darban RA, Hashemy SI. Unveiling the Promising Role of Substance P/Neurokinin 1 Receptor in Cancer Cell Proliferation and Cell Cycle Regulation in Human Malignancies. Curr Med Chem [Internet]. 2024 Jul 11 [cited 2025 May 21];31. Available from: https://pubmed.ncbi.nlm.nih.gov/38988156/

183. Zhang YX, Li XF, Yuan GQ, Hu H, Song XY, Li JY, et al. β-Arrestin 1 has an essential role in neurokinin-1 receptor-mediated glioblastoma cell proliferation and G2/M phase transition. J Biol Chem [Internet]. 2017 May 26 [cited 2025 May 21];292(21):8933–47. Available from: https://pubmed.ncbi.nlm.nih.gov/28341744/

184. Digiacomo G, Volta F, Garajova I, Balsano R, Cavazzoni A. Biological Hallmarks and New Therapeutic Approaches for the Treatment of PDAC. Life (Basel) [Internet]. 2021 Aug 1 [cited 2025 May 17];11(8). Available from: https://pubmed.ncbi.nlm.nih.gov/34440587/

185. Matsuda Y, Yoshimura H, Ishiwata T, Sumiyoshi H, Matsushita A, Nakamura Y, et al. Mitotic index and multipolar mitosis in routine histologic sections as prognostic markers of pancreatic cancers: A clinicopathological study. Pancreatology [Internet]. 2016 [cited 2025 May 17];16(1):127–32. Available from: https://pubmed.ncbi.nlm.nih.gov/26585687/

186. Lafaro KJ, Melstrom LG. The Paradoxical Web of Pancreatic Cancer Tumor Microenvironment. Am J Pathol [Internet]. 2019 Jan 1 [cited 2025 May 17];189(1):44. Available from: https://pmc.ncbi.nlm.nih.gov/articles/PMC6315325/

187. Ren B, Cui M, Yang G, Wang H, Feng M, You L, et al. Tumor microenvironment participates in metastasis of pancreatic cancer. Mol Cancer [Internet]. 2018 Jul 30 [cited 2025 May 17];17(1). Available from: https://pubmed.ncbi.nlm.nih.gov/30060755/

188. Pernot S, Evrard S, Khatib AM. The Give-and-Take Interaction Between the Tumor Microenvironment and Immune Cells Regulating Tumor Progression and Repression. Front Immunol [Internet]. 2022 Apr 13 [cited 2025 May 17];13. Available from: https://pubmed.ncbi.nlm.nih.gov/35493456/

189. Villablanca AC, Hanley MR. 17beta-estradiol stimulates substance P receptor gene expression. Mol Cell Endocrinol [Internet]. 1997 Dec 12 [cited 2025 Apr 20];135(2):109–17. Available from: https://pubmed.ncbi.nlm.nih.gov/9484906/

190. Freire VS, Burkhard FC, Kessler TM, Kuhn A, Draeger A, Monastyrskaya K. MicroRNAs May Mediate the Down-Regulation of Neurokinin-1 Receptor in Chronic Bladder Pain Syndrome. Am J Pathol [Internet]. 2010 [cited 2023 Jan 13];176(1):288. Available from: /pmc/articles/PMC2797891/

191. Eapen PM, Rao CM, Nampoothiri M. Crosstalk between neurokinin receptor signaling and neuroinflammation in neurological disorders. Rev Neurosci [Internet]. 2019 Apr 1 [cited 2025 May 17];30(3):233–43. Available from: https://pubmed.ncbi.nlm.nih.gov/30260793/

192. Ruggierii A, Anticoli S, D'ambrosio A, Giordani L, Mora M. The influence of sex and gender on immunity, infection and vaccination. Ann Ist Super Sanita [Internet]. 2016 [cited 2025 Jun 2];52(2):198–204. Available from: https://pubmed.ncbi.nlm.nih.gov/27364394/

193. Migliore L, Nicolì V, Stoccoro A. Gender Specific Differences in Disease Susceptibility: The Role of Epigenetics. Biomedicines [Internet]. 2021 Jun 1 [cited 2025 Jun 2];9(6). Available from: https://pubmed.ncbi.nlm.nih.gov/34200989/

194. Forsyth KS, Jiwrajka N, Lovell CD, Toothacre NE, Anguera MC. The conneXion between sex and immune responses. Nature Reviews Immunology 2024 24:7 [Internet]. 2024 Feb 21 [cited 2025 Jun 2];24(7):487–502. Available from: https://www.nature.com/articles/s41577-024-00996-9

195. Schnittert J, Bansal R, Prakash J. Targeting Pancreatic Stellate Cells in Cancer. Trends Cancer [Internet]. 2019 Feb 1 [cited 2025 Apr 20];5(2):128–42. Available from: https://pubmed.ncbi.nlm.nih.gov/30755305/

196. Ferdek PE, Jakubowska MA. Biology of pancreatic stellate cells-more than just pancreatic cancer. Pflugers Arch [Internet]. 2017 Sep 1 [cited 2025 May 17];469(9):1039–50. Available from: https://pubmed.ncbi.nlm.nih.gov/28382480/

197. Valkenburg KC, De Groot AE, Pienta KJ. Targeting the tumour stroma to improve cancer therapy. Nat Rev Clin Oncol [Internet]. 2018 Jun 1 [cited 2025 May 21];15(6):366–81. Available from: https://pubmed.ncbi.nlm.nih.gov/29651130/

198. Patil K, Khan FB, Akhtar S, Ahmad A, Uddin S. The plasticity of pancreatic cancer stem cells: implications in therapeutic resistance. Cancer Metastasis Rev [Internet]. 2021 Sep 1 [cited 2025 May 21];40(3):691. Available from: https://pmc.ncbi.nlm.nih.gov/articles/PMC8556195/

199. Rubin JB, Lagas JS, Broestl L, Sponagel J, Rockwell N, Rhee G, et al. Sex differences in cancer mechanisms. Biol Sex Differ [Internet]. 2020 Apr 15 [cited 2025 Apr 20];11(1):17. Available from: https://pmc.ncbi.nlm.nih.gov/articles/PMC7161126/

200. Wong ML, Medrano JF. Real-time PCR for mRNA quantitation. Biotechniques [Internet]. 2005 [cited 2025 Apr 20];39(1):75–85. Available from: https://pubmed.ncbi.nlm.nih.gov/16060372/

201. Guo Y, Xiao P, Lei S, Deng F, Xiao GG, Liu Y, et al. How is mRNA expression predictive for protein expression? A correlation study on human circulating monocytes. Acta Biochim Biophys Sin (Shanghai) [Internet]. 2008 May [cited 2025 Apr 20];40(5):426–36. Available from: https://pubmed.ncbi.nlm.nih.gov/18465028/

202. Edfors F, Danielsson F, Hallström BM, Käll L, Lundberg E, Pontén F, et al. Gene-specific correlation of RNA and protein levels in human cells and tissues. Mol Syst Biol [Internet]. 2016 Oct [cited 2025 Apr 20];12(10). Available from: https://pubmed.ncbi.nlm.nih.gov/27951527/

203. Muñoz M, Rosso M, Pérez A, Coveñas R, Rosso R, Zamarriego C, et al. The NK1 receptor is involved in the antitumoural action of L-733,060 and in the mitogenic action of substance P on neuroblastoma and glioma cell lines. Neuropeptides [Internet]. 2005 Aug [cited 2025 Apr 20];39(4):427–32. Available from: https://pubmed.ncbi.nlm.nih.gov/15939468/

204. Pelechano V, Wei W, Steinmetz LM. Extensive transcriptional heterogeneity revealed by isoform profiling. Nature 2013 497:7447 [Internet]. 2013 Apr 24 [cited 2025 Apr 20];497(7447):127–31. Available from: https://www.nature.com/articles/nature12121

205. Vogel C, Marcotte EM. Insights into the regulation of protein abundance from proteomic and transcriptomic analyses. Nature Reviews Genetics 2012 13:4 [Internet]. 2012 Mar 13 [cited 2025 Apr 20];13(4):227–32. Available from: https://www.nature.com/articles/nrg3185

206. Pandol S, Edderkaoui M, Gukovsky I, Lugea A, Gukovskaya A. Desmoplasia of Pancreatic Ductal Adenocarcinoma. Clin Gastroenterol Hepatol [Internet]. 2009 Nov [cited 2025 May 17];7(11 0):S44. Available from: https://pmc.ncbi.nlm.nih.gov/articles/PMC4573641/

207. Rucki AA, Zheng L. Pancreatic cancer stroma: Understanding biology leads to new therapeutic strategies. World Journal of Gastroenterology :

WJG [Internet]. 2014 [cited 2025 May 17];20(9):2237. Available from: https://pmc.ncbi.nlm.nih.gov/articles/PMC3942829/

208. Yu X, Abbas-Aghababazadeh F, Chen YA, Fridley BL. Statistical and Bioinformatics Analysis of Data from Bulk and Single-Cell RNA Sequencing Experiments. Methods Mol Biol [Internet]. 2021 [cited 2025 May 17];2194:143. Available from: https://pmc.ncbi.nlm.nih.gov/articles/PMC7771369/

Appendix A: Histograms to Cell Cycle Analysis

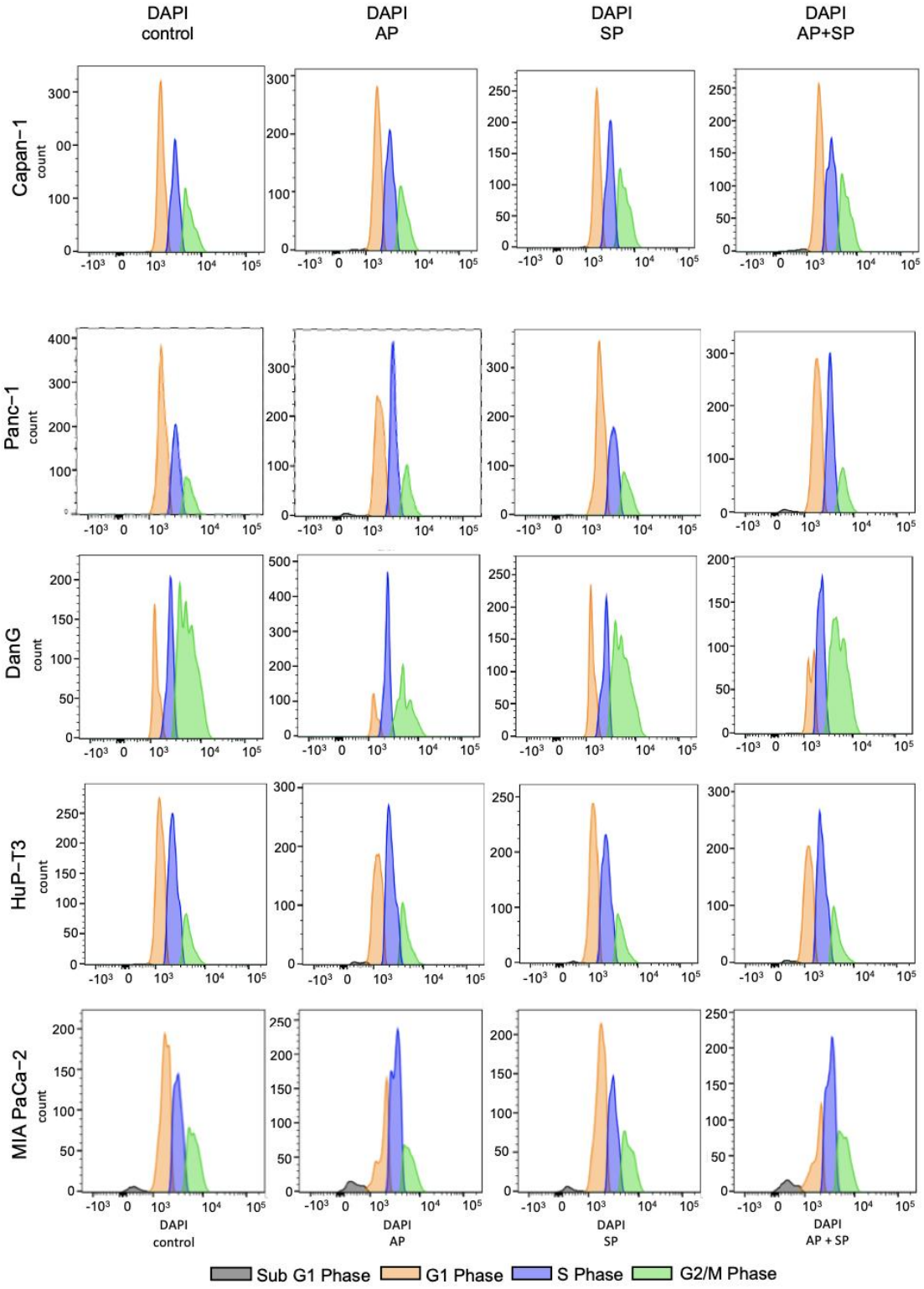

Figure 20: Histograms adding to Figure 10. Displayed is DAPI staining measured through Flow Cytometry after AP, SP, and AP+SP treatment for cell cycle analysis.

Appendix B: PRJNA1133919: High vs Low - Top 20 positive

PRJNA1133919 - High 25 % vs Low 25 % Top								
GeneID	Base mean	log2 (FC)	StdErr	Wald-Stats	P-value	P-adj	Chromo-some	Gene name
ENSG00000251546.1	413.39	5.32	0.71	7.47	7.75E-14	8.56E-10	chr2	*IGKV1D-39*
ENSG00000254709.8	90.66	6.54	0.87	7.55	4.22E-14	8.56E-10	chr22	*IGLL5*
ENSG00000234965.3	191.36	7.72	1.14	6.77	1.26E-11	9.29E-08	chr22	*SHISA8*
ENSG00000115353.11	54.58	6.36	0.94	6.73	1.69E-11	9.32E-08	chr2	*TACR1*
ENSG00000151892.16	572.69	5.62	0.86	6.54	6.26E-11	2.76E-07	chr10	*GFRA1*
ENSG00000102924.12	110.94	6.73	1.04	6.45	1.11E-10	3.51E-07	chr16	*CBLN1*
ENSG00000290698.1	141.42	5.78	0.89	6.47	9.86E-11	3.51E-07	chr17	*ENSG00000290698*
ENSG00000105369.10	2006.17	6.03	0.98	6.17	6.69E-10	1.85E-06	chr19	*CD79A*
ENSG00000239975.3	309.08	6.23	1.02	6.12	9.11E-10	2.02E-06	chr2	*IGKV1D-33*
ENSG00000163273.4	73.34	6.94	1.13	6.12	9.13E-10	2.02E-06	chr2	*NPPC*
ENSG00000242766.1	121.27	5.94	0.98	6.04	1.55E-09	3.11E-06	chr2	*IGKV1D-17*
ENSG00000123243.15	1441.02	3.51	0.61	5.78	7.31E-09	1.35E-05	chr10	*ITIH5*
ENSG00000170011.14	80.67	5.55	0.97	5.71	1.12E-08	1.90E-05	chr3	*MYRIP*
ENSG00000206579.9	39.14	5.27	0.93	5.69	1.27E-08	2.01E-05	chr8	*XKR4*
ENSG00000211593.2	31.29	6.26	1.12	5.59	2.26E-08	3.33E-05	chr2	*IGKJ5*
ENSG00000181234.10	264.42	5.54	1.00	5.54	2.97E-08	4.10E-05	chr12	*TMEM132C*
ENSG00000187922.14	105.04	6.22	1.13	5.50	3.69E-08	4.80E-05	chr9	*LCN10*
ENSG00000205056.9	164.78	6.51	1.19	5.48	4.21E-08	5.17E-05	chr12	*LINC02397*
ENSG00000104921.15	630.89	6.27	1.15	5.44	5.24E-08	6.10E-05	chr19	*FCER2*
ENSG00000159958.7	908.33	5.39	1.00	5.40	6.83E-08	7.55E-05	chr22	*TNFRSF13C*

Appendix C: PRJNA1133919: High vs Low - Top 20 negative

GeneID	Base mean	Log2 (FC)	StdErr	Wald - Stats	P-value	P-adj	Chro-mo-some	Gene name
ENSG00000137745.13	64.005487	-4.02	0.84	-4.80	1.56E-06	8.60E-04	chr11	MMP13
ENSG00000227496.3	77.969597	-4.44	1.04	-4.29	1.77E-05	5.22E-03	chr1	ENSG0000 0227496
ENSG00000237973.1	9109.6172	-3.54	0.87	-4.08	4.52E-05	1.13E-02	chr1	MTCO1P12
ENSG00000233377.1	92.466412	-4.85	1.21	-4.01	6.06E-05	1.42E-02	chr10	MTND4P20
ENSG00000173838.12	59.007023	-3.96	1.01	-3.93	8.66E-05	1.82E-02	chr17	MARCHF10
ENSG00000198763.3	504230.88	-3.39	0.86	-3.92	8.80E-05	1.84E-02	chrM	MT-ND2
ENSG00000232229.8	161.98599	-2.77	0.71	-3.91	9.08E-05	1.84E-02	chr10	LINC00865
ENSG00000198804.2	2000158.4	-3.25	0.83	-3.92	9.04E-05	1.84E-02	chrM	MT-CO1
ENSG00000248527.1	29241.161	-3.40	0.88	-3.88	1.04E-04	1.95E-02	chr1	MTATP6P1
ENSG00000198888.2	600281.17	-3.33	0.87	-3.84	1.22E-04	2.18E-02	chrM	MT-ND1
ENSG00000287335.2	121.24265	-3.80	1.00	-3.80	1.47E-04	2.46E-02	chr20	ENSG0000 0287335
ENSG00000152422.16	388.28625	-2.36	0.63	-3.74	1.81E-04	2.81E-02	chr5	XRCC4
ENSG00000198695.2	107732.16	-2.96	0.80	-3.69	2.26E-04	3.18E-02	chrM	MT-ND6
ENSG00000248810.4	257.57103	-4.01	1.09	-3.68	2.32E-04	3.19E-02	chr4	LINC02432
ENSG00000210196.2	4575.9107	-3.17	0.86	-3.68	2.32E-04	3.19E-02	chrM	MT-TP
ENSG00000251442.8	378.08347	-4.08	1.11	-3.68	2.37E-04	3.23E-02	chr4	LINC01094
ENSG00000198886.2	1026674.5	-3.14	0.86	-3.65	2.62E-04	3.46E-02	chrM	MT-ND4
ENSG00000198840.2	269162.67	-3.24	0.89	-3.62	2.93E-04	3.74E-02	chrM	MT-ND3
ENSG00000060718.22	2929.7385	-3.56	1.00	-3.56	3.70E-04	4.29E-02	chr1	COL11A1
ENSG00000251533.2	71.339063	-3.69	1.04	-3.55	3.86E-04	4.38E-02	chr14	LINC00605

Acknowledgements

I would like to express my sincere gratitude to all those who supported me throughout this doctoral journey.

First and foremost, I am deeply grateful to PD Dr. med. Matthias Ilmer, who not only selected me for this PhD position and gave me this incredible opportunity, but also provided continuous guidance, support, and mentorship throughout this research project. Without his belief in my potential, this doctoral journey would never have been possible. His dedication, constructive feedback, and unwavering encouragement have been truly invaluable at every stage of this work.

I extend my heartfelt thanks to my doctoral father, Prof. Dr. Alexandr Bazhin, who provided exceptional support and guidance, particularly during the crucial final weeks of this thesis. His expertise and encouragement when I needed it most were instrumental in bringing this work to completion.

I am grateful to the entire team at the Surgical Research Department in Großhadern for providing an inspiring research environment. Special thanks go to Michaela Svihla, Nadine Gesse, and PD Dr. Barbara Mayer, whose expertise and practical support made many aspects of this research possible. They taught me to be accurate and precise in my work and to maintain high standards in the lab - qualities I will carry with me for life.

I am deeply grateful to my colleagues in the Anesthesia department, who stood by me throughout my PhD journey, offering encouragement in the lab and cheering me on to the finish line while I juggled both research and clinical work.

On a personal note, I am profoundly grateful to my husband, who truly is my rock. He is the most patient and understanding person with the biggest heart, and he was always there to support me whenever I struggled. My love, we have known each other for 20 years now, and we have been through it all together - from our early school days through the very end of our studies. This doctoral journey is just another chapter in our shared story, and I hope we will continue this remarkable partnership for all the years to come. I love you to the moon and back.

I owe special recognition to my mother, who has been my champion from the very beginning. She encouraged me to push beyond my limits and pursue my dreams, no matter how ambitious they seemed. Her unwavering belief in my potential and her dedication to making everything possible have been the foundation upon which all my achievements rest. This doctoral degree is as much hers as it is mine.

I would also like to thank my husband's parents for their constant encouragement and for always believing in my academic pursuits. Their support has been a source of strength throughout this process.

I am grateful to my dearest friends, Lisa and Marvin, who patiently supported me even as my thesis demanded more of my time than our friendship could spare. Though they shared that they wished we could have spent more time together, they never wavered in their support and showed extraordinary understanding throughout this demanding journey.

Finally, I must acknowledge my faithful companion, Nabi, who despite being quite the princess, remained by my side throughout the entire writing process. Her patient waiting for her next walk during those long hours at the computer provided both companionship and gentle reminders that life exists beyond the pages of a thesis.

This work would not have been possible without the collective support of all these remarkable individuals, and I am forever grateful for their contributions to both my academic and personal growth.

Affidavit

Affidavit

Ittermann, Iris

Surname, first name

Marchioninistr. 15

Street

81377 Munich, Germany

Zip code, town, country

I hereby declare, that the submitted thesis entitled:

Personalised Targeting of the Substance P/NK1R Axis in Pancreatic Ductal Adenocarcinoma: A Molecular and Sex-Specific Stratification Approach

……

is my own work. I have only used the sources indicated and have not made unauthorised use of services of a third party. Where the work of others has been quoted or reproduced, the source is always given.

I further declare that the dissertation presented here has not been submitted in the same or similar form to any other institution for the purpose of obtaining an academic degree.

Munich, 03.06.2025 Ittermann, Iris

place, date Signature doctoral candidate

Confirmation of congruency

LMU LUDWIG-MAXIMILIANS-UNIVERSITÄT MÜNCHEN | Promotionsbüro Medizinische Fakultät | MMRS

Confirmation of congruency between printed and electronic version of the doctoral thesis

Ittermann, Iris

Surname, first name

Marchioninistr. 15

Street

81377 Munich, Germany

Zip code, town, country

I hereby declare, that the submitted thesis entitled:

Personalised Targeting of the Substance P/NK1R Axis in Pancreatic Ductal Adenocarcinoma: A Molecular and Sex-Specific Stratification Approach

……

is congruent with the printed version both in content and format.

Munich, 03.06.2025

place, date

Ittermann, Iris

Signature doctoral candidate

List of publications

Please note my last name has recently changed from **Beirith to Ittermann**.

Beirith, I., Renz, B. W., Mudusetti, S., Ring, N. S., Kolorz, J., Koch, D., Bazhin, A. V., Berger, M., Wang, J., Angele, M. K., D'haese, J. G., Guba, M. O., Niess, H., Andrassy, J., Werner, J., & Ilmer, M. (2021a). Identification of the Neurokinin-1 Receptor as Targetable Stratification Factor for Drug Repurposing in Pancreatic Cancer. *Cancers*, *13*(11). https://doi.org/10.3390/CANCERS13112703

Knoblauch, M., Ma, T., **Beirith, I.**, Koch, D., Hofmann, F., Heinrich, K., Aghamaliev, U., Sirtl, S., Westphalen, C. B., Nieß, H., Reichert, M., Angele, M. K., Regel, I., Bazhin, A. V., Werner, J., Ilmer, M., & Renz, B. W. (2023). In-vitro model to mimic T cell subset change in human PDAC organoid co-culture. *Journal of Cancer Research and Clinical Oncology*, *149*(14), 13051–13064. https://doi.org/10.1007/S00432-023-05100-7

Koch, D. T., Yu, H., **Beirith, I.**, Schirren, M., Drefs, M., Liu, Y., Knoblauch, M., Koliogiannis, D., Sheng, W., De Toni, E. N., Bazhin, A. V., Renz, B. W., Guba, M. O., Werner, J., & Ilmer, M. (2023). Tigecycline causes loss of cell viability mediated by mitochondrial OXPHOS and RAC1 in hepatocellular carcinoma cells. *Journal of Translational Medicine*, *21*(1). https://doi.org/10.1186/S12967-023-04615-4

Kolorz, J., Demir, S., Gottschlich, A., **Beirith, I.**, Ilmer, M., Lüthy, D., Walz, C., Dorostkar, M. M., Magg, T., Hauck, F., von Schweinitz, D., Kobold, S., Kappler, R., & Berger, M. (2021). The Neurokinin-1 Receptor Is a Target in Pediatric Rhabdoid Tumors. *Current Oncology (Toronto, Ont.)*, *29*(1), 94–110. https://doi.org/10.3390/CURRONCOL29010008

Stein-Thoeringer, C. K., Renz, B. W., De Castilhos, J., von Ehrlich-Treuenstätt, V., Wirth, U., Tschaidse, T., Hofmann, F. O., Koch, D. T., **Beirith, I.**, Ormanns, S., Guba, M. O., Angele, M. K., Andrassy, J., Niess, H., D'Haese, J. G., Werner, J., & Ilmer, M. (2025). Microbiome Dysbiosis With Enterococcus Presence in the Upper Gastrointestinal Tract Is a Risk Factor for Mortality in Patients Undergoing Surgery for Pancreatic Cancer. *Annals of Surgery*, *281*(4). https://doi.org/10.1097/SLA.0000000000006210

Wang, J., Koch, D. T., Hofmann, F. O., Härtwig, D., **Beirith, I.**, Janssen, K. P., Bazhin, A. V., Niess, H., Werner, J., Renz, B. W., & Ilmer, M. (2023). WNT enhancing signals in pancreatic cancer are transmitted by LGR6. *Aging*, *15*(20), 10897–10914. https://doi.org/10.18632/AGING.205101